

POZZOLANIC ACTIVITY OF NATURAL ZEOLITES: MINERALOGICAL, CHEMICAL
AND PHYSICAL CHARACTERIZATION AND EXAMINATION OF HYDRATION
PRODUCTS

A THESIS SUBMITTED TO
THE GRADUATE SCHOOL OF NATURAL AND APPLIED SCIENCES
OF
MIDDLE EAST TECHNICAL UNIVERSITY

BY

SEVGİ ÖZEN

IN PARTIAL FULFILLMENT OF THE REQUIREMENTS
FOR
THE DEGREE OF DOCTOR OF PHILOSOPHY
IN
GEOLOGICAL ENGINEERING

JUNE 2013

Approval of the thesis:

**POZZOLANIC ACTIVITY OF NATURAL ZEOLITES: MINERALOGICAL,
CHEMICAL AND PHYSICAL CHARACTERIZATION AND EXAMINATION OF
HYDRATION PRODUCTS**

submitted by **SEVGİ ÖZEN** in partial fulfillment of the requirements for the degree of **Doctor of Philosophy in Geological Engineering Department, Middle East Technical University** by,

Prof. Dr. Canan Özgen
Dean, Graduate School of **Natural and Applied Sciences**

Prof. Dr. Erdin Bozkurt
Head of Department, **Geological Engineering**

Prof. Dr. M. Cemal Göncüoğlu
Supervisor, **Geological Engineering Dept., METU**

Examining Committee Members:

Prof. Dr. Asuman G. Türkmenoğlu
Geological Engineering Dept., METU

Prof. Dr. M. Cemal Göncüoğlu
Supervisor, Geological Engineering Dept., METU

Prof. Dr. Hayrettin Yücel
Chemical Engineering Dept., METU

Assoc. Prof. Dr. Lütfullah Turanlı
Civil Engineering Dept., METU

Assist. Prof. Dr. Burak Uzal
Civil Engineering Dept., AGU

Date: 25.06.2013

I hereby declare that all information in this document has been obtained and presented in accordance with academic rules and ethical conduct. I also declare that, as required by these rules and conduct, I have fully cited and referenced all material and results that are not original to this work.

Name, Surname: SEVGİ ÖZEN

Signature:

ABSTRACT

POZZOLANIC ACTIVITY OF NATURAL ZEOLITES: MINERALOGICAL, CHEMICAL AND PHYSICAL CHARACTERIZATION AND EXAMINATION OF HYDRATION PRODUCTS

Özen, Sevgi

Ph.D., Department of Geological Engineering

Supervisor: Prof. Dr. M. Cemal Göncüoğlu

June 2013, 135 pages

The mineralogical properties and the effects of different zeolitic tuffs (clinoptilolites from Gördes, Bigadiç and Aliğa; mordenite from Foça and analcime from Ayvacık, western Turkey) on pozzolanic activity were investigated. The detailed mineralogical, chemical and physical characterization was followed by investigation of the physical and chemical factors that control the pozzolanic reaction in lime-pozzolan pastes in 3 to 180 days. For this, thermogravimetric analyses and Fratini's tests were applied. Experiments showed that higher specific surface area enhances the pozzolanic activity at the initial stage but it has no significant effect on reactions thereafter. The main effect of Si/Al ratio was observed at later stages, especially after 28 days. Clinoptilolite-rich tuffs exchanged with K^+ display faster reaction rates than Ca^{2+} and Na^+ -exchanged ones at longer periods. The second part of the study covers characterization of crystalline hydration products of hardened pastes as well as compressive strength behavior of blended cement mortars containing zeolitic tuffs as replacement of Portland cement. Furthermore, morphological, chemical and microstructural properties of hydrated cement products were examined. Decreasing intensity of zeolitic peaks on XRD patterns confirms the dissolution of zeolites and their involvement in pozzolanic reactions. Based on the experimental results, the compressive strength of clinoptilolite-rich tuff from Bigadiç exhibited excellent strength performance, which is approximately 10% higher than that of control Portland cement at 28 days of hydration. The compressive strength of clinoptilolite-rich tuff from Gördes is slightly higher than the control cement. It is confirmed that high strength performance should not be only considered with regard to their ability to fix lime. Physical parameters on sample preparation have also important controls on strength e.g. by arrangement of the porosity.

Keywords: Natural Pozzolan, Zeolite, Characterization, Kinetics, Hydration, Microstructure

ÖZ

DOĞAL ZEOLİTLERİN PUZOLANİK AKTİVİTESİ: MİNERALojİK, KİMYASAL VE FİZİKSEL KARAKTERİZASYON VE HİDRATASYON ÜRÜNLERİNİN İNCELENMESİ

Özen, Sevgi

Ph.D., Department of Geological Engineering

Supervisor: Prof. Dr. M. Cemal Göncüođlu

Haziran 2013, 135 sayfa

Batı Türkiye'deki farklı zeolitler içeren tüflerin (Gördes, Aliğa ve Bigadiç bölgelerindeki klinoptilolit; Foça bölgesindeki mordenit; Ayvacık bölgesindeki analsim) mineralojik özellikleri ve puzolanik aktiviteye etkileri incelenmiştir. Detaylı mineralojik, kimyasal ve fiziksel karakterizasyon ardından, 3 günden 180 güne kadar kireç-puzolan karışımındaki puzolanik reaksiyonu kontrol eden fiziksel ve kimyasal faktörler incelenmiştir. Bu amaçla termogarvimetri ve Fratini testleri uygulanmıştır. Analizler yüksek spesifik yüzey alanının ilk aşamada puzolanik aktiviteyi arttırdığını, fakat daha sonrasında reaksiyona önemli bir katkısının olmadığını göstermiştir. Si/Al oranının ana etkisi ise ileriki aşamalarda, özellikle 28 günden sonra gözlemlenmiştir. Bu aşamada, K^+ ile değiştirilmiş klinoptilolitce zengin tüf, Ca^{2+} ve Na^+ ile değiştirilmiş olana göre daha hızlı reaksiyona girmektedir. Araştırmanın ikinci kısmı sertleşmiş kireç-puzolan karışımındaki kristal hidratasyon ürünlerinin karakterizasyonunu ve zeolitik tüf içeren çimento karışımının basınç dayanım davranışını ele almaktadır. Ayrıca, hidratasyon ürünleri morfolojik, kimyasal ve mikroyapısal olarak incelenmiştir. Zeolitlerin XRD piklerinin azalması, zeolit yapısının çözüldüğünü ve puzolanik reaksiyona katıldığını göstermektedir. Deney sonuçlarına dayanarak Bigadiç'teki klinoptilolitce zengin tüfün 28 günlük dayanımı kontrol çimentosundan %10 kadar yüksek olduğu belirlenmiştir. Gördes'teki klinoptilolitce zengin tüfün basınç dayanımı ise kontrol çimentosundan biraz daha fazladır. Yüksek dayanımın sadece yüksek kireç bağlama kapasitesine bağlı olmadığı doğrulanmıştır. Örnek hazırlamada seçilen fiziksel parametrelerin de gözenekliliği düzenleyerek dayanım üzerinde önemli bir etkisi bulunduğu belirlenmiştir.

Anahtar Kelimeler: Doğal Puzolan, Zeolit, Karakterizasyon, Kinetik, Hidratasyon, Mikroyapı

To Mom and Dad, who have supported me throughout my life

ACKNOWLEDGEMENT

This PhD study was completed with the great helps and supports of many people along this long and tiring yet fulfilling road. First of all, I would like to express my heartfelt gratitude to Prof. Dr. M. Cemal Göncüoğlu, who is my supervisor, for his great help, guidance, knowledge, motivation and support throughout my thesis. Without Prof. Göncüoğlu's supervision, constructive feedback and expertise, it would have been difficult for me to complete my thesis. I feel so lucky to have had the opportunity to work with him.

I would also like to thank my sincere gratitude to my PhD committee; Prof. Dr. Asuman Türkmenoğlu, Prof. Dr. Hayrettin Yücel and Assoc. Prof. Dr. Lütfullah Turanlı. Special thanks to Assist. Prof. Dr. Burak Uzal. I am very grateful for his scientific advice, valuable and detail comments and many instructive suggestions on the thesis throughout my work. I also appreciate Dr. Mustafa Albayrak for sharing his knowledge on the field localities and advices. I would also like to thank to METU Central Laboratory for their help, Orhan Karaman for his help during field study and Rota Mining Corporation for their guidance during field work in Gördes region.

Thanks to all staff of Department of Material and Production Engineering at Universita Degli Studi Di Napoli Federico II, Italy. I am very grateful not only for the chance to visit but also be a part of the team. Specifically, Prof. Dr. Carmine Colella, Prof. Dr. Caputo Domenico, Assoc. Prof. Dr. Bruno De Gennaro, Assist. Prof. Dr. Fabio Iucolano, Assist. Prof. Dr. Barbara Liguori, Assist. Prof. Dr. Paolo Aprea, Giovanni Albano, Paola Desidery, Dr. Francesco Pepe, Dr. Nicola Gargiulo, Mocchi Giuseppe, Lilia Catalanotti. Special thanks Drs Fabio Iucolano, Barbara Liguori, Bruno De Gennaro and Paolo Aprea for welcoming me as a friend and sorry for all the bureaucratic trouble that I gave you. I will always remember the day I arrived in Italy. Thank you very much my dear friends. Appreciation is also expressed to Prof. Dr. Piergiulio Cappelletti who made QXRD analysis and Prof. Dr. G. Diego Gatta who made helpful comments on the microprobe analysis of zeolites used in the study. I also wish to thank Andrea Risplendente providing technical assistance with electron microprobe analysis of zeolites.

I really appreciate to Civil Engineering Department of Middle East Technical University for helping me at their mechanical test laboratory. I am very grateful to my friends, Dr. Burhan Alam and Dr. S. Bahadır Keskin who have helped and supported me compressive strength analysis. Also special thanks to Burhan Alam for great help not only mechanical analysis but also ideas, comments and encouragement.

Lastly, I would like to direct a deep sense of gratitude to support and love from my family who is always by my side; Sacettin Özen, Sabahat Özen, Sibel Özen, Onur Özen, Bahar Dinçer, Ersin Dinçer and Zeynep Dinçer. I feel their great support, endless encouragement, patience and understanding all my life. This study was funded by The Council of Higher Education (YÖK) with project number: 2548, 33/a.

TABLE OF CONTENTS

ABSTRACT.....	v
ÖZ.....	vi
ACKNOWLEDGEMENT.....	viii
TABLE OF CONTENTS.....	ix
LIST OF TABLES.....	xii
LIST OF FIGURES.....	xiii
ABBREVIATIONS.....	xvii
CHAPTERS	
1. INTRODUCTION.....	1
1.1 General.....	1
1.2 Scope of the Study.....	2
2. THEORETICAL BACKGROUND AND LITERATURE REVIEW.....	5
2.1 The History of Mortar Technology.....	5
2.2 Natural Zeolites.....	7
2.3 Pozzolans and Pozzolanic Reaction of Zeolites.....	9
2.4 Literature Review.....	11
3. GEOLOGY OF THE STUDY AREA.....	15
3.1 Field work.....	15
3.2 Geology of Gördes Region.....	15
3.3 Geology of Aliağa Region.....	17
3.4 Geology of Bigadiç Region.....	19
3.5 Geology of Foça Region.....	21
3.6 Geology of Küçükkuyu Region.....	23
4. EXPERIMENTAL STUDY.....	25
4.1 Introduction.....	25
4.2 Material.....	25
4.2.1 Lime.....	25
4.2.2 Portland Cement.....	25
4.2.3 Aggregate.....	27
4.2.4 Zeolitic Tuffs.....	27

4.2.4.1	Physical Characterization of Zeolitic Tuffs.....	28
4.2.4.2	Chemical Characterization of Zeolitic Tuffs.....	28
4.2.4.2.1	Chemical Analyses of Zeolitic Tuffs.....	28
4.2.4.2.2	Quantitative Electron Microprobe Analyses of Zeolites	28
4.2.4.2.3	Evaluation of Cation Exchange Capacity (CEC) of Zeolitic Tuffs	30
4.2.4.2.3.1	Cross Exchange Method (CEM)	31
4.2.4.2.3.2	Batch Exchange Method (BEM)	31
4.2.5	Mineralogical/Petrographical Characterization of Zeolitic Tuffs.....	32
4.2.5.1	Petrography	32
4.2.5.2	Quantitative XRD.....	33
4.2.5.3	Scanning Electron Microscope (SEM) Analyses of Zeolitic Tuffs	33
4.3	Experimental Methods	34
4.3.1	Evaluation of Pozzolanic Reaction.....	34
4.3.1.1	Thermogravimetric Analyses of Zeolitic Tuffs	34
4.3.1.2	Thermogravimetric Analyses of exchanged Zeolitic Tuff.....	35
4.3.1.3	Fratini's Test.....	36
4.3.1.3.1	Comparison of Fratini's test and thermogravimetric method.....	36
4.3.1.4	Kinetic Analyses.....	36
4.3.2	Reaction Products.....	37
4.3.2.1	XRD Analyses of Hardened Lime-Zeolite Pastes	37
4.3.2.2	FTIR Analyses of Hardened Lime-Zeolite Pastes.....	38
4.3.2.3	Compressive Strength Analyses	38
4.3.2.3.1	Flow Test (ASTM C 109).....	38
4.3.2.3.2	Preparation of Mortars (ASTM C 311-98b).....	38
4.3.2.3.3	Test on Hardened Cement	39
4.3.2.3.4	Water Requirement.....	39
4.3.2.4	Microstructure of Hardened Cement Pastes	39
4.3.2.4.1	SEM Analyses of Hardened Cement	40
4.3.2.4.2	Quantitative Electron Microprobe Analyses of Hardened Cement	40
5	RESULTS.....	41
5.1	Characterization of Zeolitic Tuffs	41
5.1.1	Physical characterization of zeolitic tuffs.....	41

5.1.2	Chemical Characterization.....	42
5.1.2.1	Chemical Analyses of Zeolitic Tuffs	42
5.1.2.2	Quantitative Electron Microprobe Analyses (EPMA) of Zeolites	43
5.1.2.3	Evaluation of cation exchange capacity (CEC)	48
5.1.3	Mineralogical Charaterization.....	50
5.1.3.1	Petrography	50
5.1.3.2	Quantitative X-ray powder diffraction (XRPD)	54
5.1.3.3	SEM Analyses of Zeolitic Tuffs	55
5.2	Pozzolanic Reaction Evaluation.....	66
5.2.1	Thermogravimetric Analyses of Zeolitic Tuffs.....	66
5.2.2	Thermogravimetric Analyses of Exchanged Zeolitic Tuff	67
5.2.3	Fratini’s Test	68
5.2.3.1	Comparison of Fratini’s Test and Thermogravimetric Analysis.....	69
5.2.4	Kinetic Analyses	71
5.3	Reaction Products	72
5.3.1	XRD Analyses of Hardened Lime-Zeolite Pastes.....	73
5.4	FTIR Analyses of Hardened Lime-Zeolite Paste	82
5.5	Compressive Strength Analyses.....	89
5.6	Microstructure of Hydrated Cement Pastes	92
5.6.1	SEM Analyses of Hardened Cement.....	93
5.6.2	Quantitative Electron Microprobe Analyses of Hardened Cement.....	105
6	DISCUSSION	113
7	CONCLUSIONS AND RECOMMENDATIONS	117
	REFERENCES	121
	CURRICULUM VITAE.....	135

LIST OF TABLES

TABLES

Table 4.1 Physical properties and chemical composition of Portland cement	26
Table 4.2 Physical properties of aggregate used in this study (*OD: Oven Dry, SSD: Saturated Surface Dry).	27
Table 4.3 Particle size distributions of aggregate.....	27
Table 5.1 Physical properties of the zeolitic tuffs	41
Table 5.2 Chemical composition of the zeolitic tuffs (wt %).	43
Table 5.3 Representative electron microprobe analyses of zeolites in tuffs (wt %).	44
Table 5.4 Theoretical, Expected and Experimental CECs and exchangeable cations of zeolitic tuffs.....	48
Table 5.5 Quantitative mineralogical composition of zeolite bearing tuff samples.	55
Table 5.6 Fratini's test results quantified using Equation 4.3.	70
Table 5.7 Compressive strength test results of the zeolite blended and control cement mortar...	90
Table 5.8 Electron microprobe analysis of hardened cement (wt %).	106

LIST OF FIGURES

FIGURES

Figure 2.1 Classification of pozzolanas (Massazza, 1998).	11
Figure 3.1 Location map of the study area.....	15
Figure 3.2 Simplified geologic map of Gördes region with sample location (after Göktaş, 1996).	16
Figure 3.3 Photograph illustrating massive Gökyar tuff, which is fine-grained, compact and white in color.	17
Figure 3.4 Simplified geologic map of Aliğa region with sample location (after Albayrak and Özgüner, 2013).	18
Figure 3.5 A view from Foça Tuff, which is soft, homogeneous and white in color.....	19
Figure 3.6 Simplified geologic map of Bigadiç region with sample location (after Ercan et al., 1984b).	20
Figure 3.7 Photograph shows Beğendikler Tuff, which is light green, very hard and homogeneous.	21
Figure 3.8 Simplified geologic map of Foça region with sample location (after Lengeranlı et al., 1998).	22
Figure 3.9 Photograph illustrating Foça Tuff, which is whitish yellow in color and very hard. .	22
Figure 3.10 Simplified geologic map of Foça region with sample location (after Çelik et al., 1999).	23
Figure 3.11 Photograph showing Arıklı tuff, which is homogenous and yellow in color.	24
Figure 4.1 Particle size distribution of ordinary Portland cement.	26
Figure 4.2 The design of standard electron and x-ray optics of a combined SEM-EMPA (Figure taken from http://serc.carleton.edu/research_education/geochemsheets/techniques/SEM.html)	29
Figure 4.3 Experimental set-up for cross exchange method (CEM).....	32
Figure 4.4 Vacuum filtration setup of hardened paste after washing with acetone.	35
Figure 5.1 Particle size distributions of zeolitic tuffs.	42
Figure 5.2 Back scattered image shows very small prismatic clinoptilolite crystals 1µm in length distinguished from cryptocrystalline matrix and one microprobe analyze spot (Cli: clinoptilolite; Sample: CLI-G).	45
Figure 5.3 Back scattered image showing clinoptilolite-rich tuff (Sample: CLI-A).	46
Figure 5.4 Back scattered image showing CLI-B, which display denser structure.....	46

Figure 5.5 Back scatter image displaying mordenite fibers, which form by alteration of volcanic glass (Sample: MOR). 47

Figure 5.6 Back scattered image showing analcime bearing tuff (Sample: ANA). 47

Figure 5.7 The cation exchange capacity (CEC) and the amount of exchangeable cations (Na^+ , K^+ , Ca^{2+} and Mg^{2+}) determined by BEM method..... 49

Figure 5.8 Photomicrograph showing biotite and quartz phenocryst as well as relict volcanic glass shard (Sample: CLI-G, GS: glass shard, Bio: biotite, PPL). 50

Figure 5.9 Photomicrograph of homogeneous clinoptilolite rich tuff, which consist of cryptocrystalline feldspar and quartz mineral (Sample: CLI-A, PPL). 51

Figure 5.10 Photomicrograph showing relict volcanic glass shards in darker groundmass (Sample: CLI-B, GS: glass shard, PPL). 52

Figure 5.11 Photomicrograph displaying direct alteration of mordenite from edge of volcanic glass and precipitation of cristobalite (Sample: MOR, Mor: mordenite, Crs: cristobalite, PPL). 53

Figure 5.12 Photomicrograph showing thin section view of analcime-bearing vitric tuff (Sample: ANA, PPL). 54

Figure 5.13 Scanning electron micrograph shows clinoptilolite crystals displaying laths and tabular plates (Sample: CLI-G, Cli: clinoptilolite). 56

Figure 5.14 Scanning electron micrograph of well-formed clinoptilolite crystals and corresponding EDX measurement (Sample: CLI-G, Cli: clinoptilolite, Mor: mordenite). 57

Figure 5.15 Scanning electron micrograph of well-formed clinoptilolite crystals (Sample: CLI-A, Cli: clinoptilolite). 58

Figure 5.16 Scanning electron micrograph shows lath-shaped clinoptilolite crystals (Sample: CLI-A, Cli: clinoptilolite). 59

Figure 5.17 Scanning electron micrograph of clinoptilolite aggregate and corresponding EDX spectra (Sample: CLI-B, Cli: clinoptilolite). 60

Figure 5.18 SEM image sample showing anhedral to subhedral clinoptilolite aggregates and corresponding EDX spot (Sample: CLI-B, Cli: clinoptilolite). 61

Figure 5.19 SEM image shows mordenite needles growing on the edge of the volcanic glass shard (Sample: MOR, Mor: mordenite PF: pumice fragment). 62

Figure 5.20 SEM image showing characteristic morphology of mordenite (Sample: MOR). 63

Figure 5.21 Scanning electron image of fibers of mordenite at high magnification (Sample: MOR). 64

Figure 5.22 Scanning electron micrograph of cubo-octahedral analcime. Honeycomb smectite and quartz are also present (Sample ANA, Ana: analcime, Sme: smectite, Qtz: quartz). 65

Figure 5.23 Amounts of fixed lime in zeolitic tuff-lime pastes. 67

Figure 5.24 Amounts of of fixed lime in CLI-B exchanged with K^+ , Na^+ and Ca^{2+} cations-lime pastes.....	68
Figure 5.25 Results of Fratini's test to evaluate pozzolanicity of blended cements.	69
Figure 5.26 Correlation between pozzolanic activity of Fratini's test (8 days) and thermogravimetric analysis (7, 28 and 90 days).	70
Figure 5.27 Pozzolanic reaction kinetics in zeolitic tuff-lime pastes.....	71
Figure 5.28 Pozzolanic reaction kinetics in CLI-B exchanged with K^+ , Na^+ and Ca^{2+} cations-lime pastes.....	72
Figure 5.29 X-ray diffraction patterns of bulk material (CLI-G) and hardened paste (CLI-G-R at 3 days) (P: portlandite, Cli: clinoptilolite, H: hydrotalcite, Qtz: quartz).	74
Figure 5.30 XRD patterns of a) CLI-A (bulk) and CLI-A-R (3 days), b) CLI-B (bulk) and CLI-B-R (3 days).....	75
Figure 5.31 X-ray diffraction patterns and identified phases of a) MOR (bulk) and MOR-R (3 days), b) ANA (bulk) and ANA-R (3 days) (Mor: mordenite, Ana: analcime, Qtz: quartz).	77
Figure 5.32 X-ray diffraction patterns and identified phases of the CLI-G-R at ages 3 days to 180 days (P: portlandite, Cli: clinoptilolite, H: hydrotalcite).....	78
Figure 5.33 X-ray diffraction patterns and identified phases of the a) CLI-A-R, b) CLI-B-R at ages 3 days to 180 days (P: portlandite, Cli: clinoptilolite).	79
Figure 5.34 XRD patterns and identified phases of CLI-G-R, CLI-A-R and CLI-B-R at 180 days (P: portlandite, Cli: clinoptilolite, H: hydrotalcite).....	80
Figure 5.35 X-ray diffraction patterns and identified phases of the a) MOR-R, b) ANA-R at ages 3 days to 180 days (Mor: mordenite, Ana: analcime, P: portlandite, Kfs: K-feldspar).	81
Figure 5.36 X-ray diffraction patterns and identified phases of the CLI-G-R, CLI-A-R, CLI-B-R, MOR and ANA samples at 180 days of hydration (H: hydrotalcite, Kfs: K-feldspar, Qtz: quartz, M: mordenite, Ana: analcime, P: portlandite).....	82
Figure 5.37 FTIR spectrum of bulk material (CLI-G) and corresponding blended paste at 3 days (CLI-G-R).	83
Figure 5.38 FTIR spectrum of a) bulk material (CLI-A) and corresponding blended paste at 3 days (CLI-A-R), b) bulk material (CLI-B) and corresponding blended paste at 3 days (CLI-B-R).	84
Figure 5.39 FTIR spectrum of a) bulk material (MOR) and corresponding blended paste at 3 days (MOR-R), b)) bulk material (ANA) and corresponding blended paste at 3 days (ANA-R).	86
Figure 5.40 FTIR spectra of CLI-G-R/lime pastes after 3, 7, 28, 56 90 days.....	87
Figure 5.41 FTIR spectra of CLI-A-R/lime pastes after 3, 7, 28, 56 90 days.....	87
Figure 5.42 FTIR spectra of CLI-B-R/lime pastes after 3, 7, 28, 56 90 days.	88

Figure 5.43 FTIR spectra of MOR-R/lime pastes after 3, 7, 28, 56 90 days.....	88
Figure 5.44 FTIR spectra of ANA-R/lime pastes after 3, 7, 28, 56 90 days.	89
Figure 5.45 The compressive strength of blended cements at 7, 28, 56, 90 days.	90
Figure 5.46 Scanning electron micrographs showing general microstructure of a) CLI-G-R, b) CLI-B-R at low magnification.	93
Figure 5.47 Scanning electron micrograph showing the characteristic polygonal morphology of cement grain (alite), CSH coating and sponge-like CSH found in the cavity (Sample: CLI-B-R).	94
Figure 5.48 Scanning electron micrograph displaying round belite crystals and corresponding EDX spectra of belite (Sample: Control-R).	95
Figure 5.49 Scanning electron micrograph of gehlenite hydrate and corresponding EDX analysis (Sample: ANA-R).	97
Figure 5.50 SEM image displaying branched fibrous CSH and mordenite needles and corresponding EDX spectra of the CSH (Sample: MOR-R).....	98
Figure 5.51 Scanning electron image of CSH radiate outward from the remnant cement particles (Sample: ANA-R).	99
Figure 5.52 Scanning electron image of CSH and prismatic clinoptilolite crystals (CLI-A-R).	100
Figure 5.53 Scanning electron image illustrating thin porous CSH coatings (CLI-G-R).	101
Figure 5.54 Scanning electron micrographs of a) CLI-G, b) CLI-A, c) CLI-B, d) MOR, d) ANA.	102
Figure 5.55 SEM-EDX characterization of hardened cement pastes after 28 days of curing; prismatic clinoptilolites in the a)CLI-G, b) CLI-A, c) CLI-B and corresponding EDX spectrums.	104
Figure 5.56 SEM image of clinoptilolites embedded in the cement matrix (Sample: CLI-A-R, Cli: clinoptilolite).	105
Figure 5.57 Backscattered electron image of cement paste showing general microstructure (Sample: CLI-G-R).....	107
Figure 5.58 Backscattered electron image of a) CLI-A, b) MOR.	108
Figure 5.59 Backscattered image of blending cement paste showing the ferrite phase (Sample: CLI-B-R).	109
Figure 5.60 Backscattered image of blending cement paste showing the aluminate phase (Sample: CLI-B-R).....	110
Figure 5.61 Backscattered electron images of a) CLI-G-R, b) CLI-A-R, c) CLI-B-R, d) MOR-R, e) ANA-R cement pastes.	112

ABBREVIATIONS

XRD	: X-ray Diffraction
FTIR	: Fourier Transform Infrared Spectroscopy
SEM	: Scanning Electron microscopy
EDX	: Energy Dispersive X-ray Analysis
ICP-OES	: Inductively Couple Plasma-Optical Emission Spectroscopy
ASTM	: American Society for Testing and Materials
BET	: Brunauer Emmett Teller
SCMs	: Supplementary Cementitious Materials

CHAPTER 1

INTRODUCTION

1.1 General

A pozzolan is defined in ASTM C125 as “a siliceous and aluminous material, which contains constituent possessing little or no cementitious properties in themselves but which will, in finely divided form and in presence of moisture, react with calcium hydroxides at ordinary temperatures to form relatively stable and water insoluble compounds with cementitious properties”. Since Roman times, pozzolans were widely used for the constructional purposes, acquiring their name from today’s village of Pozzuoli, Naples, Italy.

During cement manufacturing, raw materials generate chemical reactions that result in CO₂ emission. The substitution of natural or artificial pozzolan to Portland cement clinker is one of the succeeding processes developed for reducing CO₂ emissions in cement industry. They also have many advantages on the physical aspect of the resulting concrete (Malhotra and Mehta, 1996; Sersale, 1992). Pozzolans are known to lower hydration heat and thermal expansion (Mehta, 1987; Sersale and Frigione, 1983; Collepardi et al., 1978), increase sulfate resistance (Janotka et al., 2004), enhance durability (Cook, 1986), decrease permeability (Mehta and Monteiro, 2006), minimize the risk of alkali-aggregate reaction (Mielenz, 1950) and improve resistance to chemical attack (Sersale and Frigione 1983; Janotka and Krajci, 2003). On the other hand, since the pozzolanic reaction progresses slowly, the strength of mortars takes place gradually over long periods of time (Collepardi et al., 1978; Fragoulis et al., 1997) and zeolite-blended cements require more water owing to large specific surface area (Drzaj et al., 1978). Obvious economic and environmental benefits attract not only industrial but also scientific research towards supplementary cementitious materials (SCMs).

Natural materials used as pozzolan are zeolites, diatomaceous earth, volcanic glass, and so on. Fly ash, calcined clay, silica fume, ground granulated blast furnace slag and burnt gaize are reported as artificial pozzolans (Massazza, 1998). Natural zeolites are hydrated aluminosilicates including high amounts of reactive SiO₂ and Al₂O₃ (Tsitsishvili et al., 1992). As zeolites show excellent pozzolanic activity regardless of their distinct crystalline structure (Sersale, 1992; Drzaj et al., 1978; Massaza, 1998), they have been widely used since Roman times as admixtures in cement for all kinds of constructions. Reactivity of natural zeolites is mainly attributed to their highly porous structure which is related to large external surface area giving interaction of zeolite with lime (Janotka and Krajci, 2003; Mostafa et al., 2001; Perraki et al., 2003; Lea, 1998), ability of ion exchange and meta-stability, which support dissolution of zeolitic crystals and precipitation of hydrated calcium silicates and aluminates under interaction

of OH⁻ ions available in the saturated lime solution (Drzaj et al., 1978; Janotka et al., 2004; Sersale and Frigione, 1985; Caputo et al., 2008).

The pozzolanic property of different kind of materials from different countries was investigated by several authors (Caputo et al., 2008; Fragoulis et al., 1997; Kitsopoulos and Dunham, 1996; Mertens et al., 2009; Martiniz Ramirez et al., 2006; Ortega et al., 2000; Poon et al., 1999; Perraki et al., 2003; Sersale and Frigione, 1985; Shi and Day, 2000; Turkmenoglu and Tankut, 2002; Uzal et al., 2010; Uzal and Turanlı, 2012; Yılmaz et al., 2007 and reference therein). A number of authors have examined pozzolanic activity assessment using direct methods such as the evaluation of lime reduction with time by thermogravimetric analysis (TGA), Fratini's test, X-ray powder diffraction (XRD) or chemical analysis (Caputo et al., 2008; Mertens et al., 2009; Perraki et al., 2005; Uzal and Turanlı, 2012), whereas others have tried to define reactivity by indirect methods monitoring mechanical properties of mortars such as compressive strength, electrical conductivity, conduction calorimetry, pore-size distribution of pastes or microstructural properties of zeolite-blended cements (Uzal and Turanlı, 2012; Uzal et al., 2010; Poon et al., 1999). Even though, numerous studies were carried out on the usage of zeolitic tuffs to produce blended cements, factors controlling the reactivity are even scarcer (Caputo et al., 2008; Mertens et al., 2009; Uzal and Turanlı, 2012). Therefore, the main goal of this study is to fulfill this requirement. Furthermore, more research is needed to investigate at which stage of reactions what kind of parameters is effective.

Considerably large zeolitic tuff deposits situated in the western part of Turkey have potential economic value. Nevertheless, published literature of zeolite blended cement is scarcer (Uzal et al., 2010; Uzal and Turanlı, 2012; Yılmaz et al., 2007; Turkmenoglu and Tankut, 2002). Even though Gördes and Bigadic deposits were studied (Uzal and Turanlı, 2012; Yılmaz et al., 2007), the literature lacks information from Aliğa and Foça regions for blending cement. Ayvacık, on the other hand, had been only evaluated on the basis of analcime formation (Özen and Göncüoğlu, 2012). Therefore, the study also includes determining the possible industrial utilization of zeolitic tuffs as blended cement. In order to be able to apply the results industrially, the mechanical behavior of blended cement, prepared by mixing cement with zeolitic tuffs from various localities and their reaction products are examined.

1.2 Scope of the Study

The main aim of the present work was to determine mineralogical, physical and chemical factors influencing the pozzolanic activity by comparing the behavior of zeolites during the pozzolanic reaction stages, and to investigate experimental results on the mechanical behavior of zeolitic blended cements.

For this purpose, an investigation on characterization from the mineralogical, physical and chemical point of view of different kind of zeolites acquired from major deposits in western

Turkey and evaluation of their reactivity as pozzolanic additives in lime paste was examined. In order to quantitatively evaluate and compare the pozzolanic activity of different kind of zeolites in the tuffs, thermal analysis, one of the most suitable techniques, has been used (Perraki et al., 2005). The pozzolanic activity has also been evaluated by Fratini's test (EN 196/5), which is a commonly used direct method. The European Standard Method, the Fratini's test, and thermogravimetric method are compared to be sure on the validity of experimental procedure. The pozzolanic activity of exchanged tuff samples was conducted to investigate further findings about the relationship between cation content of zeolites and its ability to fix calcium. Furthermore, the examination of the kinetic analyses using modified Jander's equation was conducted to investigate both the hydration mechanism and the rate of reaction.

Attempts have then been made to identify the hydration products generated in the pozzolanic reaction in zeolite-lime pastes. Detection and the progress of the reaction products are monitored by X-ray diffraction (XRD) and Fourier Transform Infrared Spectroscopy (FTIR) analyses. Since alteration of volcanic glass present in volcanic tuff is well known and common in Turkey, which represent huge source of natural zeolites, it is important to examine the possible industrial utilization of the zeolitic tuff deposits from the western part of Turkey. Therefore, blended cement, which is one of the most promising uses of natural zeolites because of both technical and economic advantages, were prepared to investigate the compressive strength analysis. The morphological, chemical and microstructural properties of hydrated products were also examined on mortars after 28 days of hydration, which is also not frequently realized on local material.

CHAPTER 2

THEORETICAL BACKGROUND AND LITERATURE REVIEW

2.1 The History of Mortar Technology

The discovery of binding properties of lime dates back to the Neolithic ages most probably when fire was used to cook or to heat the limestone cave (Kingery, 1980, Aitcin, 2008). The earlier mortar consisting of calcined limestone was found to be made 22 600 years ago in Nevalı Çözü in Turkey (Felder-Casagrande et al., 1997). Lime or gypsum had started to be used as renders 8000 years ago (Tunca, 2004). The use of lime was prevalent not only to the Mediterranean region but also in the Chinese province of Ganow (Güleç and Tulun 1997, Thornton, 1996), whereas gypsum was used more frequently in the East.

Although the use of lime preceded the use of gypsum, the common mortar which is similar to the today's system is first met with masonry constructions of the Egyptians by joining stones with a mortar, consisting of blending sand with burning gypsum at about 15 000 years ago (Blezard, 1998, Stark and Wicht, 1999). In spite of the fact that many researchers believe the Great Pyramid was made from limestone, Champbell (1999) proved by chemical analysis that Egyptians did not use burned limestone until Roman period. Lucas (1968) claimed that the reason for using gypsum in place of lime by Egyptians is the simplest processed material requiring lower temperature and thus lower fuel for its calcinations. Gypsum dehydrates heating up to 120 to 150°C and rehydrates at ambient temperature. Since it easily loses its durability in a humid environment, the most ancient use of gypsum was found in Egypt where desert climate dominated (Aitcin, 2008). Torres and Emeric (1999) stated that gypsum as a binder in mortar was dated in a fresco found in Çatal Höyük in Turkey, made 9 000 BC.

Even though lime was not used by early Egyptians, it was employed to the architectural use by the Greeks and then by the Romans (Martinet et al., 1992). The processing of hydrated lime was controversial at the time of the construction of the Palace of Versailles. Lorient (1774) suggested that the storing lime conditions recommended by ancient writers in question and proposed that lime had to be slaked at the time of use. De la Faye (1777) and Faujas de Saint-Fond (1778), however, objected the topic and stated that lime should be slaked immediately and then immersed in water. Finally, Rondelet (1805) concluded that the durability of constructions depends on the thoroughness of mixing and ramming but not the slaking or composition of the lime.

The finely ground volcanic material mixing with lime and sand was known by the Greeks and then the Romans (Blezard, 1998). Indeed, pozzolanic materials were used to a lesser extent

during the Neolithic period (Malinowski and Garfinkel, 1991). The Phoenicians had revealed the pozzolanic mortar made of fired clay waste (Aitcin, 2008). The Greeks used the volcanic Santorin Earth with pozzolanic properties at about 500-300 BC (Idorn, 1997). The use of pozzolanic material consist of volcanic tuff found near the Mount Vesuvius in mortar was also seen in Roman buildings around the 3rd century BC (Blezard, 1998). Because the best quality of this material was acquired from Pozzuoli near Vesuvius, the name of material is given as “pozzolana”. Vitruvius (1826) suggested this corresponding material as the species of sand found in abundance in the Baie which possesses cementitious properties even under water as ordinary cement if mixed with lime and rubble. The pozzolanic mortars were an important technological invention since they could be produced under water. Thus, the discovery of hydraulic mortars gives way to constructions of bridge footings, harbors, line aqueducts and so on (Oleson et al., 2004). Romans also mentioned about true selection of source rock, burning processes and proportions of pozzolana. Furthermore, Romans used a mixture of lime and powdered tiles whenever volcanic tuff was not available, which produce a similar effect as volcanic tuff (Baronio et al., 1997). Therefore, Romans were the first to change properties of cementitious material. After Romans, during the Middle Ages lime technology began to decline as has been found by studying Saxon and Norman buildings. They show evidence of poorly calcined lime and badly mixed mortar even this was not always the case (Blezard, 1998, Adams et al., 1993). But, the quality again started to improve with beginning of the twelfth century.

The first known scientific mortar made of lime was prepared by John Smeaton, a British engineer, in order to rebuild the lighthouse on the Eddystone Rock (Bogue, 1952). Smeaton started to make investigation as to the best mortar comparing the hardening properties of lime in different origin. After chemical analyses of different materials by dissolving them in nitric acid he realized that lime from the Aberthaw limestone which gave better results as mortars includes considerable amount of clay minerals that would harden under water. As a result of this discovery he rebuilt the Eddystone lighthouse in 1759 (Bogue 1952, Blezard 1998). At about the time of the breakthrough of hydraulic lime, James Parker discovered the first hydraulic binder made by calcination of argillaceous limestone known as septaria. He called his binder as Roman Cement and he obtained a patent for it in 1796 (Papadakis and Venuat 1966). This was the first natural cement made by burning septaria containing approximately 30% clay. Actually, the meaning of Roman Cement is misleading since it was not similar to the Roman mortar.

Roman Cement was quick setting natural cement and useful to work in contact with water. The most productive period was reached until about 1850. From that moment its use gradually decreased due to the lower prices of artificial Portland cement. Vicat (1818) was the first to determine the optimum proportion of limestone (chalk) and clay in producing hydraulic lime. This process may be considered as a real milestone of the manufacture of Portland cement. Thereafter, the knowledge of cement mineralogy increased because hydraulic binders started to be examined by optical microscopy. The next step in the history of hydraulic cement stands out by Joseph Aspdin, an English mason, applying improved double kilning method first described by Vicat (1837). In 1824, he obtained a patent for it and named as Portland cement since its

color looks like that of the stone of Portland Island. Gradually, strength of Portland cement increased compared with that of Roman cement and manufacture of Portland cement was greatly improved by William Aspdin, Joseph Aspdin's son.

The addition of gypsum during clinker grinding to retard the setting carried out by Giron at about 1990 (Draffin 1943) was an important chemical invention from the point of view of manufacturing technique. Another important technological innovation was the improvement of the rotary kiln, which replaced the intermittent kiln (Blezard 1998). Obviously, many other developments were applied and gradually slow evolution are recognized from lime to hydraulic lime, from hydraulic lime to natural cement and from natural cement to present day Portland cement (Aitcin, 2008).

2.2 Natural Zeolites

Freiherr Axel Cronstedt (1756), Swedish mineralogist, was the first scientist to define a new type of mineral displaying frothing features when heated in a blow-pipe flame and therefore he named as zeolite from the Greek words meaning "boiling stone" (Hay, 1978; Gottardi and Galli, 1985). At present the term correspond to over 40 naturally occurring species and 206 different frameworks and is the largest group of aluminosilicates (Tsitsishvili et al., 1992; IZA, 2013). Natural zeolites are crystalline, micro porous, hydrated aluminosilicates with three dimensional framework structures based on TO_4 tetrahedra, where T is Si or Al atom, linked to each other by sharing all oxygens by two tetrahedra that yields numerous island structures, chains and sheets (Gottardi and Galli, 1985). The replacement of Si^{4+} by Al^{3+} results in a negative charge being neutralized by the extraframework cations located outside the tetrahedra (e.g. Na^+ , K^+ , Ca^{2+}). The framework structure of zeolites contains channels filled with water molecules and loosely bound cations which can be easily exchanged that leads to unique ion exchange property (Tsitsishvili et al., 1992).

The general chemical formula of the natural zeolites is shown equation 2.1 (Gottardi, 1978):



where M is monovalent cations, D is divalent cations, the part in square brackets is the framework atoms which are not exchanged under ordinary conditions and the part outside the square brackets is the extraframework atoms which are substituted easily and m is the number of water molecules per unit cell (Gottardi, 1978; Barrer, 1982). The Si/Al ratio in natural zeolites ranges from 1 to 6. The ratio, $R = Si:(Si+Al+Fe)$, representing the percentage of the tetrahedra occupied by Si lies within the limits of 0.50 to 0.87 (Gottardi, 1978). The content of zeolitic water which can be removed at high temperature (150 to 400°C) without destruction of the crystal structure and re-adsorbed it again at room temperature depends on the character of the exchangeable cations and conditions of crystallization. Water as an intracrystalline fluid is well able to penetrate into the zeolitic cavity. Consequently, under ordinary conditions the measure of

the approximate free volume of channels in the zeolite structure can be determined by the volume of the liquid water released under heating (Tsitsishvili et al., 1992). When zeolitic phase dehydrated, it may re-adsorb a variety of molecules in addition to water (e.g. gases, vapours and fluids) that related to the catalytic property and selective sorbents of zeolites.

Three classification systems are recently used for zeolites (Armbruster and Gunter, 2001). The first classification of zeolites depends on the structural type. In accordance with this classification the topology of distinct frameworks of any given zeolite are represented by three-letter code that specifies the zeolite structure (Meier et al. 1996). These letters define various orderings of framework the given topology. For example, natrolite, mesolite, scolecite and gonnardite have similar frameworks and all are described by the code NAT although their chemical compositions are different. The next classification system is based on the geometric arrangement of tetrahedra. Because silicate group of minerals are so diverse, Meier (1968) introduced a concept termed “secondary building units” (SBU) based on small group of linked tetrahedra, which are linked together to generate the structure of zeolite. In the SBU Si or Al is present at each corner and numerous frameworks could be build, including those of all the natural and synthetic zeolites (Tsitsishvili et al., 1992). The third classification method is introduced by Gottardi and Galli (1985) on the basis of the finite or infinite complex structural units of tetrahedra, which are connected to form the actual frameworks.

At the beginning, zeolite minerals were thought to be only formed in geodes in volcanic rocks since sedimentary zeolites are microcrystalline and well developed large crystals was the main point of interest in mineralogical studies. It was only possible to ascertain a wide distribution of zeolites in sedimentary rocks after X-ray powder diffraction (XRD) technique and then these deposits start to gain a practical importance. In recent years most of the efforts has centered not only their occurrences but also on their unique chemical and physical properties and their potential applications in industry. Although there are a wide variety of authigenic zeolite minerals that occurred in nature, only eight are common in sedimentary deposits; they are analcime, clinoptilolite, chabazite, erionite, mordenite, phillipsite, heulandite and laumontite (Hay and Sheppard,2001). Zeolites can be formed from a variety of materials including volcanic glass, pre-existing zeolites, feldspars, feldspathoids, biogenic silica or clay minerals. Most zeolites are originated by alteration of volcanic glass being the major precursor material with pore water by dissolution-precipitation process, with or without an intermediate gel stage (Mumpton, 1973b). Early formed zeolite species also react further to yield other zeolites as a results of change in the chemical environment or the availability of time in order to transform from less stable phase to more stable phase (Hay and Sheppard, 2001). Others formed by the alteration of pre-existing aluminosilicate minerals.

Natural or synthetic zeolites are being used in the various agricultural and industrial areas in many countries. The major industrial applications which make use of zeolites include filler in the paper industry, oil spills clean up, ion-exchangers in water purification and pollution-abatement processes, in the separation of oxygen and nitrogen from air, herbicides, desiccant material,

nuclear remediation, antibiotics, detergent builder, soil conditioner, dietary supplements in animal husbandry, in pozzolanic cements and concrete, lightweight aggregate and so on (Mumpton, 1978; Passaglia and Galli, 1991).

Even though most early work had assumed zeolite formation in only amygdules in igneous rocks, today the natural zeolite reserves are in fact numerous as major constituents of Cenozoic sedimentary rocks of volcanic origin all over the world. Approximately 3-3.5 million tons of zeolites in tuff are currently mined each year worldwide as an important industrial mineral (Virta, 2002). According to the United States Geological Survey minerals Yearbook in 2008, the estimated production countries are; Turkey 100,000 ton, Japan 150,000 ton, the United States 60,000 ton, Hungary 30,000 ton, New Zealand 17,000 ton, Greek 5,000 ton, Bulgaria 15,000 ton, China 2.5 million ton, Jordan 400,000 ton, the Republic of Korea 160,000 ton, Slovakia 60,000 ton, Indonesia 40,000 ton, Cuba 16,500 ton, Italy 10,000 ton, Mexico 700 ton, Canada 5,000 ton and South Africa 15,000 ton (USGS, 2008; Gottardi and Galli, 1985; Mumpton, 1978). Although zeolitic tuffs are widely distributed and billion-ton deposits are estimated in many countries worldwide, the information is limited on the production of zeolitic tuffs as blending cement. Nevertheless, a rough estimate of the worldwide zeolitic tuff utilization in the cement industry is at least about 2×10^6 tons per year (Colella et al., 2001).

Turkey has very high reserves of sedimentary zeolite deposit especially in central and western Anatolia regions. The important and well-known deposits of clinoptilolite, one of the most common zeolite in Turkey, are found in Gördes (Manisa) and Bigadiç (Balıkesir) regions with approximately 20 million tons and 500 million tons of apparent reserves, respectively (DPT, 1996). There are some quarries producing a wide range of natural zeolite products in the Gördes region. Among them, the biggest one is Rota Mining which exports its products to more than 45 countries all over the world. No detail studies have been governed for the other regions, but it has been estimated that approximately 50 billion tons zeolite reserves (clinoptilolite, analcime, chabasite and erionite) are available in Şaphane (Kütahya), Urla (İzmir), Emet-Yukarı Yoncağağaç, Gediz-Hisarçık and Amasya-Doğantepe (DPT, 1996). Even though zeolitic tuffs are widely distributed and billion-ton deposits are estimated in Turkey, the production is limited. Only the occurrences of clinoptilolite is mined and processed for water purification, soil amendment, animal feed additive, fertilizer additive, agricultural and animal litter purposes in Turkey and they are exported to some companies in United States, Europe and Israel (Özaydın et al., 2006).

2.3 Pozzolans and Pozzolanic Reaction of Zeolites

ASTM C618 defined that pozzolans are siliceous and aluminous materials, which in themselves possess little or no cementitious property, but they are able to combine with calcium hydroxide ($\text{Ca}(\text{OH})_2$) at ordinary temperatures and in the presence of water to form new reaction compounds possessing binding character. There are several types of natural and artificial

pozzolans (Figure 2.1). Natural pozzolans do not require any processes in addition to grinding. Artificial pozzolans, on the other hand, results from chemical/structural modifications of original material as well as residue of certain product (Massazza, 1998). Nevertheless, the separation between natural and artificial pozzolans is not certain. For instance, some rhyolitic tuff includes not only volcanic glass but also contain considerable amount of clay minerals which can possess cementitious properties only by firing (Massazza, 1998). Some natural pozzolans are one of the oldest construction materials. Santorin earth, glassy rhyolite, zeolitic tuffs, clays, diatomaceous earth and gaize are given as examples. Fly ash, silica fume, ground blast-furnace slag, burned clay and shale, microsilica and burned rice hask are examples of artificial pozzolans.

The capability of material to react easily with lime in the presence of water is named as pozzolanic activity. Quality and quantity of active phases in pozzolanic material determine the maximum amount of lime combined. As well as the nature and amount of active phases, the amount of combined lime depends on their silica-alumina content, the ratio of lime/pozzolan, length of curing, specific surface area, water/solid mix ratio and temperature (Massazza, 1998).

Zeolites are regarded as materials which demonstrate excellent pozzolanic reactivity. The process of pozzolanic activity of zeolites is not simple and is influenced by a number of factors at the same time: surface area, particle-size, Si/Al ratio, CEC capacity, mineralogy, chemistry etc. Simply, when lime and zeolitic material are added into water, this results in a rapid hydration process included spontaneous release of alkali-earth cations and (AlOH_4^-) from the zeolite channels into the pore solution, resulting an unstable zeolite structure (Zhang et al., 1995). At the same time, $\text{Ca}(\text{OH})_2$ starts to dissolve as Ca^{2+} and OH^- ions and the solution achieves a high pH value and Ca^{2+} goes from pore solution into the zeolite structure (Caputo et al., 2008). While the chemical reactions between Ca^{2+} and (AlOH_4^-) to form hydrated calcium aluminate (CAH), electrical neutrality of unstable zeolite is maintained by replacement of O^- by OH^- resulting dissolve and/or breakdown of zeolite structure in a high pH solution (Perraki et al., 2003; Caputo et al., 2008) and release of silica ($\text{Si}(\text{OH})_4$) because of the weak Si-OH-Si bonds in zeolite structure (Zhang et al., 1995). Simultaneously, the reaction of $\text{Si}(\text{OH})_4$ with Ca^{2+} forms hydrated calcium silicates (CSH) formed on the surface of zeolites. If the rate of formation of CSH is higher than that of dissolution of $\text{Si}(\text{OH})_4$, CSH gel phase is formed directly on the surface of zeolite crystals (Draj et al., 1978; Urhan, 1987) and dissolution stops (Urhan, 1987; Fraay et al., 1989). Otherwise dissolution continues. During the pozzolanic reaction, alkalinity of solution increases while Ca^{2+} concentration decreases (Caputo et al., 2008; Perraki et al., 2003). The pozzolanic reactivity of zeolites is strongly related with their chemical composition, ability of ion-exchange and the structure comprised a large number of cavities which offers large internal and external surface area (Caputo et al., 2008; Perraki et al., 2003; Massazza, 1998).

The use of pozzolans is of increasing interest because their substitution reduces CO_2 emission and they provide low energy requirement during production. They also have technical advantages on the physical properties of the resulting concrete (Malhotra and Mehta, 1996; Sersale, 1992). Pozzolans are known to reduce the amount and rate of heat of hydration and

thermal expansion (Mehta, 1987; Sersale and Frigione, 1983; Collepardi et al., 1978), improve the durability (Cook, 1986), high ultimate strength, give way to easier workability (Sersale and Frigione, 1983), minimize the risk of alkali-silica reaction (Janotka and Krajci, 2003) and improve resistance to chemical attack (Sersale and Frigione, 1983; Janotka and Krajci, 2003). On the other hand, since the pozzolanic reaction progresses slowly, the strength of mortars takes place gradually over long periods of time (Mielenz, 1950; Collepardi et al., 1978) and zeolite-blended cements require more water owing to large specific surface area (Fragoulis, 1997).

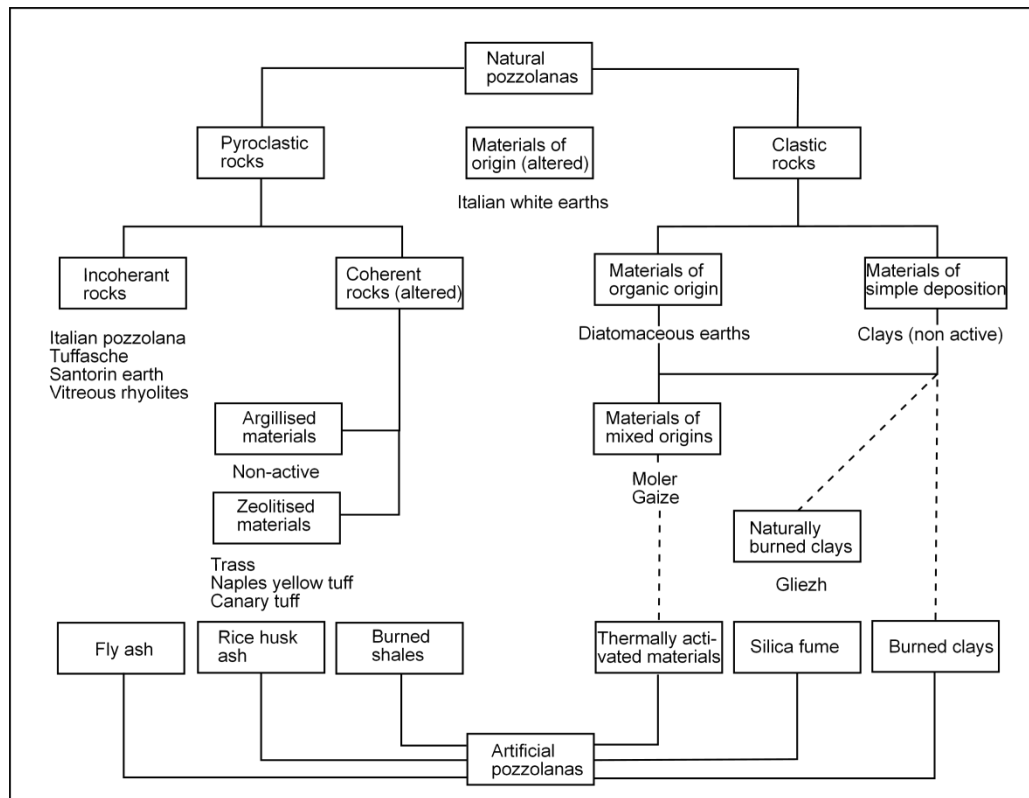


Figure 2.1 Classification of pozzolanas (Massazza, 1998).

2.4 Literature Review

Several researchers have examined the pozzolanic activity and the usage of natural zeolites as SCMs.

Drzaj et al. (1978) studied mechanism and kinetics of zeolitic tuff (analcime, clinoptilolite, heulandites) - lime system on pozzolanic reaction at increased temperature by XRD and SEM. They defined that zeolitic tuff-CaO reactions produce a series of diffusion controlled

topochemical reactions, where a layer of unstable CSH gel phase is formed on the surface of starting zeolite and the final product (tobermorite) is the results of heterogeneous nucleation on the solid-liquid interface.

Sersale (1992) studied zeolite tuff from Italian deposits as a manufacture of blended cements. He reported that adding zeolitic tuff in Portland cement clinker in order to product blended cement has many advantageous e.g. increased compressive strength, increased minimization of expansion due to alkali-silica reaction and greater durability. In addition, they suggested using the superplasticizer since zeolitic tuffs generate decrease in workability when compared with pozzolan, which includes volcanic glass.

Fragoulis et al. (1997) reported the strength performances of Milos pozzolana and tuffaceous rocks transformed to mordenite and clinoptilolite tuffs blended with Portland cement at various replacement levels. They reported that the compressive strength of mordenite cement is higher than clinoptilolite cement and Milos pozzolana. The higher zeolite and reactive silica content of mordenite tuff was concluded as a possible explanation for higher strength. It was also pointed out that zeolite-rich tuffs need more water to produce cement pastes at the same consistency. They concluded that cement blended with mordenite-rich and clinoptilolite-rich tuffs is promising. In order to use zeolitic tuffs for concrete, superplasticizer must be added to control workability of the mixture.

Poon et al. (1999) investigated that the hydration rate of natural zeolite blended cement pastes with respect to fly ash and silica fume. They observed that natural zeolite is a pozzolanic material and the degree of pozzolanity examined for natural zeolite is lower than silica fume and higher than fly ash. They also noticed that blended cement pastes with lower water to cementitious ratio undergo increased strength results of the pastes. Furthermore, it was stated that replacement of 15% of zeolite resulted in lower porosity, but higher replacement level (25%) increases the porosity at all the studied ages.

Ortega et al. (2000) studied the properties of alkali-activated clinoptilolite hydrated with calcium hydroxide and compared them with other alkali activated waste-derived and naturally occurring pozzolana. They concluded that when particle size, curing conditions and the amount of Ca(OH)_2 content were optimized, hydrated products contain compacted materials comprising 20% Ca(OH)_2 with average compressive strength of 38.7 MPa. He also stated that physical properties are connected with sample preparation methods, clinoptilolite particle size, curing conditions and amount of alkali addition. XRD analysis proved that portlandite was consumed during hydration and it was finished in fully cured materials.

Türkmenoğlu and Tankut (2002) studied tuffs from central Turkey as admixture in blended cements. They stated that alkali content of tuffs display variation content and seem to relate inversely with compressive strength of mortar specimens. They also concluded that petrographical analysis is fast and easily accessible technique in order to determine

petrographical characteristics, that may have important control on mechanical behavior of material.

Perraki et al. (2003) investigated that the effect of natural zeolites, which is characterized as “heulandites type II”, on the early hydration and hydrated product. They concluded that natural zeolite displays a good pozzolanic reactivity. Furthermore, they reported that the incorporation of natural zeolite in Portland cement contributes to the consumption of lime and generation of hydrated cement products. But, an increase of zeolite replacement in cement did not promote the lime consumption.

Canpolat et al. (2004) studied the use of natural zeolite, fly ash and coal bottom ash as replacement pozzolan in cement production. They determined volume expansion, setting time, compressive strength and water demand of the mortars. They put forward that the replacement of zeolite up to 15% brings about an increase in mechanical strength at early ages. But, combination of zeolite and fly ash resulted in a decrease in compressive strength.

Martinez-Ramirez et al. (2006) analyzed pozzolanic reactivity of zeolitic rocks with calcium hydroxide. They also characterize the hydrated products produced as well as determine the relationship between composition and structure of pozzolan on capacity to lime fixation. They stated that pozzolanic activity of zeolitic tuffs resulted in CSH formation. But, the formation of calcium aluminate hydrate was not observed.

Yılmaz et al. (2007) reported the chemical, mechanical and microstructural properties of clinoptilolite blended cements. They also determined the ion exchange capacity of zeolite depending on the calcium hydroxide ($\text{Ca}(\text{OH})_2$) level in the solution. They concluded that clinoptilolite can be used as pozzolanic cement because of reactive SiO_2 content and ion exchange capacity. Water demand of zeolite blended cement increases since structure of zeolite contains micropores.

Caputo et al. (2008) investigated the effect of zeolite structure on pozzolanic activity. They used blended cements mixed with artificial zeolites (zeolite A and zeolite X) and ordinary Portland clinker. They determined that both zeolites are effective as pozzolanic materials. They introduced the reaction steps of pozzolanic activity, including a) cation exchange, b) decomposition of zeolitic structure c) formation of gel phase d) and finally precipitation of hydrated calcium aluminates and silicates. The pozzolanic activity was depended on zeolite structure. Although zeolite A reacts more than zeolite X, the latter, being slightly more siliceous one, generates greater mechanical resistance at short curing times.

Mertens et al. (2009) studied pozzolanic reactions of natural zeolites with portlandite and parameters affecting the reactivity. They concluded that surface area only influences initial stage of hydration, whereas the cation content has an affect on both early and later stages and Si/Al

ratio has powerful effect on long term reactivity. They also stated that silica rich zeolites react faster than aluminum rich counterparts.

Uzal et al. (2010) compared pozzolanic activity of clinoptilolite with silica fume, fly ash and non-zeolitic natural pozzolan. After complete characterization of the materials, they were evaluated pozzolanic reactivity of materials with various test methods including free lime content, electrical conductivity, compressive strength and pore size distribution of hardened pastes. They reported that the reactivity of clinoptilolite was comparable to silica fume and was higher than non-zeolitic pozzolan and fly ash. Reactive silica content and specific surface area is accepted as the reason of the high reactivity. Poor strength of clinoptilolite in spite of high lime consuming is attributed to large pore size distribution.

Uzal and Turanlı (2012) recently investigated blended cements comprising high volume of natural zeolites. They reported properties and hydration characteristics of blended cement composed of 55% by weight clinoptilolite rich tuff. For this, free lime content, hydration products and decomposition of crystal structure of clinoptilolite were examined. In addition, pore size distribution and microstructure of hardened cement were determined. They concluded that lime was totally consumed and complete decomposition of clinoptilolite crystal structure at the end of 28 days of hydration. They determined presence of tetra calcium aluminate hydrate as a hydration product of pozzolanic activity and similar strength results with control Portland cement. They also suggested the usage of melamine-based superplasticizer rather than naphthalene based one.

CHAPTER 3

GEOLOGY OF THE STUDY AREA

3.1 Field work

Field work was done at the summer period of 2011. Representative five samples, up to 5 kg were taken, from each tuff from the outcrops. Clinoptilolite-rich tuffs marked as CLI-G are from Gördes (Manisa), CLI-A from Aliğa (İzmir) and CLI-B from Bigadiç (Balıkesir), mordenite-bearing tuff marked as MOR is from Foça (İzmir) and analcime-bearing tuff marked as ANA is from Ayvacık (Çanakkale) region (Figure 3.1).

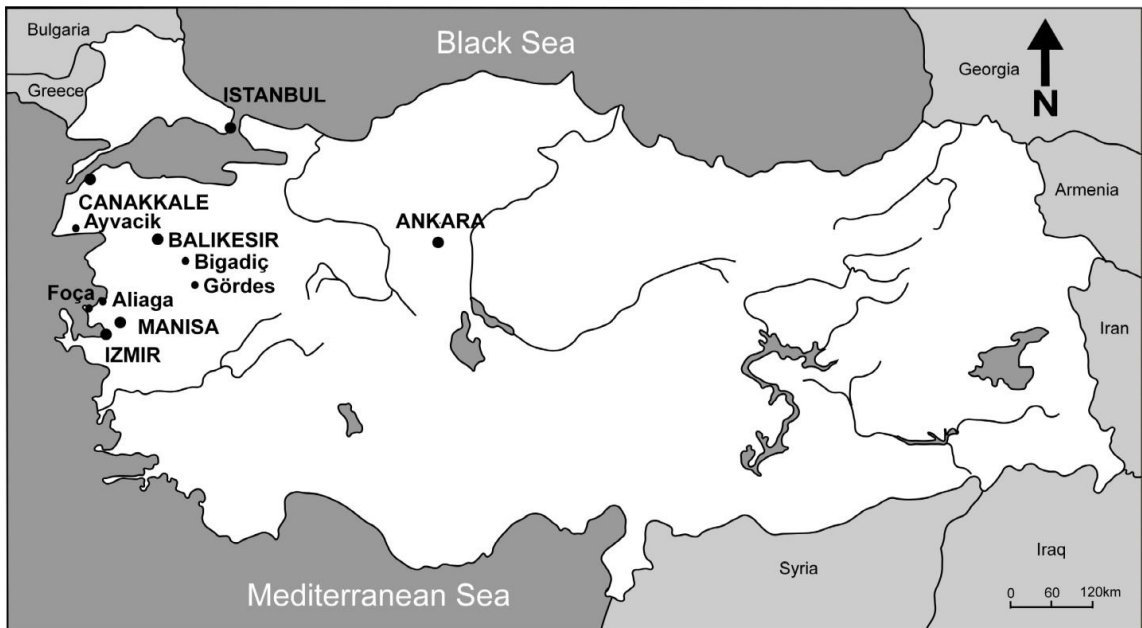


Figure 3.1 Location map of the study area.

3.2 Geology of Gördes Region

Gördes zeolitic tuffs are located in the Neogene Gördes Basin in Western Anatolia. The Neogene continental sedimentary succession in this basin is 2000 m thick and divided into lower Miocene Gördes Group and upper Miocene Kavakalan Group (Göktaş, 1996; Ercan et al., 1978). In the sampled area, Gördes Group is represented by the Kurtköyü and Yeniköy formations,

Gökyar tuff (Göktaş, 1996; Yağmurlu, 1983; Yılmaz, 1977; Esenli, 1992) and the Tekkedere formation (Göktaş, 1996) in ascending order (Figure 3.2). The Menderes Massif metamorphics constitute the basement rocks in this region and consist mainly of gneiss, migmatite, micaschist and quartzite. It is unconformably overlain by alluvial fan deposits of Kurtköyü formation marked by its red color. Kurtköyü formation, made up of muddy flow levels interbedded with conglomerates is Lower Miocene in age and unconformably overlain by 800 m thick lacustrine sediments of the Yeniköy formation. Lower Miocene calc-alkaline volcanism, which is transitional with the volcano-sedimentary facies consist of agglomerate, tuff and lavas. Rhyolitic Gökyar tuff is homogeneous, generally white and occasionally light gray in color and widely distributed in the study area. Sample (CLI-G) was collected from Gökyar tuff (Figure 3.3). It reaches 250 m thickness in northeast of Gördes. It is generally classified as vitric tuff, but crystal tuff and lithic-crystal tuff is also determined. Gökyar tuff is deposited from subaerial to subaqueous environmental conditions. Extensive zeolitization has taken place in Gökyar tuff as a result of diagenetic alteration (Göktaş, 1996; Esenli and Özpeker, 1993; Albayrak, 2008; Albayrak, 2010).

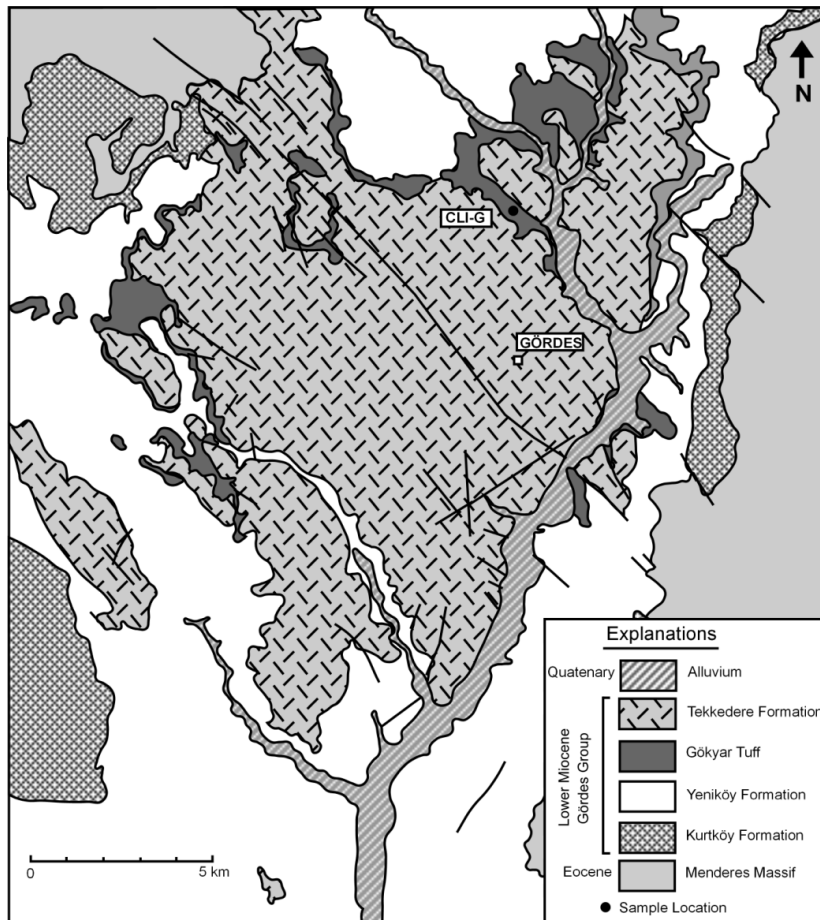


Figure 3.2 Simplified geologic map of Gördes region with sample location (after Göktaş, 1996).

Tekkedere formation conformable overlies the Gökyar tuff and is made up of shale, mudstone and limestone alternating with tuffs, which also include zeolites (Esenli and Özpeker, 1994; Albayrak, 2008). Quaternary alluvial sediments overlay all other units (Göktaş, 1996).



Figure 3.3 Photograph illustrating massive Gökyar tuff, which is fine-grained, compact and white in color.

3.3 Geology of Aliğa Region

The Aliğa area, which is composed of shallow lacustrine volcano-sedimentary rocks is located in north of Aliaga, Izmir. It is bounded to the east by Çaltılıdere Village, to the west by the Gulf of Çandarlı. Middle Miocene basement rocks within the study area are made up of subaqueous uppermost part of Yuntdağ Volcanics, which consists of grey laminated tuff and shale interlayers. They are gradually overlain by Foça rhyolites including two different volcanic successions in the area (Figure 3.4). The first basal section occurs around and west of Sarıkaya Hill and consists of massive volcanoclastics alternating with thin bedded tuffs and local small rhyolitic intrusions. These intrusions are covered by hyaloclastic breccias and perlites in the northern and western parts of the Sarıkaya Hill. The second phase of Foça rhyolitic volcanism consist of pyroclastic flows and base surge deposits at north of Kalabasar Hill (Akay and Erdoğan, 2004). These pyroclastic flow deposits are covered by rhyolitic ash fall deposits laterally passing into authigenically altered subaqueous zeolitic tuff unit, Foça tuff, (Kaya and Savaşçın, 1981) and the overlying smectitic tuff level. The studied sample was collected from

Foça tuff (Figure 3.5). The tuffs are overlain by gastropoda-bearing lacustrine Aliğa limestone. The youngest magmatic phase in the region is named as the Bozdevlit Dağ Volcanics. Sporadically extruded brownish-black andesitic basalts of this unit discordantly cover the Aliğa limestone (Albayrak and Özgüner, 2013).

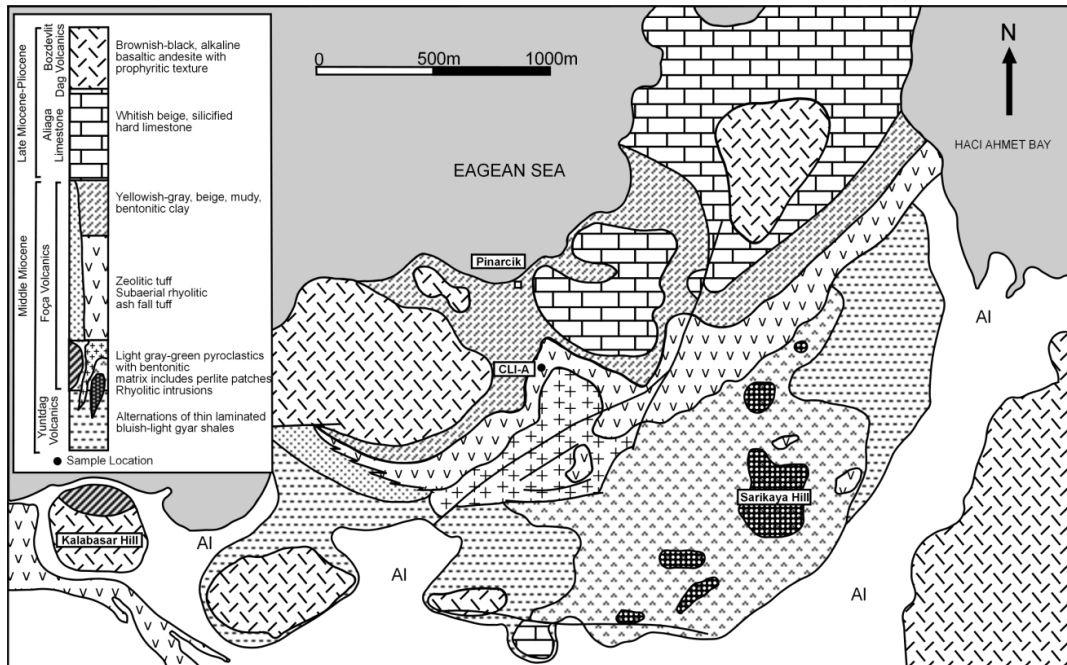


Figure 3.4 Simplified geologic map of Aliğa region with sample location (after Albayrak and Özgüner, 2013).



Figure 3.5 A view from Foça Tuff, which is soft, homogeneous and white in color.

3.4 Geology of Bigadiç Region

Bigadiç volcano-sedimentary succession consists of basaltic to rhyolitic lavas and volcanoclastic rocks intercalated with borate-bearing lacustrine units (Helvacı and Alaca, 1991). The stratigraphic unit cropping out around İskele-Beğendikler-Çamköy villages starts with Lower Miocene Dedetepe formation (Figure 3.6). It comprises rhyolite, dacite, tuff and agglomerate (Ulusoy and Albayrak, 2009). The following quite hard and irregular Middle Miocene Çandağ basalt including basalt, trachy-basalt, agglomerate and tuffs is unconformably overlain by Bigadiç formation comprising from bottom to top five members; Güvemçetmi limestone, Akçakertil tuffite, Yeniköy limestone, Beğendikler tuff and İskele limestone member, (Ercan et al., 1984; Ercan et al., 1984b). Dacitic, rhyodacitic Akçakertil tuffite conformably overlies the Güvemçetmi limestone.

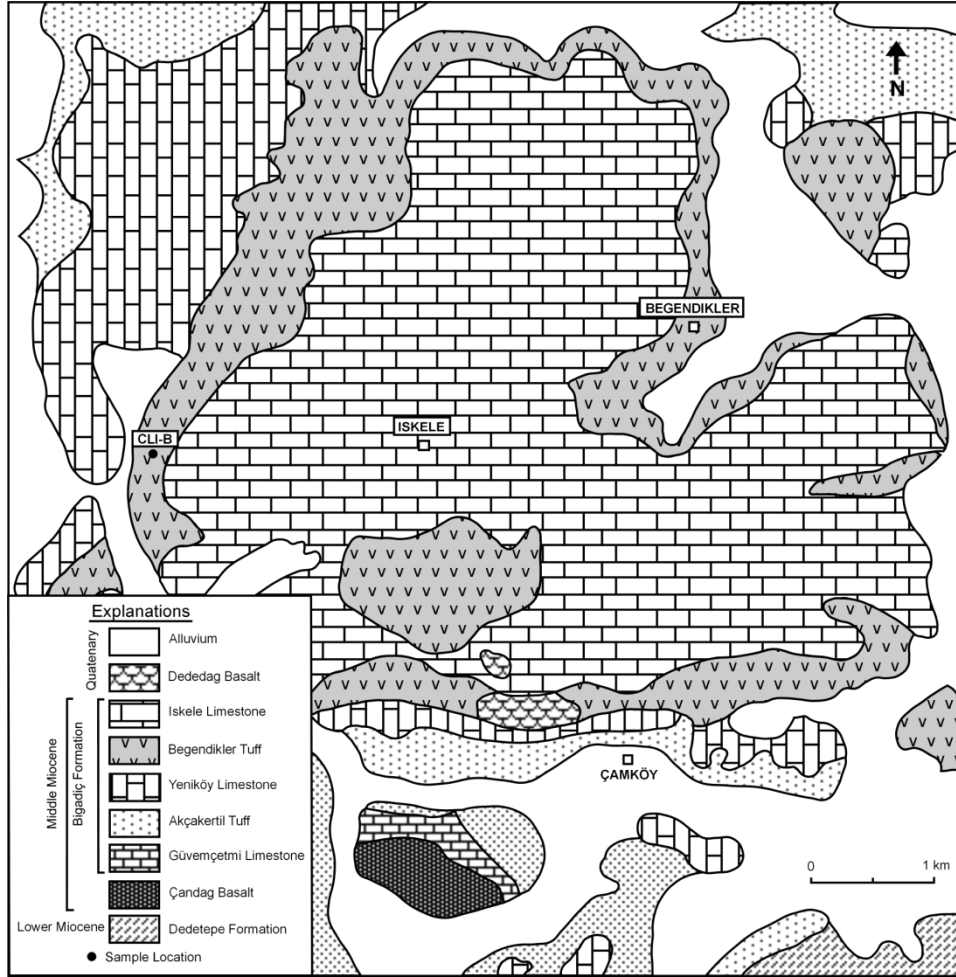


Figure 3.6 Simplified geologic map of Bigadiç region with sample location (after Ercan et al., 1984b).

Ataman (1977) observed the clinoptilolite formation in the light gray, white yellowish tuff of Akçakertil tuffite member. Borate bearing Yeniköy limestone consists of limestone, marl, sandstone and siltstone alternations. Beğendikler tuffite member is formed by deposition of rhyolitic tuffs in a lacustrine environment and they also include clinoptilolite. The studied sample was collected from Beğendikler tuff (Figure 3.7). The youngest member, İskele limestone, is very rich in borate. Quaternary alluvium in the study area is represented by loose material of pebble, sand and clay (Ercan et al., 1984b).



Figure 3.7 Photograph shows Beğendikler Tuff, which is light green, very hard and homogeneous.

3.5 Geology of Foça Region

In this area, widespread Middle Miocene volcano-sedimentary succession outcrop. Yuntdağ volcanic sequence (Akyürek and Soysal, 1978; Kaya and Savaşçın, 1981) is represented by calc-alkaline red-gray andesites, which consist of massive andesitic/trachyandesitic lava flows and interbedded pyroclastic flow deposit is the lowermost part of the unit. It is overlain by the Foça volcanics comprising dominantly of rhyolitic pyroclastic sequences associated with small rhyolitic domes, dykes and lava flows (Akay and Erdogan, 2004). The pyroclastics cropping around Foça were named as the Foça Tuff (Figure 3.8), which is up to 400 m thick (Kaya and Savaşçın, 1981). The studied sample was collected from Foça Tuff (Figure 3.9). The white to yellow, well-bedded Aliğa limestone is transitional with these two units in different stratigraphic levels. Quaternary alluvium, showing alternations of different block, gravel, sand, silt, clay sediments forms the uppermost unit (Lengeranlı et al., 1998).

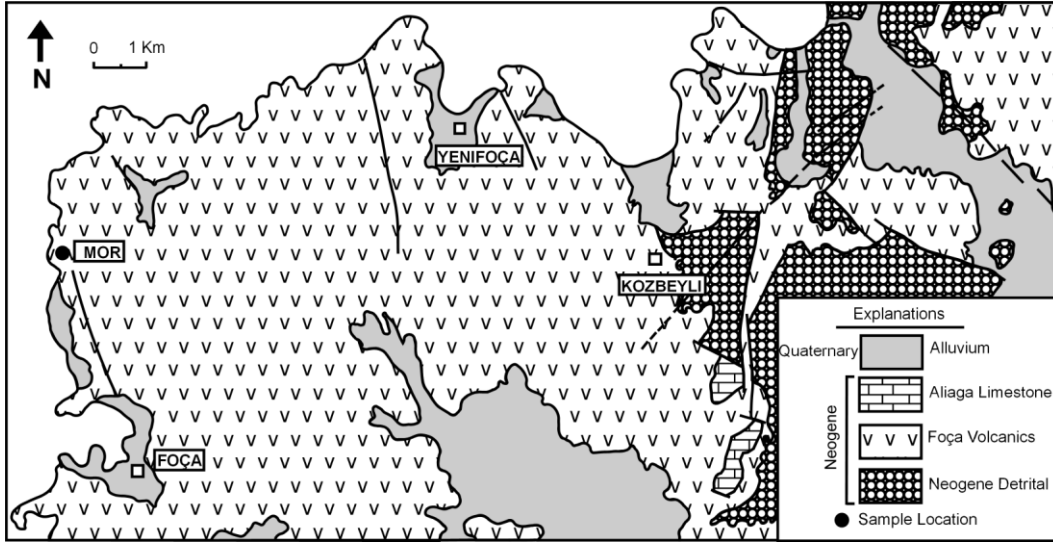


Figure 3.8 Simplified geologic map of Foça region with sample location (after Lengeranlı et al., 1998).



Figure 3.9 Photograph illustrating Foça Tuff, which is whitish yellow in color and very hard.

3.6 Geology of Küçükkuşu Region

The study area comprises four main rock units; the ophiolitic basement rocks, volcanics, lacustrine sediments and alluvium. The Çetmi Ophiolitic Melange forms the basement (Göncüođlu et al., 1997). It is disconformably overlain by Lower-Middle Miocene calc-alkaline volcanic rocks (Behram Volcanics) and detrital sediments (Borsi et al., 1972; Ercan et al., 1995). Behram Volcanics are made up of andesite, andesitic agglomerate and tuff (Figure 3.10). Early Miocene Küçükkuşu Formation represented by turbiditic lacustrine sediments includes an alternating sequence of conglomerate, sandstone, claystone, mudstone and shale (İnci, 1984).

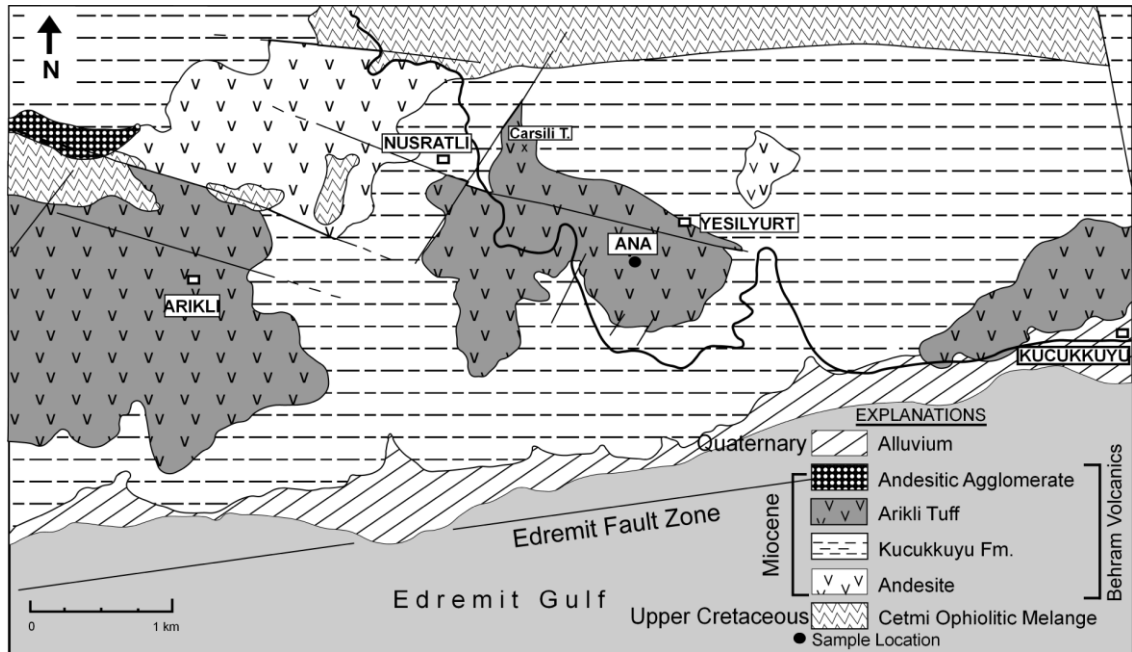


Figure 3.10 Simplified geologic map of Foça region with sample location (after Çelik et al., 1999).

The dacitic-rhyolitic Arıklı Tuff (Figure 3.10) within the tuffs of the Behram Volcanics represents the main pyroclastic products of the volcanic activity. The massive and bedded tuffs are white, light green, yellow, and light yellow in color. The studied sample was collected from Arıklı Tuff (Figure 3.11). The analcime formation in this unit was evaluated by Özen and Göncüođlu (2012). The age of Arıklı Tuff is Early-Middle Miocene (Çelik et al., 1999). Quaternary alluvium comprises of loose material of pebble, sand and clay.



Figure 3.11 Photograph showing Arikki tuff, which is homogenous and yellow in color.

CHAPTER 4

EXPERIMENTAL STUDY

4.1 Introduction

The experimental study is carried out in three main stages. The first stage consists of complete characterization of the zeolitic tuffs. In the second part of the research, experimental methods are used to evaluate the pozzolanic activity of materials. The examination of hydration products are described at the third stage of the study.

4.2 Material

This chapter provides information on the materials used to produce pastes and mortars for subsequent methods. For all blended specimens in this study, the materials used are lime, Portland cement, aggregate and natural zeolitic tuff.

4.2.1 Lime

Reagent grade $\text{Ca}(\text{OH})_2$ is used to prepare lime-zeolitic tuff pastes in thermogravimetric (TG), X-ray diffraction (XRD) and Fourier transform infrared spectroscopy (FTIR) analysis.

4.2.2 Portland Cement

Ordinary Portland cement (CEM I 42.5 R) was used in Fratini's test and mortars for compressive strength analysis in this study. The physical properties and chemical composition of ordinary Portland cement are given in Table 4.1. Particle size distribution was determined using a Malvern Mastersizer 2000 Laser Particle Size Analyser in Central Laboratory, Middle East Technical University, Turkey and shown in Figure 4.1.

Table 4.1 Physical properties and chemical composition of Portland cement

Chemical Composition	
SiO ₂ ,%	19.18
Al ₂ O ₃ ,%	5.04
Fe ₂ O ₃ ,%	3.05
CaO,%	62.89
MgO,%	2.12
SO ₃ ,%	2.62
Na ₂ O,%	0.26
K ₂ O,%	0.69
Loss on ignition, %	3.45
Physical Properties	
Specific Gravity	3.15
Blaine fineness, m ² /kg	385
Compressive strength, MPa	
	7 days 41.5
	28 days 52.9

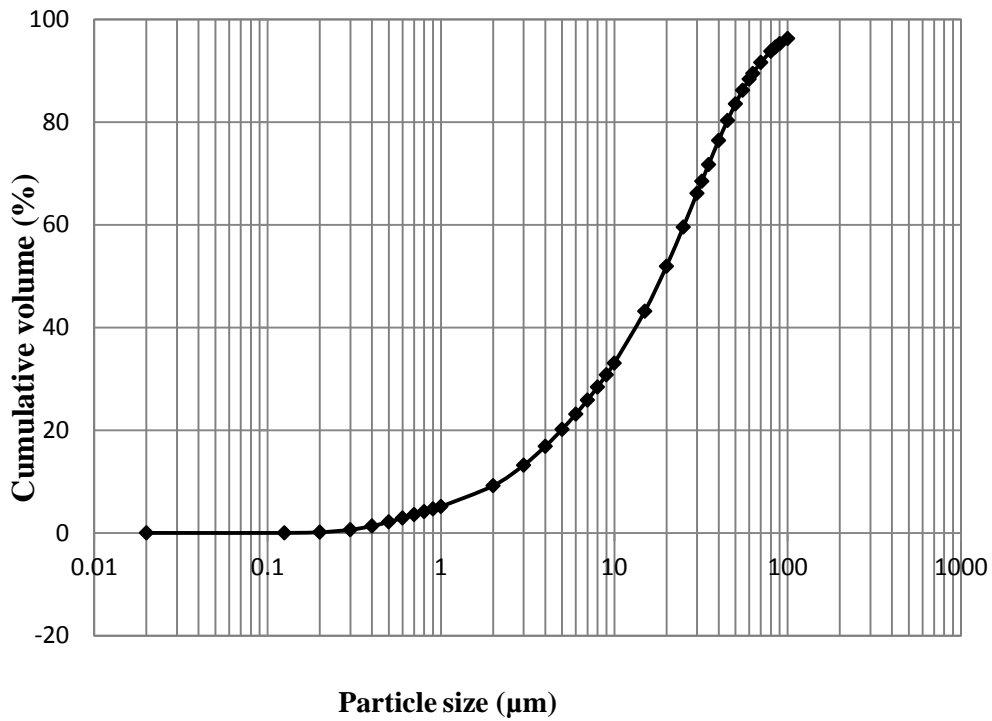


Figure 4.1 Particle size distribution of ordinary Portland cement.

4.2.3 Aggregate

The physical properties of the aggregate used in this study, CEN standard sand (EN 196-1), are given in Table 4.2 and particle size distributions is given in Table 4.3.

Table 4.2 Physical properties of aggregate used in this study (*OD: Oven Dry, SSD: Saturated Surface Dry).

Aggregate type	Specific Gravity			Water Absorption (%)
	OD*	SSD*	Apparent	
CEN Standard Sand	2.56	2.52	2.54	0.68

Table 4.3 Particle size distributions of aggregate

Sieve size		Cumulative passing (%)
Inch	mm	CEN Standard Sand
3/8	9.5	100
No. 4	4.76	99.73
No.8	2.38	88.73
No.16	1.19	66.02
No.30	0.59	38.07
No.50	0.297	15.1
No.100	0.149	5.1
Passing No.100		0

4.2.4 Zeolitic Tuffs

In this study, different kind of zeolitic tuffs, acquired from the major deposits in the western Turkey were investigated for the evaluation of pozzolanic activity.

4.2.4.1 Physical Characterization of Zeolitic Tuffs

Representative amount of zeolitic tuff samples were crushed with a hammer to small pieces, which is then used to grind to a fine powder by MG171 Automatic Swing Mill, using Cr-steel set of rings. The samples are run through 90 μm after dry sieving and approximately 80% passing through 45 μm sieve after wet sieving. The grain size distribution of the tuffs was determined using a Malvern Mastersizer 2000 laser particle size analyser in Central Laboratory, Middle East Technical University, Turkey. Surface area was obtained by BET method (Brunauer et al., 1938) using a Micromeritics Gemini 2360 apparatus after activation under vacuum at 150 $^{\circ}\text{C}$ for 5 h in Department of Material and Production Engineering, Universita Degli Studi di Napoli Federico II, Italy. Blaine surface area was determined according to ASTM C 204 standard method in chemistry laboratory of Civil Engineering Department, Middle East Technical University, Turkey.

4.2.4.2 Chemical Characterization of Zeolitic Tuffs

4.2.4.2.1 Chemical Analyses of Zeolitic Tuffs

A microwave digestion system is used to determine the chemical composition of tuff samples. The standard solution is prepared by using an acid mixture of 1 ml of HNO_3 , 4 ml of HF and 1 ml of HCl. After addition of H_3BO_3 (24 ml) to mask free fluoride ions and re-dissolve fluoride precipitates, the solution is subsequently analyzed by inductively coupled plasma-atomic emission spectroscopy (ICP-OES) by Perkin Elmer Multiwave 3000 in Department of Material and Production Engineering, Universita Degli Studi di Napoli Federico II, Italy. Loss on ignition (LOI) was measured by thermogravimetric analysis (Netzsch STA409 PCLuxx apparatus; alumina crucibles; N_2 gas flow; heating rate: $10^{\circ}\text{C}/\text{min}$) in Department of Material and Production Engineering, Universita Degli Studi di Napoli Federico II, Italy.

4.2.4.2.2 Quantitative Electron Microprobe Analyses of Zeolites

Electron microscopy (EM) technique has an important role in many ways (e.g. image, analyze) in characterization of materials, which cannot be observed with optical microscopy. In this study, the most commonly used electron microscope techniques namely electron microprobe (EMPA) and scanning electron microscope (SEM), which provide valuable information related to morphology, texture and composition of materials, were used. Although both instruments have the same basic principle of operations, the EMPA is primarily used for quantitative chemical analysis. SEM, on the other hand, is mainly used for three dimensional imaging. The next paragraph introduces basic principles of electron microscope technique.

In the Electron Microscope (EM), a beam of high energy electrons is produced from an electron gun. An accelerated and finely focused primary electron beam obtained from a tungsten wire passes through pairs of electromagnetic fields and lenses in the electron column and bombards the surface of the solid sample resulting in a number of different waves (back-scattered electrons, cathodoluminescence, secondary electrons, x-rays, Auger electron etc.) being emitted (Figure 4.2). In this manner, it is obtained information about the sample's structure, morphology and chemical composition. The secondary electrons are used for morphology while x-rays provide chemical information (Goldstein et al., 1981).

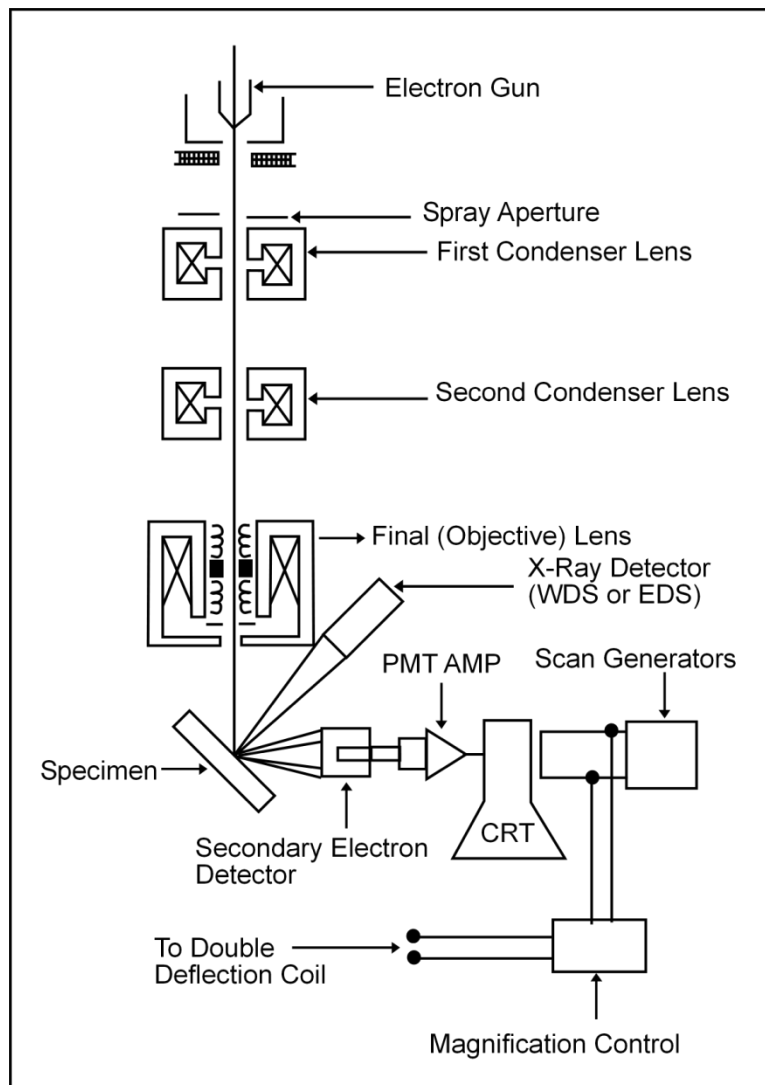


Figure 4.2 The design of standard electron and x-ray optics of a combined SEM-EMPA
 (Figure taken from http://serc.carleton.edu/research_education/geochemsheets/techniques/SEM.html)

Electron microprobe (EMPA) analysis is a useful tool to determine the quantitative chemical analysis of very small inorganic solid materials. An accelerated and finely focused electron beam bombards the polished sample resulting in the atoms of individual elements excited to higher energy states. As they gain their initial lower energy states, x-rays are emitted which are detected at particular wavelength. The amounts obtained from individual elements are compared those for the same element of a known composition in order to determine the amount of each element in quantitatively (Wittry, 1958).

Quantitative chemical compositions of zeolites were analysed using a Jeol JXA-8200 electron microprobe in wavelength dispersive mode (EPMA-WDS) in Department of Earth Sciences, Università degli Studi di Milano. In order to reduce the crystal dehydration due to the electron bombardment, the system was operated using a defocused electron beam (diameter: 5 -10 nm), an accelerating voltage of 15 kV, a beam current of 10 nA measured by a Faraday cup and counting times of 20s on the peaks and 5s on the backgrounds. Natural crystals of K-feldspar (for Si, K, Al), ilmenite (for Ti), forsterite (for Mg), fayalite (for Fe), wollastonite (for Ca), barite (for Ba), celestite (for Sr), omphacite (for Na), were used as standards. The results were corrected for matrix effects using a conventional ZAF routine in the Jeol suite of programs. The crushed clinoptilolite-rich, mordenite and analcime-bearing tuff samples were polished and mounted in a resin for accurate quantitative analysis.

4.2.4.2.3 Evaluation of Cation Exchange Capacity (CEC) of Zeolitic Tuffs

The Cation Exchange Capacity (CEC) which is an important characterization parameter of zeolites is the measure of the quantity of exchangeable cations in mili-equivalent per grams. The total CEC comes from the existence of loosely bound cations (Na^+ , K^+ , Ca^{2+} and Mg^{2+}) in the structure of zeolites.

Two methods have been recommended to characterize the cation exchange capacity (CEC) of zeolites. These are the batch exchange method (BEM) and the cross exchange method (CEM) (Cerri et al., 2002; Semmens, 1984). Even though the CEM method was found to be successful to determine CEC of the chabazite and phillipsite-bearing tuff (Colella et al., 2002), Cerri et al. (2002) showed that the CEM gave unreliable results for determining the CEC of the clinoptilolite-bearing tuff. BEM, however, was proposed to be the most reliable method in the determination of clinoptilolite-bearing material (Cerri et al. 2002).

In the present study, the cross exchange method (CEM) was used to measure the cation exchange capacity (CEC) of clinoptilolite-rich tuff (CLI-B) and the batch exchange method (BEM) described by Cerri et al. (2002) was used to measure the cation exchange capacity (CEC) of zeolitic tuffs (CLI-G, CLI-A, CLI-B, MOR, ANA). For the BEM method NH_4Cl was used as the replacement cation since Cerri et al., (2002) showed that NH_4^+ and Cs^+ resulted in the best CEC through various cations (Na^+ , K^+ , Li^+ , Cs^+ , NH_4^+ , Ca^{2+} , Mg^{2+} , Sr^{2+}). Furthermore, they proved that the particle size has no significant affect on exchange process.

After the analyses, the results of the same sample (CLI-B) are compared with each other and with literature to re-prove that the experimental CEC is dependent on the method used (e.g. Ming et al., 1993; Bottale et al., 1998; Cerri et al., 2002). The exchanged zeolite-rich tuff samples (CLI-B-Na, CLI-B-Ca, CLI-B,K) were washed and filtered after CEM analysis, then left it to air dry, which was used to determine pozzolanic activity of exchanged zeolitic tuffs.

4.2.4.2.3.1 Cross Exchange Method (CEM)

The procedure given as follows was used. For this method, CLI-B is divided into three parts. Saturated solution was made by adding of 0.5 M KNO₃, NaCl and Ca(NO₃)₂ to 1 lt distilled water. 10 ml of saturated solution was stored to measure the concentration of blank. 15 g of clinoptilolite-rich tuff (CLI-B) was placed in a 1000 ml glass beaker. 900 ml of previously prepared saturated solution was added to the beaker. After the beaker was covered with parafilm, it was left by Falc mixer during 10 hours, left overnight (Figure 4.3). 10 ml exchanged solution was stored to measure the concentrations of cations. The exchanged solution was then pumped. Sample was remained on the beaker. The procedure was repeated until the cation concentration of exchanged solution becomes less than 0.1 mg.l⁻¹, adding fresh solutions each time. The Na, K, Ca concentrations of the last exchange cycle was measured by inductively coupled plasma-atomic emission spectroscopy (ICP-OES) as meq/g and the result was used to calculate the CEC value.

4.2.4.2.3.2 Batch Exchange Method (BEM)

The method comprises from weighing 0.5 g tuff samples and then placing in tubes together with 35 ml aliquots of 0.5 M NH₄Cl solution at 60 °C under continuous rotating device. After 2 h, the solution was centrifuged. The clear liquid was disposed and the procedure repeated 10 times. Cations released from zeolites were analyzed by inductively coupled plasma-atomic emission spectroscopy (ICP-OES) and from their concentration the CEC, in meq/g, was estimated.



Figure 4.3 Experimental set-up for cross exchange method (CEM).

4.2.5 Mineralogical/Petrographical Characterization of Zeolitic Tuffs

4.2.5.1 Petrography

The thin sections of zeolitic tuffs were prepared in the thin section preparation laboratory in Department of Earth Sciences, Università degli Studi di Milano, Italy. Five thin sections are examined under a Nikon polarizing microscope in order to identify the mineralogy and to determine the petrographical and textural features of the zeolitic tuffs. After investigation of thin sections, photographs were taken by using image analyzer system attached the Nikon camera in the Geological Engineering Department, Middle East Technical University, Turkey.

4.2.5.2 Quantitative XRD

Rietveld quantitative phase analysis is a powerful method to measure an amount of crystalline and amorphous phases in multiphase components. Although the Rietveld profile refinement method was developed for the refinement of nuclear and magnetic structures from neutron diffraction data, the method can also be applied for X-ray powder diffraction (Rietveld, 1969). The Rietveld refinement method can be used for quantitative measurement since the scale factors of refined minerals are related to the weight percentage of minerals (Hill and Howard, 1987; Bish and Howard, 1988). Basic requirements for the Rietveld refinement method are reasonable starting structural model and accurate diffraction data. In the Rietveld method, the observed pattern must fit to the calculated pattern using the model for crystal structure and diffraction peak profiles. Because only the crystalline phases can be quantified by Rietveld refinement method, known amount of internal standard must be added to calculate the amount of amorphous phases (Chung, 1974). Besides, grain size must be 10 μm or less. For this, wet grinding using the McCrone Micronizing Mill which is the most effective method is recommended in order to prevent the formation of an amorphous layer around the grains (Kosanovic et al., 1993; Buhrke et al., 1998). Further information about quantitative phase analysis using X-ray powder diffraction can be found in Hill and Howard (1987), Bish and Howard (1988), O'Connor and Raven (1988) and Snyder and Bish (1989).

In the present study, mineralogical characterization of zeolitic tuff samples was performed using the Rietveld method with internal standard by means of TOPAS 4.2 software (BRUKER AXS Company). Before the X-ray powder diffraction (XRPD) quantitative measurements, samples with $\alpha\text{-Al}_2\text{O}_3$ internal standard in amount of 20 wt% were wet grinded through a McCrone Micronising Mill in order to obtain powders with grain size $<10\mu\text{m}$. XRPD patterns were then recorded on an automated Philips PW1730/3710 diffractometer equipped with a curved graphite crystal monochromator using $\text{CuK}\alpha$ radiation, 40 kV, 30 mA, 2θ range from 3 to 80°. Step size was 0.02° 2θ with a counting time of 10 sec. Identification of mineral phases was carried out with the Philips APD 3.6 software.

4.2.5.3 Scanning Electron Microscope (SEM) Analyses of Zeolitic Tuffs

Scanning Electron Microscope (SEM) is a powerful method for studying zeolites because of small particle size. Scanning Electron Microscope (SEM) technique has the same basic principles of function with Electron Micro Probe Analysis (EMPA). SEM uses a focused beam electrons scanning across the sample and the secondary electrons are reflected from the surface of solid specimen. Detectors collect the secondary electrons and transform them into a signal. The main goal of the SEM analysis is to generate three dimensional topographic images of the sample with high resolution (Welton, 1984). The SEM analysis is an ideal technique to observe morphology, size and three-dimensional crystal relationships especially for small size zeolites. When the crystal morphology is not enough to identify the unreacted or reacted mineral, energy

dispersive X-ray spectroscopy (EDX) measurements were also performed to qualitative elemental analyses.

Prior the SEM analysis, zeolitic tuff samples were gently broken with a hammer to an appropriate size, and they were coated with a thin layer of gold-platinum to prevent charging. Microstructural investigations were performed using a Quanta 400 F type scanning electron microscope (SEM) analyzer equipped with energy-dispersive X-ray (EDX) system in the Central Laboratory, Middle East Technical University, Turkey.

4.3 Experimental Methods

4.3.1 Evaluation of Pozzolanic Reaction

Two methods have been used for the evaluation of the pozzolanic activity of natural zeolites. Fratini test (Fratini, 1949) is used to identify whether the tuff is able to combine with $\text{Ca}(\text{OH})_2$ at 8 or 15 days of hydration of cement and therefore allows to assess the ability of pozzolanic reaction of materials. On the other hand, thermogravimetric analysis giving the amount of lime combined with pozzolan after several days provides more precise information and quantitative results.

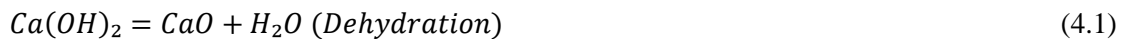
4.3.1.1 Thermogravimetric Analyses of Zeolitic Tuffs

Thermogravimetric analyses (TG) is a technique in which the weight loss of a material is measured as a function of temperature at a constant rate (Mackenzie, 1974). Since one of the purposes of this study is to compare the pozzolanic activity of zeolite bearing tuffs, the progress of the pozzolanic reactivity of the natural zeolites was quantitatively studied by thermogravimetric analysis (TGA). For the preparation of the pastes, zeolitic tuffs was blended with the commercial lime ($\text{Ca}(\text{OH})_2$) in the mixtures of 1:1 lime/pozzolan ratio and 0.5 water/solid ratio. After thoroughly mixing, the pastes were filled into sealed polyethylene containers and then left at room temperature. The pozzolanic reaction products were collected after 3, 7, 28, 56, 90, and 180 days then, they were ground manually in an agate mortar. The hydration process was stopped with acetone. After vacuum filtration (Figure 4.4), the samples were dried at 60 °C for 2 hours. Analyses were performed by Netzsch STA 409 PCLuxx in alumina crucibles in N_2 gas flow with heating rate of 10 °C/min from 25 to 1000 °C.



Figure 4.4 Vacuum filtration setup of hardened paste after washing with acetone.

The total amount of reacted Ca(OH)_2 was calculated by taking the weight loss at the 400-550 °C due to dehydration of Ca(OH)_2 (Shi and Day, 2000; Paya et al., 2003). The chemical reaction occurs as equation 4.1 (Taylor, 1997; Ramachandran, 2001).



Then, the fixed lime was calculated as percent from the difference between the initial and the final weight loss as shown in equation 4.2 (Shi and Day, 2000; Paya et al., 2003).

$$\text{Fixed Lime (\%)} = \frac{\text{CH}_i - \text{CH}_m}{\text{CH}_i} \times 100 \quad (4.2)$$

The CH_i is the initial amount of Ca(OH)_2 , which was estimated from the original lime used in the pastes and CH_m is the amount of measured Ca(OH)_2 in the zeolitic tuff paste for a particular day (Shi and Day, 2000; Paya et al., 2003).

4.3.1.2 Thermogravimetric Analyses of Exchanged Zeolitic Tuff

In order to understand the chemical influence on the pozzolanic reactivity, a study was performed aiming to compare the pozzolanic activity of clinoptilolite-rich tuff (CLI-B) exchanged with Na^+ , K^+ and Ca^{2+} cations using a cross exchange method (CEM) (Cerri et al., 2002). The detailed procedure was explained in Section 4.2.4.2.3.1. After the 15 day cycles of CEM process, washed and dried samples of Na, K and Ca exchanged materials were used for

measurement of pozzolanic activity at 3, 7, 28, 56 and 90 days of age by thermogravimetric analysis. Three mixtures of Na⁺, K⁺ and Ca²⁺ exchanged clinoptilolite (CLI-B) and lime were prepared by 1:1 lime/pozzolan ratio and 0.5 water/ solid ratio.

4.3.1.3 Fratini's Test

The Fratini's test (Fratini, 1949) standardized by EN 196:5(1994) is a commonly used chemical method performed in order to ascertain whether the material is active or not. In this test the amount of free Ca²⁺ and OH⁻ ions leached from blended cement is determined. The procedure stated in EN 196/5 (1994) consists in adding 20 g zeolitic blends to 100 ml distilled water and the mixtures were left at 40 °C for 8 days or 15 days. After this period, Ca²⁺ and OH⁻ concentrations were analyzed in the contact solution by complexometric titration with EDTA and acid-base titration. Results as mmol/l are plotted on a graph of OH⁻ on the x-axis versus Ca²⁺ on the y-axis. The test is considered positive when the points lying below the 40 °C solubility isotherm of Ca(OH)₂ after 8 days or 15 days.

4.3.1.3.1 Comparison of Fratini's test and Thermogravimetric Method

Fratini's test implies the determination of the quantity of calcium [CaO] and hydroxyl [OH] ions in contact water. Then, according to amount of Ca(OH)₂ lying below, on, or above the solubility isotherm one can say the material has pozzolanicity. However, since Fratini's test only gives qualitative result, it is required to convert the results in numeric values in order to compare with thermogravimetric analysis.

Donatello et al., (2010) succeeded to quantify the experimental Ca(OH)₂ solubility data by taken into account the distance of measured points from the solubility isotherm of Ca(OH)₂ and from the [CaO] axis at the given [OH] . It was emphasized that, based on the [OH] ions remaining in the contact solution, the theoretical maximum [CaO] concentrations can be calculated using an equation 4.3 provided from EN 196:5. Then the [CaO] reduction can be quantified by the difference between the theoretical maximum [CaO] and sample calcium concentration [CaO] in percentage (Donatello, 2010).

$$Max[CaO] = \frac{350}{[OH]-15} \quad (4.3)$$

4.3.1.4 Kinetic Analyses

The knowledge of kinetic analysis of blended material provides the clarification of the reaction mechanism. The experimental data obtained from thermogravimetric analysis was further assessed to describe the mechanism of the lime-pozzolan reaction by modified Jander's

equation. An early mathematical model of lime reactivity was developed by Jander (1927) which is based on Fick (1855)'s parabolic Law of Diffusion (equation 4.4).

$$[1 - (1 - x)^{1/3}]^2 = 2kt/r^2 = K \quad (4.4)$$

In the above equation, r is the radius of reacted sphere, x is the fraction of reacted sphere, t is the time of reaction, k and K are the rate constants. In this equation, the rate of thickening of reaction product is inversely proportional to the thickness (Jander, 1927).

Kondo et al. (1976) have modified the Jander's equation for a wider application by presenting a reaction grade N . According to the theory calculated consumption of lime fixation compared to the initial amount was used as the reaction degree (α) for three dimensional diffusion processes (equation 4.5).

$$(1 - \sqrt[3]{(1 - \alpha)})^N = Kt \quad (4.5)$$

where α is the degree of reaction, t is the reaction time, K is the reaction constant and N is the reaction grade. The equation provides classifying reaction process (Kondo et al., 1976) on the basis of the reaction grade N .

$N \leq 1$: The process is controlled by the reaction at the surface, or by the dissolution of reactants, or the precipitation of reaction products.

$1 < N \leq 2$: The process is controlled by the diffusion of reactants through a layer of porous reaction products.

$N > 2$: The process is controlled by the diffusion of reactants through a layer of dense reaction products.

4.3.2 Reaction Products

4.3.2.1 XRD Analyses of Hardened Lime-Zeolite Pastes

To investigate the preexisting phases and the formation of the new crystalline reaction products during the pozzolanic reaction, XRD analyses were carried out at various reaction times. Furthermore, to observe differences and similarities during the progress of hydration, the peak heights of identified phases were correlated to each other in the same paste from 3 days to 180 days of hydration and different blended pastes at the same days of hydration. The hardened paste samples acquired from thermogravimetric analysis were prepared with the same procedure described in Section 4.3.1.1. Powder X-ray diffraction patterns were recorded on Philips PW 1730 diffractometer with Ni-filtered, $\text{CuK}\alpha 1$ radiation, operating at 40 kV, 30 mA.

4.3.2.2 FTIR Analyses of Hardened Lime-Zeolite Pastes

In addition to XRD of hardened cement analysis, the detection of the newly formed phases during hydration was carried out using a Fourier Transform IR spectrophotometer (FTIR). Samples for FTIR analyses were prepared by mixing 1 mg of tuffs with 150 mg of KBr and pressed into pellet. Then, infrared spectra were obtained using the Perkin Elmer 880 spectrophotometer at a resolution of 1 cm^{-1} , over the range from 400 to 4000 cm^{-1} at various times ranging from 3 days to 90 days. The complete determination of the spectra is achieved by comparison with available data of the lime, zeolites and hydration products. Accordingly, first the lime and zeolites are characterized by this technique and then FTIR spectra of 3, 7, 28, 56 and 90 days pastes are presented.

4.3.2.3 Compressive Strength Analyses

Mechanical characterization of zeolitic tuffs was investigated by the compressive strength analyses of specimens according to ASTM C 311-98b. Before the preparation of mortars, a Flow Test was performed.

4.3.2.3.1 Flow Test (ASTM C 109)

Flow analysis was made to decide the amount of water content necessary to prepare mortars for the same flow spread (standard consistency) and was performed according to ASTM C 109, Standard Test Method for Compressive Strength of Hydraulic Cement Mortars. The flow test was performed with a standard flow table, which is described in ASTM C 230. Standard mold was placed at the center of the standard flow table. The mold was filled in two layers. Each layer was tamped for 20 times with a tamper. After removing mold, the flow table was exposed to 25 drops during 15 sec through a height of 13 mm. Then the average diameter of mortar was measured and reported as percentage of increase of the original base diameter (ASTM C 109).

4.3.2.3.2 Preparation of Mortars (ASTM C 311-98b)

Mortars were prepared with zeolitic tuffs/cement by using 0.485 water-to-solid ratio. The materials were mixed mechanically in accordance with ASTM C 305-99. 242 g water, 400 g cement and 100 g zeolitic tuff were mechanically mixed at slow speed ($140\pm 5\text{ r/min}$) for 30 s. Then, 1375 g CEN standard sand (EN 196-1) were slowly added over 30 sec during mixing at slow speed. The mortar was mixed for another 30 sec at medium speed ($285\pm 10\text{ r/min}$). The mixer was stop for 90 sec. Through the first 15 sec, mortar that collected on the side of the bowl was scraped down and was waited. After that, the mortar was mixed for 60 sec at medium speed. The fresh pastes were then cast into 50X50X50 mm moulds and stored 24 h covering with a wet

towel. The prisms were removed from the moulds after 24 h and stored in water at 23 °C until testing day.

4.3.2.3.3 Test on Hardened Cement

Compressive strengths of cubic specimens were determined in accordance with ASTM C 109, using universal testing machine at 7, 28, 56 and 90 days of age. The compressive strength values were calculated from the average of six cubes for each test ages.

Strength Activity Index (SAI)

After the compressive strength analysis, the strength activity indices (SAI) of the all blended cements were determined according to ASTM C 311 to evaluate the field performance of the natural zeolites. The method was applied by determining the compressive strength of blended cements with respect to the control Portland cement. The calculation of strength activity index as follows (ASTM C 311) (equation 4.6):

$$SAI = \frac{A}{B} \times 100 \quad (4.6)$$

where A is average compressive strength of blended mortar (MPa), B is average compressive strength of control Portland cement (MPa).

4.3.2.3.4 Water Requirement

Water requirement of blended cements were measured in accordance with ASTM C 311. The calculation of water requirement as follows (equation 4.7):

$$Water\ Requirement = \frac{Y}{242} \times 100 \quad (4.7)$$

where Y is water required for the blended cement.

4.3.2.4 Microstructure of Hardened Cement Pastes

This part of the study is focussed on the microstructural observations of clinoptilolite, mordenite and analcime blended cement after 28 days of hydration.

4.3.2.4.1 SEM Analyses of Hardened Cement

The use of scanning electron microscopy (SEM) is important to observe the morphology of hydrated phases. Besides, EDX analysis can also be performed to obtain semi-quantitative chemical analysis. For this reason, to investigate the microstructure and hydration properties of blended cements cured for 28 days, scanning electron microscope (SEM) using a Quanta 400 F device, equipped with energy-dispersive X-ray (EDX) system was employed in the Central Laboratory, Middle East Technical University, Turkey.

When the hardened pastes were crushed for the compressive strength analysis at 28 days of hydration, small pieces (typically 3 to 7 mm in size) were removed and immersed in acetone in order to stop further hydration. The pieces were then subsequently cured in an oven at 60°C during 10 hours. After curing, the specimens were coated gold-platinum before SEM analysis.

4.3.2.4.2 Quantitative Electron Microprobe Analyses of Hardened Cement

The chemical composition of hydration products generated by the pozzolanic reaction in cement paste after 28 days of curing was analyzed by Jeol JXA-8200 electron microprobe in wavelength dispersive system (EPMA-WDS) by using an accelerating voltage of 10kV. The true selection of accelerating voltage for the microanalysis is very important to prevent analytical errors. Microprobe analysis was used to determine the extent of reaction of zeolites. The knowledge of the reaction products will be determinant for the complex chemical reactions occurred during the hydration of cement. This method was selected specifically since it provides the best opportunity to collect chemical information of reacted zeolites as well as having the smallest analytical volume. Furthermore, this method has the obvious advantage of comparing the data directly with chemical analysis observed bulk material.

The other half of specimens that has already been used for morphological investigation by SEM analysis was polished and mounted in a resin. Since polished surface is necessary for quantitative analysis, great care must be taken to generate during polishing of the hydrated cement paste. Quantitative chemical compositions of reacted zeolites and hydration products were analyzed using a Jeol JXA-8200 electron microprobe in wavelength dispersive mode (EPMA-WDS) in Department of Earth Sciences, Università degli Studi di Milano.

CHAPTER 5

RESULTS

5.1 Characterization of Zeolitic Tuffs

5.1.1 Physical Characterization of Zeolitic Tuffs

The physical properties and grain size distribution of the finely ground zeolitic tuffs are given in Table 5.1 and Figure 5.1, respectively.

Table 5.1 Physical properties of the zeolitic tuffs

	CLI-G	CLI-A	CLI-B	MOR	ANA
Specific Gravity	2.12	2.09	2.12	2.17	2.3
BET surface area, m ² /g	39.9	28.01	17.57	27.3	26.19
Blaine surface area, m ² /g	7436	8209	4769	6328	5076
Fineness					
Passing 90 μm, %	100	100	100	100	100
Passing 45 μm, %	92	99	90	77	95

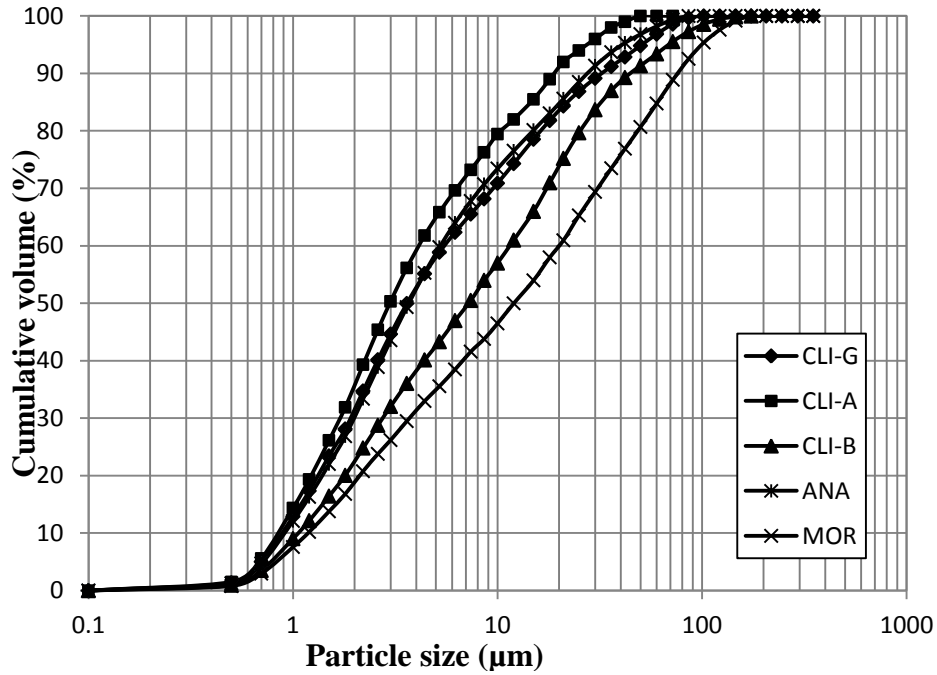


Figure 5.1 Particle size distributions of zeolitic tuffs.

From these results, it is seen that CLI-G offers the largest specific surface area ($39.9 \text{ m}^2/\text{g}$). The BET surface area of the CLI-B is smaller than those of CLI-G and CLI-A. From Figure 5.1, it is obvious that the particle size of CLI-A is slightly smaller than CLI-G and ANA, whose grain size distributions are very similar. Particles of CLI-B, on the other hand, are much bigger than CLI-G and CLI-A. MOR has the largest grain size distribution. Although particle size of CLI-A is slightly smaller than CLI-G, BET specific surface area of CLI-G is much higher than CLI-A most probably presence of smectite in CLI-G. The reverse relationship was established between BET and Blaine surface among CLI-G and CLI-A.

5.1.2 Chemical Characterization

5.1.2.1 Chemical Analyses of Zeolitic Tuffs

Determination of major element oxides of zeolite bearing tuff samples were carried out by ICP-OES and the results of chemical analyses are presented in Table 5.2.

Table 5.2 Chemical composition of the zeolitic tuffs (wt %).

	CLI-G	CLI-A	CLI-B	MOR	ANA
Chemical Composition (%)					
SiO ₂	67.54	67.18	66.30	68.72	69.13
Al ₂ O ₃	12.27	12.31	11.70	13.86	15.12
Fe ₂ O ₃	1.18	0.39	0.97	0.89	1.99
CaO	2.32	2.57	2.66	1.76	0.30
MgO	1.25	1.03	1.32	0.08	0.65
K ₂ O	2.31	2.77	3.38	4.09	6.04
Na ₂ O	0.27	0.25	0.22	1.38	3.17
MnO	0.01	-	-	0.02	0.04
LOI	12.85	13.50	13.45	9.20	3.56
Sum	100	100	100	100	100

From this table, it is seen that in the zeolites SiO₂ has the highest major oxide content and ranges between 66.14 to 70.21 %. The sum of SiO₂ and Al₂O₃ constitute more than 77%, which is suitable for pozzolanic reaction. The chemical compositions of CLI-G and CLI-A are very similar. CLI-B, on the other hand, has higher K₂O and CaO values than others. MOR is characterized by higher K₂O value. Among the samples, ANA has the highest Na₂O and K₂O contents with 3.02 %, 7.16 %, respectively.

5.1.2.2 Quantitative Electron Microprobe Analyses (EPMA) of Zeolites

Polished thin sections of zeolitic tuff samples were used for chemical analyses of zeolite phases, obtained through wavelength dispersive mode of microanalyser (EPMA-WDS). Zeolites from each locality were analyzed using 3 to 6 spots. The results of microprobe analyses of zeolites are presented in Table 5.3. Electron microprobe analyses showed that zeolite in CLI-G is chemically very similar to that of CLI-A. Clinoptilolite in CLI-B, on the other hand, includes high amounts of K⁺ (1.61%) and lower Si/Al ratio (4.40) than other clinoptilolites. The concentrations of Na⁺ in clinoptilolites are lower than 1%. The content of Na⁺ and Ca²⁺ in mordenite is higher and K⁺ is slightly lower than clinoptilolites. Analcime is characterized by highest Na⁺ content (12.82%) and low K⁺ and Ca²⁺ contents (0.03 and 0.02%, respectively). Si/Al ratio of the analyzed CLI-G, CLI-A and CLI-B is more than 4, which are clearly characteristic for clinoptilolite according to Coombs et al (1998).

Figure 5.2 shows a back scattered electron image (BSE) of clinoptilolite-rich tuffs (CLI-G). In Figure 5.2, it is difficult to distinguish clinoptilolite crystals from cryptocrystalline matrix. Very small prismatic clinoptilolite crystals 1µm in length can only be separated near the cavity (Figure 5.2). Because clinoptilolites have very small crystal sizes, collecting data using a

microprobe spot analyzer was performed on assemblages of prismatic clinoptilolite crystal rather than single crystal. Analyzed points were taken from the most representative regions and Figure 5.2 shows only one spot point.

Table 5.3 Representative electron microprobe analyses of zeolites in tuffs (wt %).

	CLI-G	CLI-A	CLI-B	MOR	ANA
SiO ₂	68.61	65.40	67.24	71.71	58.16
Al ₂ O ₃	11.75	11.64	12.98	10.91	21.58
Fe ₂ O ₃	0.1	0.03	0.07	0.06	0.11
MgO	1.11	0.86	1.08	0.05	0.01
CaO	3.01	3.05	3.23	2.91	0.03
Na ₂ O	0.12	0.15	0.12	1.64	11.42
K ₂ O	2.08	2.12	2.89	1.45	0.04
SrO	-	0.25	-	0.01	0.06
MnO	0.01	-	0.01	-	-
BaO	0.04	0.13	0.08	0.02	-
Total	86.85	83.63	87.70	88.76	91.41
LOI	13.15	16.37	12.30	11.24	8.59
Oxygen	72	72	72	96	96
Si	30.04	29.87	29.41	40.86	33.68
Al	6.06	6.27	6.69	7.33	14.73
Fe	0.03	0.01	0.02	0.03	0.05
Mg	0.72	0.59	0.71	0.04	0.01
Ca	1.41	1.49	1.52	1.78	0.02
Na	0.10	0.13	0.10	1.81	12.82
K	1.16	1.24	1.61	1.05	0.03
Sr	-	0.07	-	-	0.02
Mn	-	-	-	-	-
Ba	0.01	0.02	0.01	-	-
Si/Al	4.95	4.77	4.40	5.58	2.29
Na/K	0.09	0.11	0.06	1.72	-
E%	9.39	9.81	8.08	12.77	13.74

$$E\% = [Al - (Na + K) - 2(Ca + Mg + Sr + Ba)] / [Na + K + 2(Ca + Mg + Sr + Ba)]$$

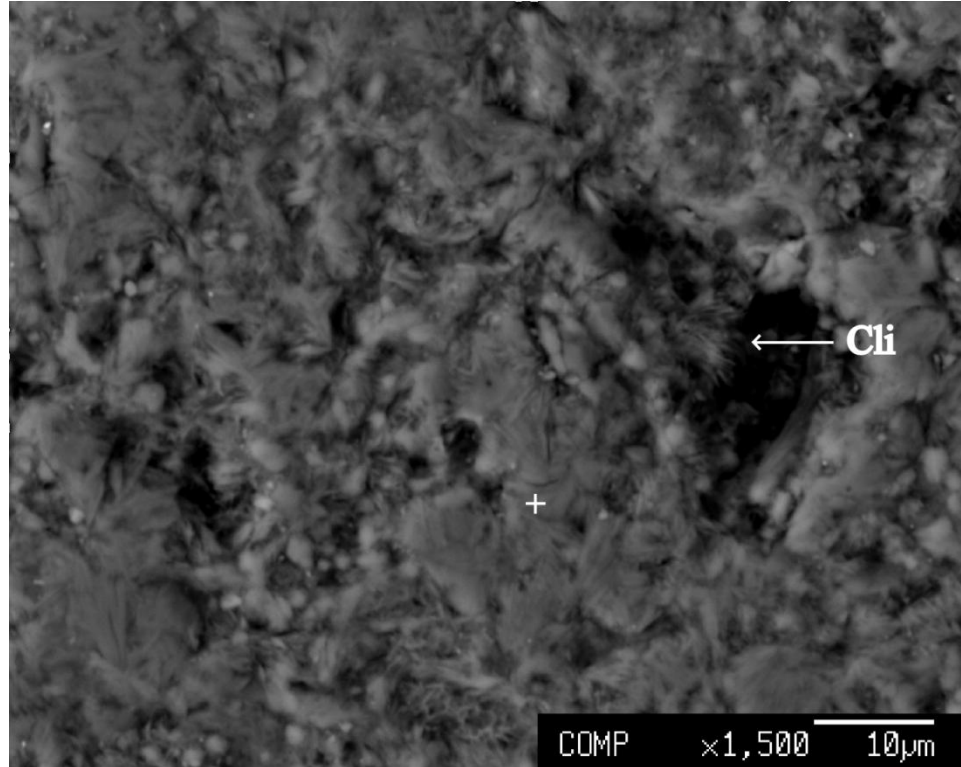


Figure 5.2 Back scattered image shows very small prismatic clinoptilolite crystals 1µm in length distinguished from cryptocrystalline matrix and one microprobe analyze spot (Cli: clinoptilolite; Sample: CLI-G).

Figures from 5.3 to 5.6 show back scattered electron images (BSE) of zeolite bearing tuffs (CLI-A, CLI-B, MOR and ANA, respectively). For clinoptilolite rich ones, it is again difficult to differentiate single crystals and analyses were taken from an assemblage of clinoptilolite crystals (Figure 5.3, 5.4). Sample CLI-B represents denser structure. Mordenite forms fiber like crystals (Figure 5.5). Spot analyses were taken from the cavity where mordenite start to form. Analcime aggregates are differentiated by their euhedral morphology (Figure 5.6).

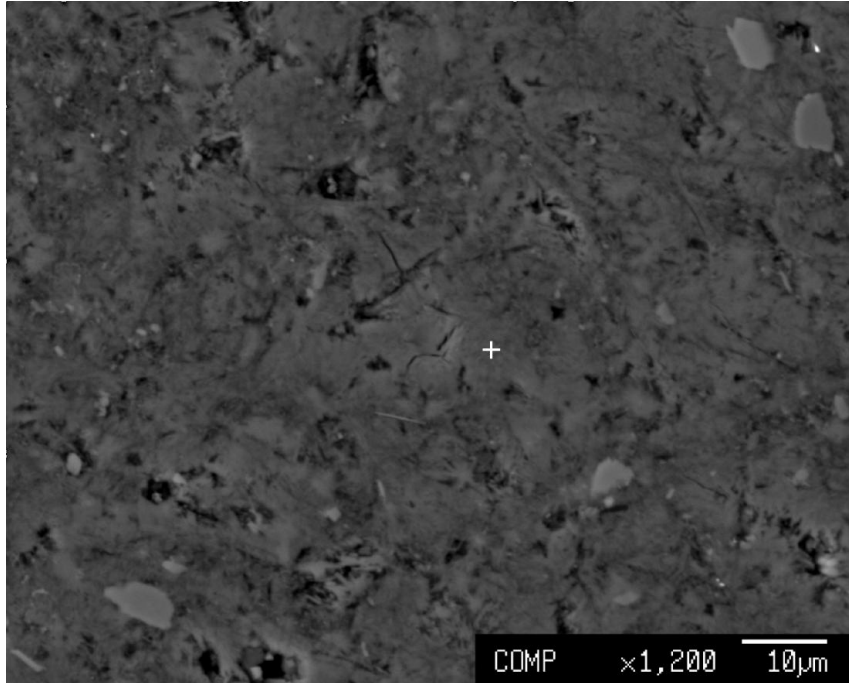


Figure 5.3 Back scattered image showing clinoptilolite-rich tuff (Sample: CLI-A).

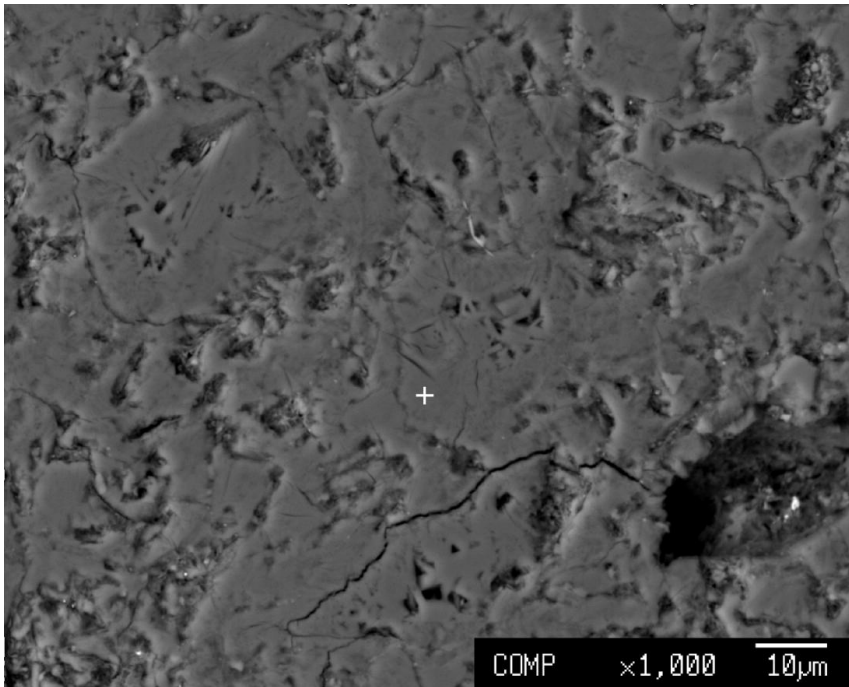


Figure 5.4 Back scattered image showing CLI-B, which display denser structure.

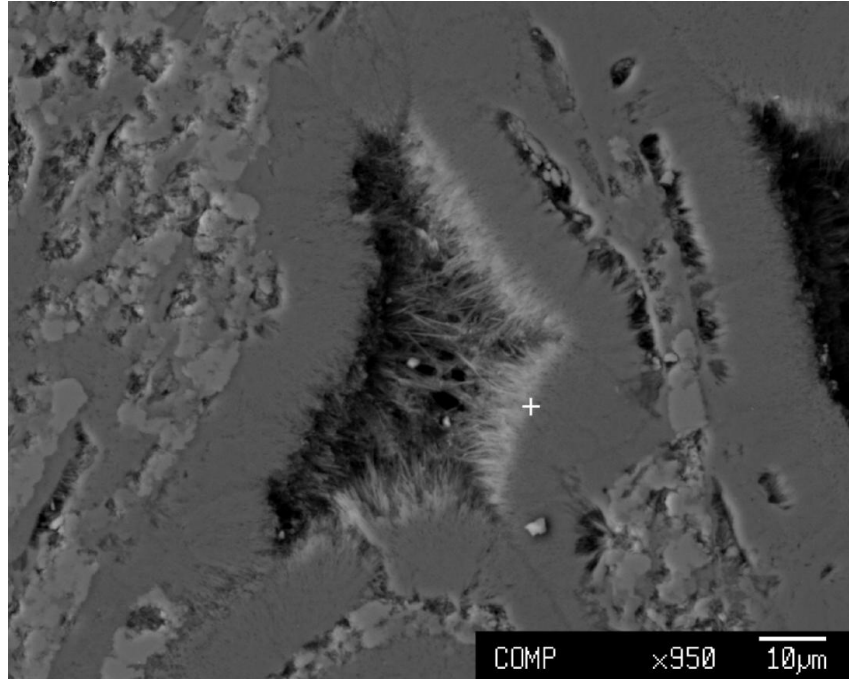


Figure 5.5 Back scatter image displaying mordenite fibers, which form by alteration of volcanic glass (Sample: MOR).

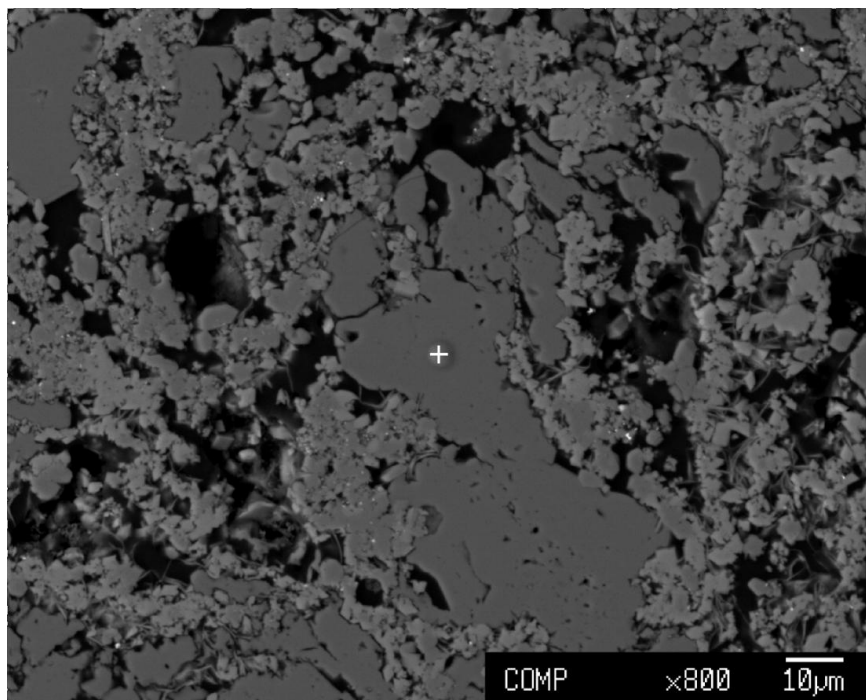


Figure 5.6 Back scattered image showing analcime bearing tuff (Sample: ANA).

5.1.2.3 Evaluation of Cation Exchange Capacity (CEC)

Zeolite bearing tuffs were investigated in order to determine their cation exchange capacities (CECs). Two methods were used to characterize CECs of zeolitic tuffs, namely the cross exchange method (CEM) and the batch exchange method (BEM) (Colella et al., 2001; Cerri et al., 2002). The theoretical CECs reported in literature (Breck, 1974; Mumpton, 1999), expected CECs calculated from mineralogical percentage of zeolitic tuffs and experimental CECs determined by the BEM are listed in Table 5.4.

Table 5.4 Theoretical, Expected and Experimental CECs and exchangeable cations of zeolitic tuffs

Sample	Cation Exchange Capacity CEC (meq/g)			Exchangeable cations (meq/g)			
	Theoretical	Expected	Experimental	Na	K	Ca	Mg
CLI-G	2.40	1.80	1.75	0.0450	0.4280	0.8740	0.4050
CLI-A	2.40	1.80	1.78	0.0650	0.4586	0.9356	0.3218
CLI-B	2.40	1.80	1.72	0.0401	0.5944	0.8593	0.2270
MOR	2.29	0.62	0.60	0.1800	0.1180	0.2850	0.0176
ANA	0.60	0.12	0.17	0.0586	0.0166	0.0800	0.0131

The theoretical CEC of pure clinoptilolite, mordenite and analcime are reported in literature (Breck, 1974; Mumpton, 1999). Expected CEC of zeolitic tuffs was estimated from the zeolite content and the theoretical CECs of each tuff sample. The amount of expected CEC is calculated as follows.

$$\text{Expected CEC} = \text{Theoretical CEC} \times \frac{\text{Mineralogical content of zeolite}}{100} \quad (5.1)$$

The CEC values determined by BEM method are very close to the CEC values reported in literature as can be seen in Table 5.4. Since the BEM resulted in values of about 1-4 % lower than the expected CEC in clinoptilolite-rich samples, the analyses suggest that the BEM method is suitable for cation exchange capacity measurements of clinoptilolite (e.g. Cerri et al., 2002). MOR, on the other hand, has higher experimental value than expected and ANA has nearly same result. The CEC value of CLI-B determined by CEM is 1.01 meq/g, which is about 39% lower than the expected CEC of clinoptilolite (1.8 meq/g). Therefore, CEM method leads to inaccurate result for clinoptilolite-rich tuffs as discussed in Cerri et al. (2002).

The amount of exchangeable cations (Na^+ , K^+ , Ca^{2+} and Mg^{2+}) and cation exchange capacity (CEC) of zeolitic bulk rock samples established by BEM method is given in Figure 5.7. According to XRPD analysis (Table 5.5), zeolite is the only exchangeable phase in CLI-B, CLI-A and ANA samples, whereas CLI-G and MOR samples contain also clay minerals, for which the influence on cation exchange capacity is negligible since their percentage is very low. The analysis revealed that CLI-G and CLI-A have the highest CEC (1.75 meq/g, 1.78 meq/g,

respectively) and ANA has the lowest (0.17 meq/g) values. MOR also has lower CEC (0.60 meq/g). These results are in agreement with the mineralogical compositions of the analyzed samples (Table 5.5). In fact, MOR and ANA contain only a modest amount of zeolitic phase. Besides, analcime is known as a scarce exchanger. Concerning the clinoptilolite-rich tuff samples, despite the samples have the same zeolite content, the CLI- B shows slightly lower ion exchange capacity (1.72 meq/g) than CLI-G and CLI-A. Results from CEC also suggest that exchangeable cations consists of $\text{Ca} > \text{K} > \text{Mg} > \text{Na}$ with decreasing abundance for clinoptilolite rich tuffs.

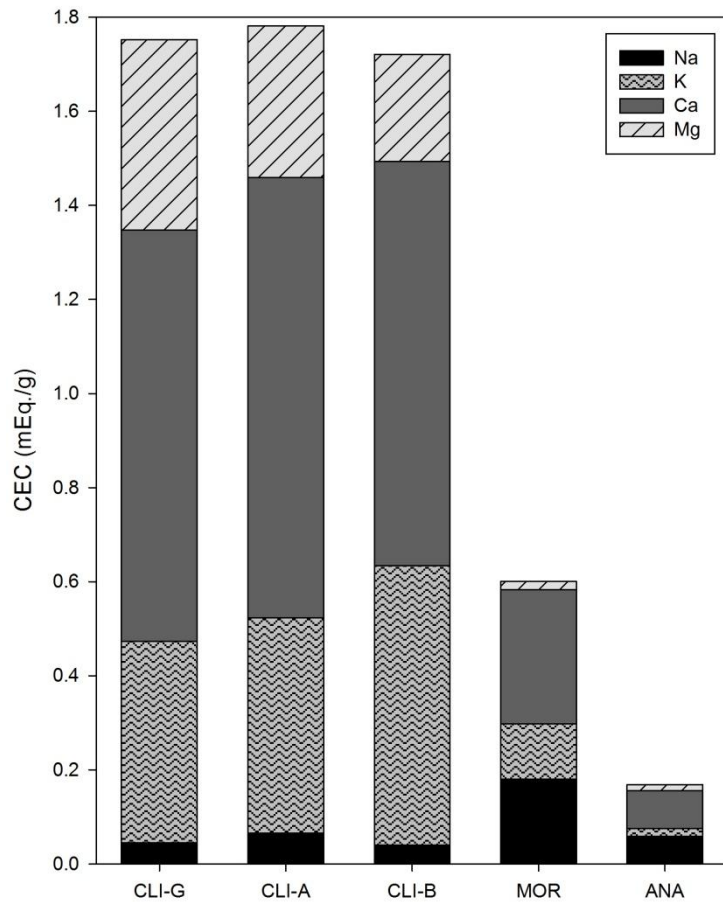


Figure 5.7 The cation exchange capacity (CEC) and the amount of exchangeable cations (Na^+ , K^+ , Ca^{2+} and Mg^{2+}) determined by BEM method.

5.1.3 Mineralogical Characterization

5.1.3.1 Petrography

For petrographical purposes five thin sections were prepared, collected from each locality of the study areas. Microscopical study reveals that the zeolitic tuff samples can be classified as fine tuff based on grain size (Fisher and Schmincke, 1984). In addition, all samples were named as vitric tuff.

CLI-G consists of minor amount of quartz, feldspar and biotite (Figure 5.8). The phenocryst content is about 5%. Grains of quartz are clear and anhedral. Biotite crystals are brown pleochroic. Small phenocrysts of feldspar are colorless and display low birefringence. The glassy material consists of relict glass shards in small amount (~5%). It was not be able to determine zeolite mineral on thin section studies because of the minute grain size of this diagenetic mineral.

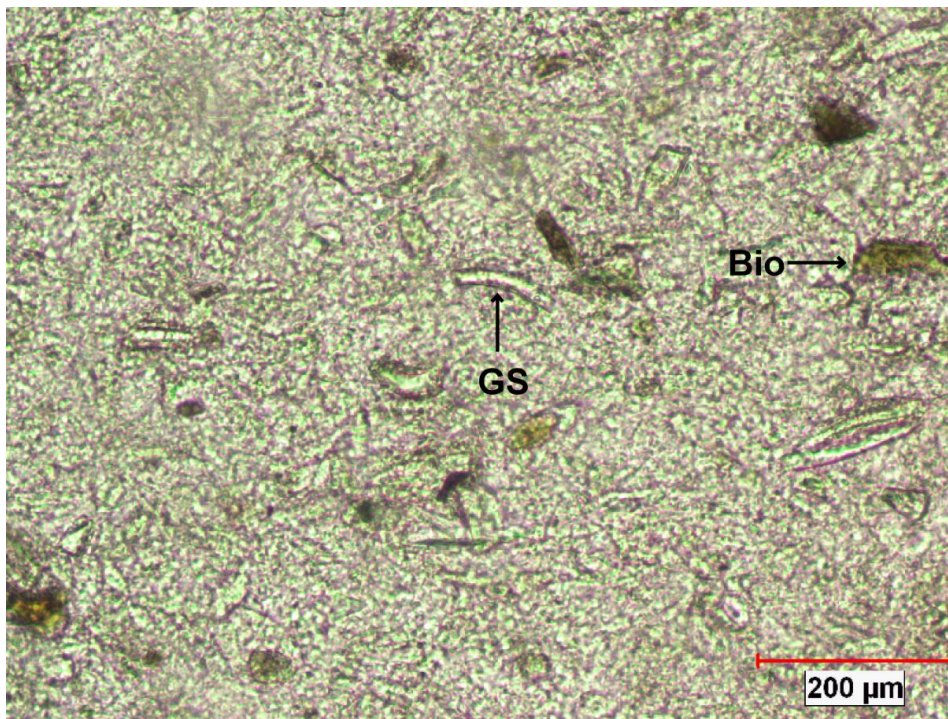


Figure 5.8 Photomicrograph showing biotite and quartz phenocryst as well as relict volcanic glass shard (Sample: CLI-G, GS: glass shard, Bio: biotite, PPL).

The size of CLI-A is found smaller and more homogeneous than CLI-G in the studied thin section (Figure 5.9). Primary minerals, which comprises of quartz, feldspar and trace amount of

biotite are less than 5%. Tiny feldspar crystals in the matrix can be differentiated by low birefringence. Quartz, which is anhedral in shape, occurs as single crystals.

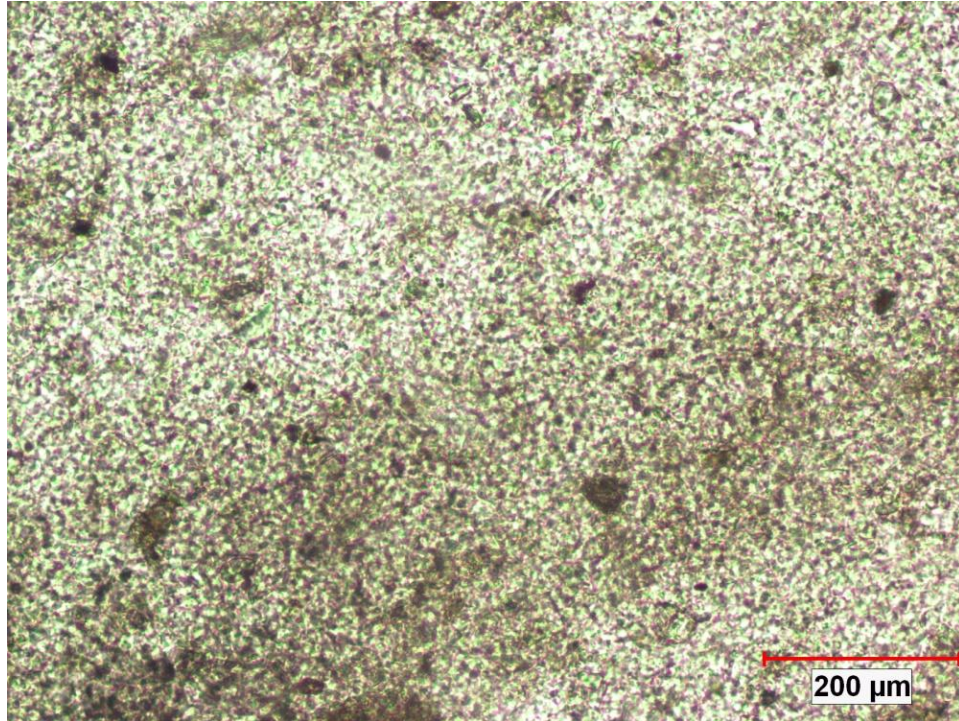


Figure 5.9 Photomicrograph of homogeneous clinoptilolite rich tuff, which consist of cryptocrystalline feldspar and quartz mineral (Sample: CLI-A, PPL).

CLI-B has the same type phenocryst, which makes up about 5% as CLI-G and CLI-A, but it appears darker in color (Figure 5.10). Relict glass shards in the matrix are common and about 15% in amount. Quartz is found slightly more than previous two thin sections. Colorless quartz crystals display subhedral outlines. Trace amounts of biotite are brown in color.

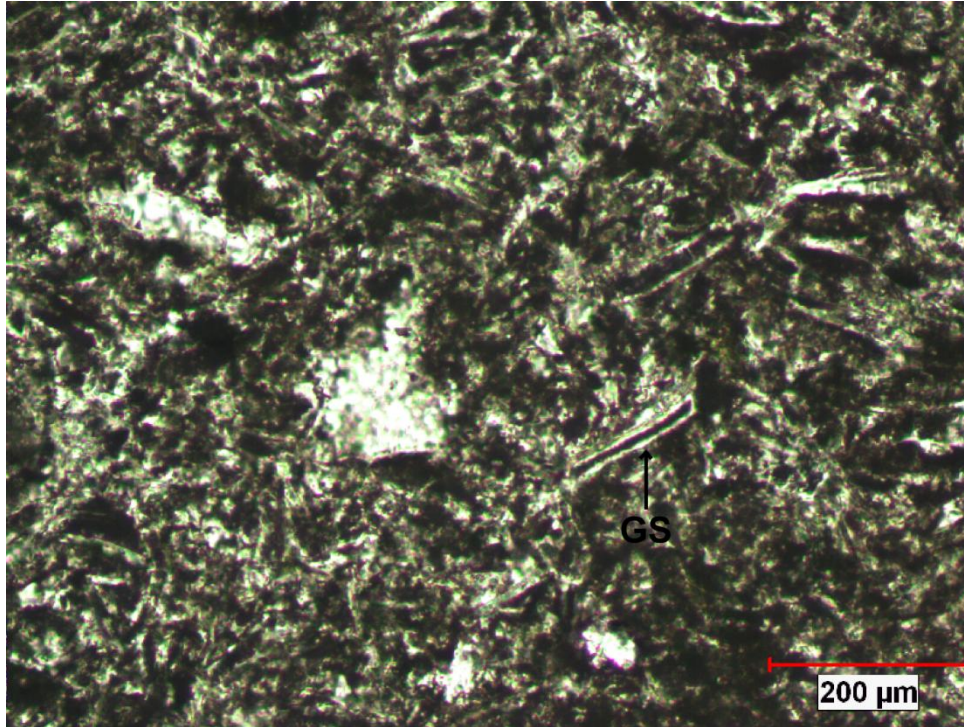


Figure 5.10 Photomicrograph showing relict volcanic glass shards in darker groundmass (Sample: CLI-B, GS: glass shard, PPL).

Primary minerals make up approximately 5 % of the MOR. Mordenite fibers can be clearly differentiated by morphological features (Figure 5.11). Widespread diagenetic mordenite fibers are well present at the edge of pumice fragment and they grow from edge to the inside by direct alteration of volcanic glass. In addition, precipitation of cristobalite in pores of pumice fragment can be found as a secondary mineral.

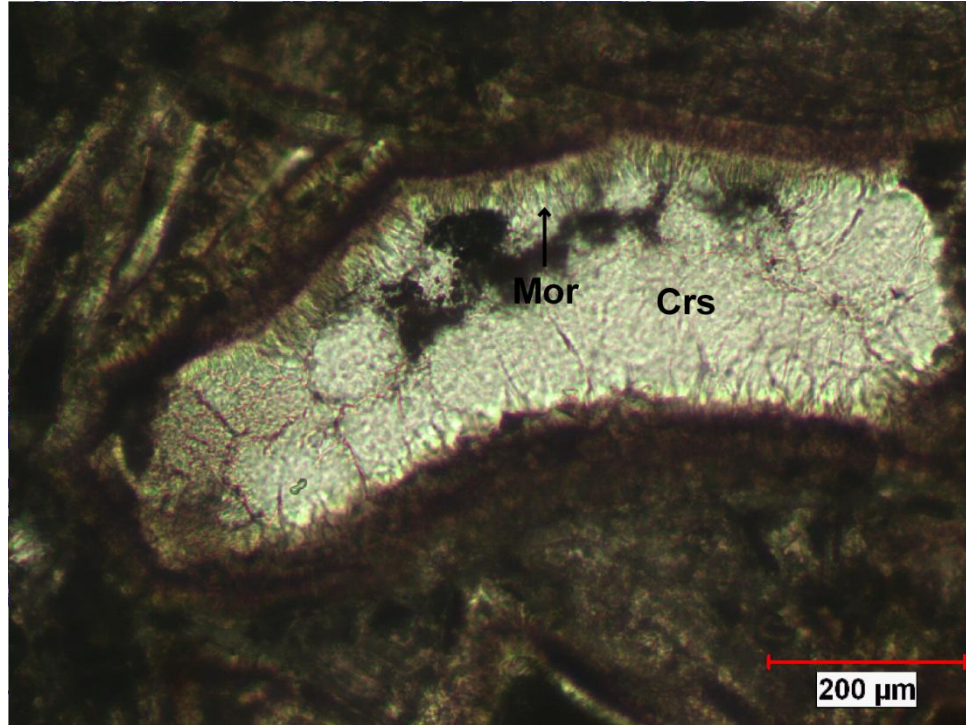


Figure 5.11 Photomicrograph displaying direct alteration of mordenite from edge of volcanic glass and precipitation of crystobalite (Sample: MOR, Mor: mordenite, Crs: crystobalite, PPL).

Figure 5.12 displays thin section view of ANA. The primary minerals constitute approximately 5% of the tuff. Colorless, clear quartz phenocrysts with low birefringence have subhedral outlines. Feldspars typically exhibit low birefringence. Fine-grained, colorless, low relief and isotropic analcime crystals are differentiated in the matrix, but its percentage cannot be determined.

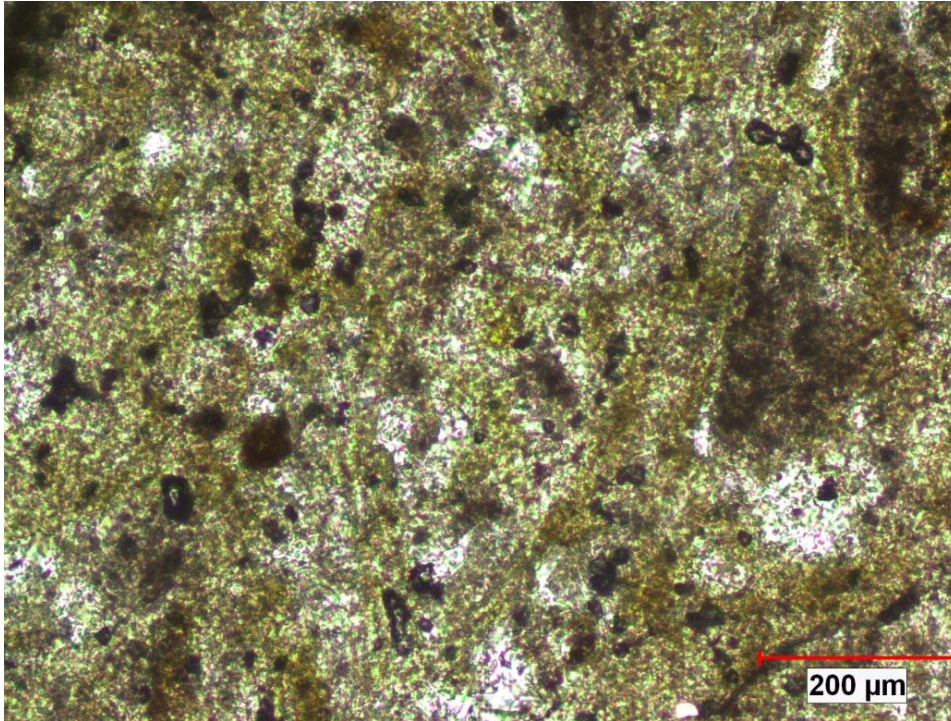


Figure 5.12 Photomicrograph showing thin section view of analcime-bearing vitric tuff (Sample: ANA, PPL).

5.1.3.2 Quantitative X-ray Powder Diffraction (XRPD)

Quantitative mineralogical composition (XRPD) of zeolitic tuffs is summarized in Table 5.5. The main phase of CLI-G, CLI-A and CLI-B is clinoptilolite, with minor amounts of feldspar, quartz and biotite. Their zeolite content in them is similar, about 80%. MOR and ANA, on the other hand, appeared to contain less zeolites (27.3% and 20.3%, respectively). Feldspar contents are higher in MOR and ANA (19.4, 45.6, respectively). The presence of insignificant amount of smectite (4.6%) and kaolinite (5.7%) is also relevant. It is important to notice that each sample also includes volcanic glass especially high in quantity in MOR and ANA, which could have a role on pozzolanic activity.

Table 5.5 Quantitative mineralogical composition of zeolite bearing tuff samples.

Sample	CLI-G	CLI-A	CLI-B	MOR	ANA
Clinoptilolite	76.4	82.9	84.7		
Mordenite				27.3	
Analcime					20.3
Feldspar	3.5	6.5	5.4	19.4	45.6
Quartz	1.1	0.5	2.2		16.5
Opal	5.3	6.1	2.9	13.1	
Smectite	4.6				
Biotite	3	2.1	2.8		0.9
Kaolinite				5.7	
Volcanic Glass	6.1	1.9	2	34.5	16.7
Total	100	100	100	100	100

5.1.3.3 SEM Analyses of Zeolitic Tuffs

The morphology of zeolites was investigated by means of scanning electron microscopy (SEM) equipped with energy dispersive X-ray microanalyser (EDX). The crystals of clinoptilolites have characteristic morphology of blades, tabular plates and laths, some of which have coffin-shaped crystals (Mumpton and Ormsby, 1978).

The scanning electron micrograph of Gördes (Manisa) clinoptilolites is shown in Figure 5.13. In the micrograph, well-formed clinoptilolite crystals occur as euhedral laths approximately 1 μm in length and tabular plates is observed.

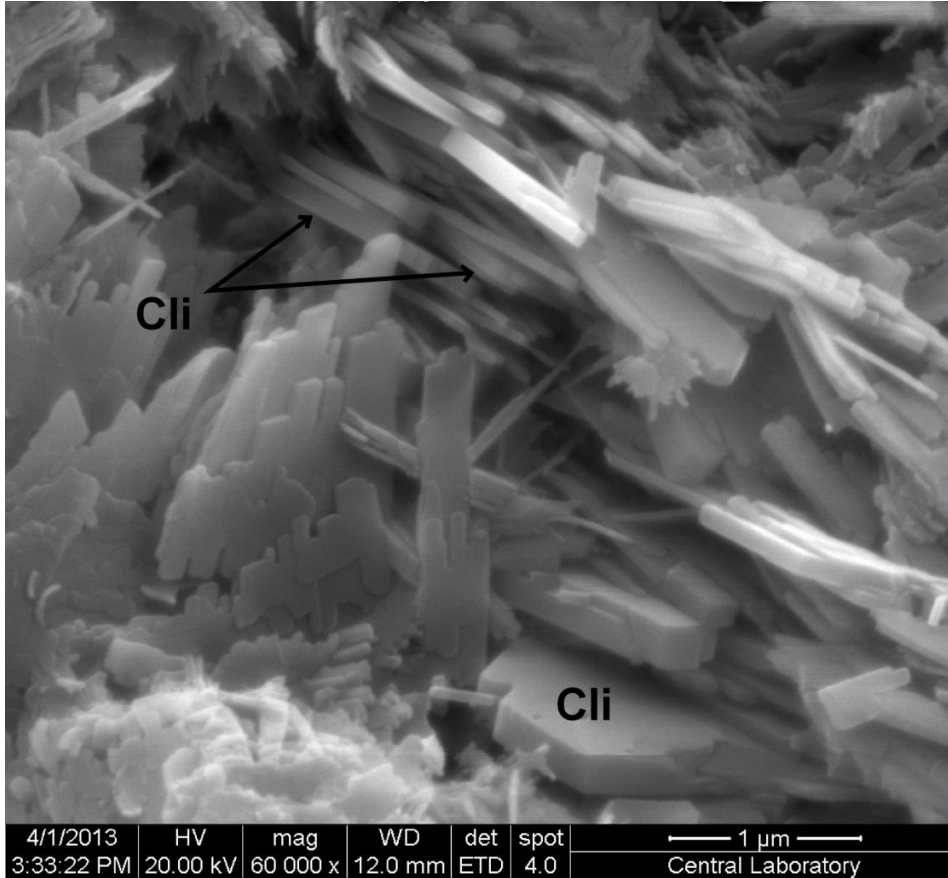


Figure 5.13 Scanning electron micrograph shows clinoptilolite crystals displaying laths and tabular plates (Sample: CLI-G, Cli: clinoptilolite).

Closely spaced lath-shaped clinoptilolite crystals occurring together are shown in Figure 5.14. Identification is based on their morphology and EDX analysis displaying the major elements of clinoptilolite (Si, Al, Ca, K, Mg) as shown in Figure 5.14. The fibers coating the clinoptilolites are probably mordenite.

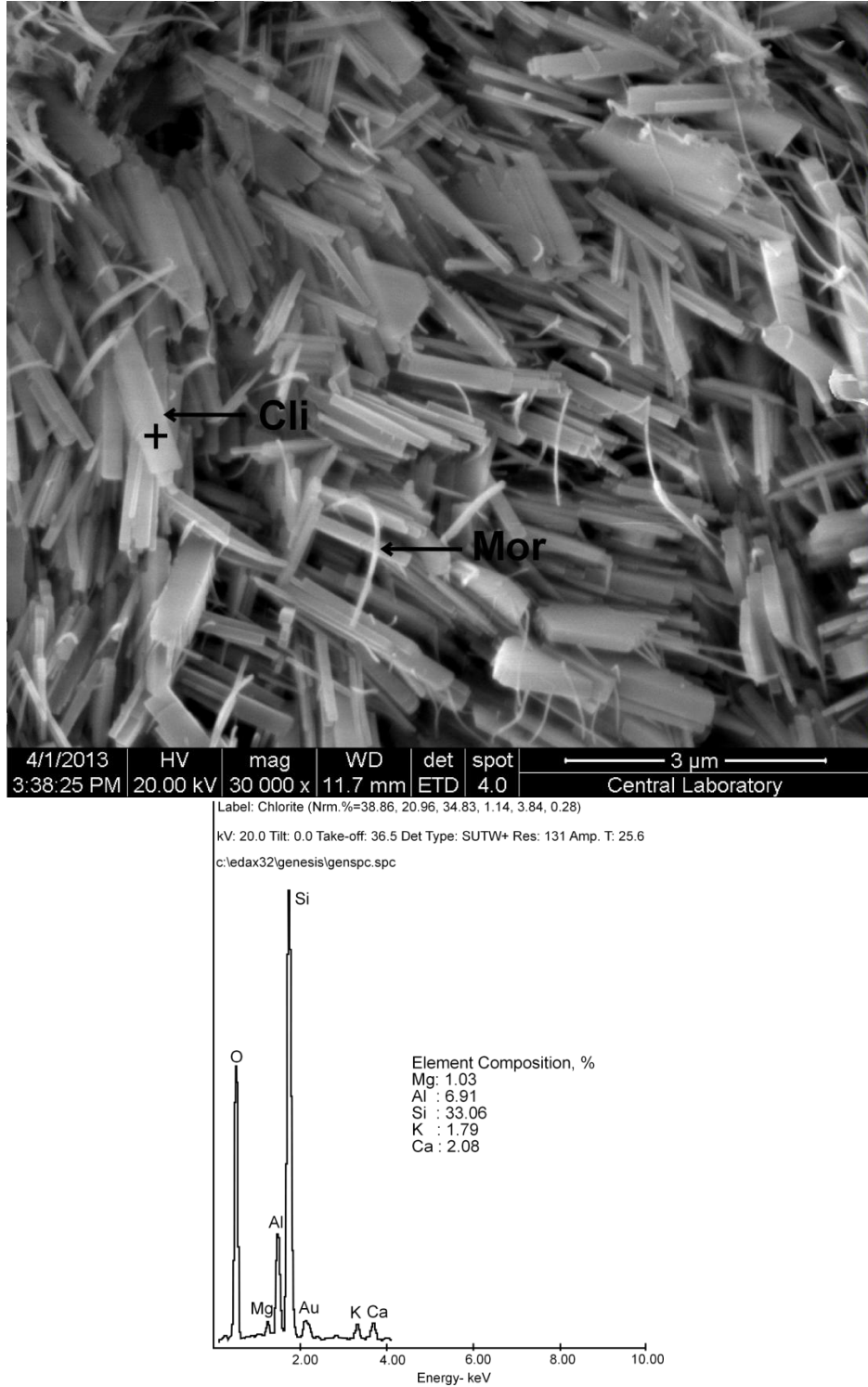


Figure 5.14 Scanning electron micrograph of well-formed clinoptilolite crystals and corresponding EDX measurement (Sample: CLI-G, Cli: clinoptilolite, Mor: mordenite).

The morphology of clinoptilolites from Aliğa region is similar to that of the Gördes clinoptilolite. Figure 5.15 shows well-developed clinoptilolite plates from Aliğa, İzmir (CLI-A).

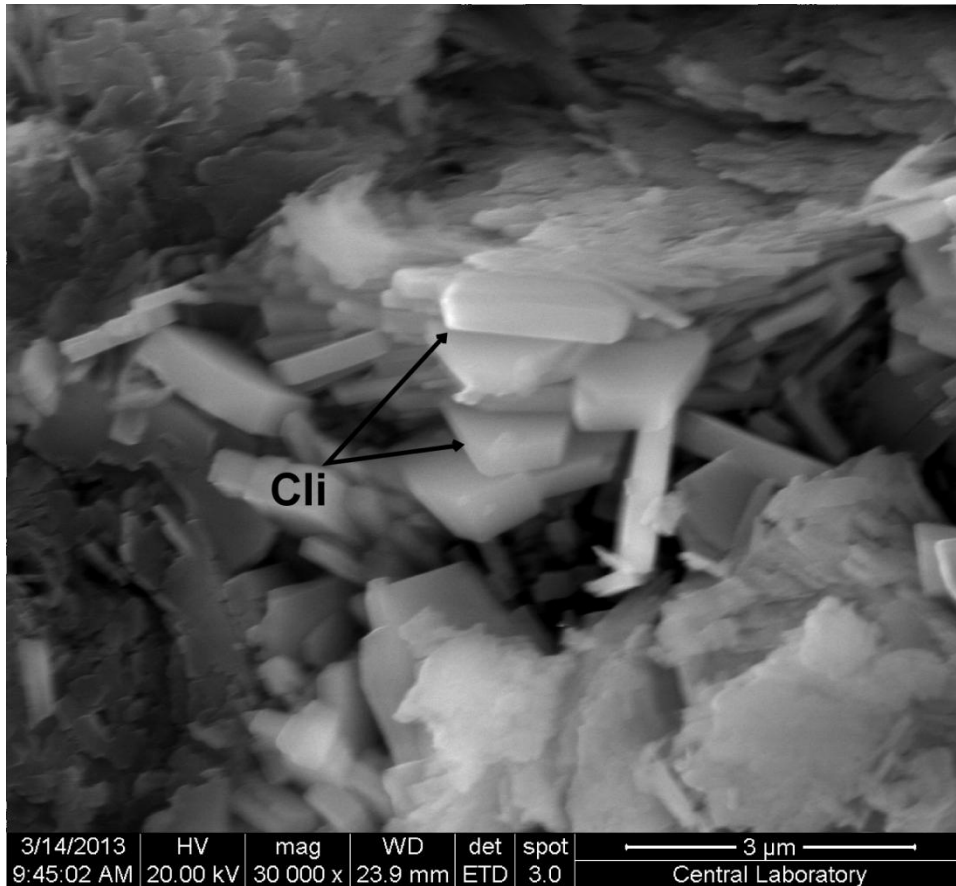


Figure 5.15 Scanning electron micrograph of well-formed clinoptilolite crystals (Sample: CLI-A, Cli: clinoptilolite).

Lath-shaped crystal morphology is also observed in Aliğa clinoptilolite and is illustrated in Figure 5.16. The average size of the clinoptilolite crystals is 1 μm in diameter.

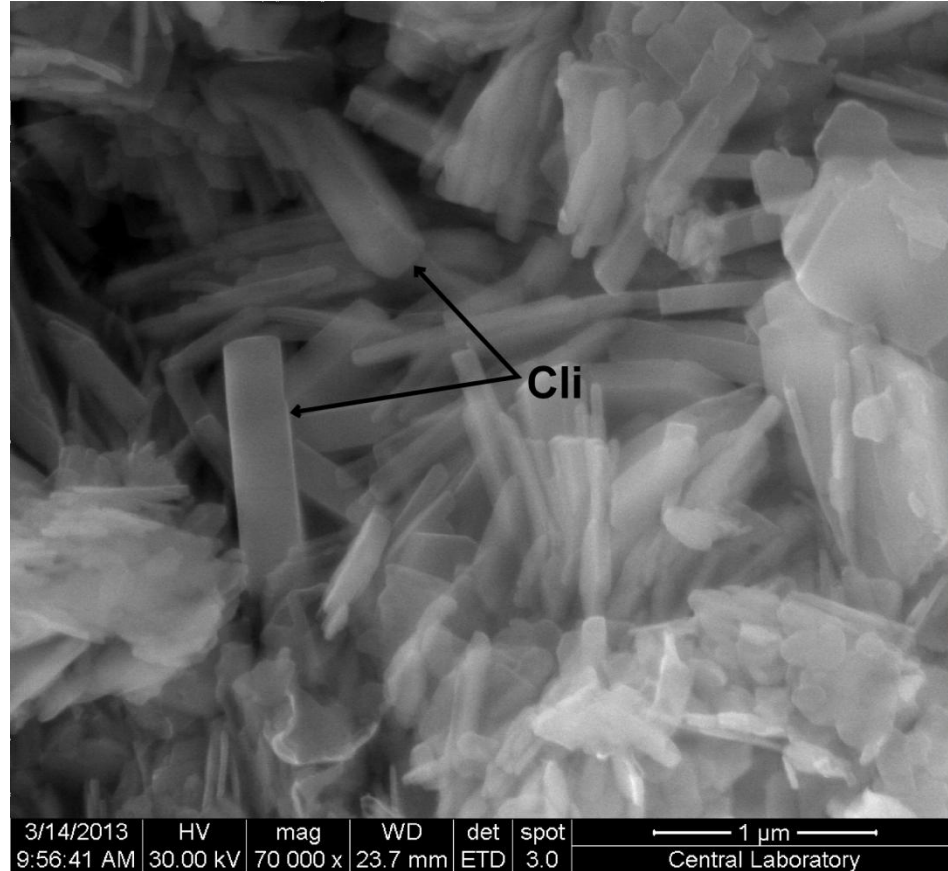


Figure 5.16 Scanning electron micrograph shows lath-shaped clinoptilolite crystals (Sample: CLI-A, Cli: clinoptilolite).

Clinoptilolites from Bigadiç region, on the other hand, have different morphologies than Gördes and Aliağa samples. Clinoptilolites occur as aggregates presented by lath-shaped morphology (Figure 5.17). Their identification is based on morphology and EDX analysis that yielded the principal constituents of clinoptilolite (Si, Al, Ca, K and Mg) as shown in Figure 5.17.

Another SEM image from the CLI-B showing masses of anhedral to subhedral clinoptilolite aggregates is illustrated in Figure 5.18. The identification is based on EDX analysis because of ambiguous morphology. The EDX spectra on the upper left corner of Figure 5.18 demonstrate the presence of Si, Al, Ca, K, Mg elements, which constitute the clinoptilolite composition.

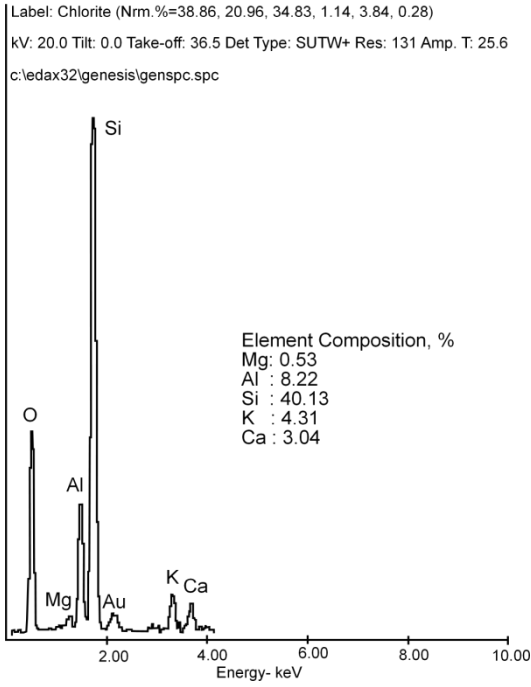
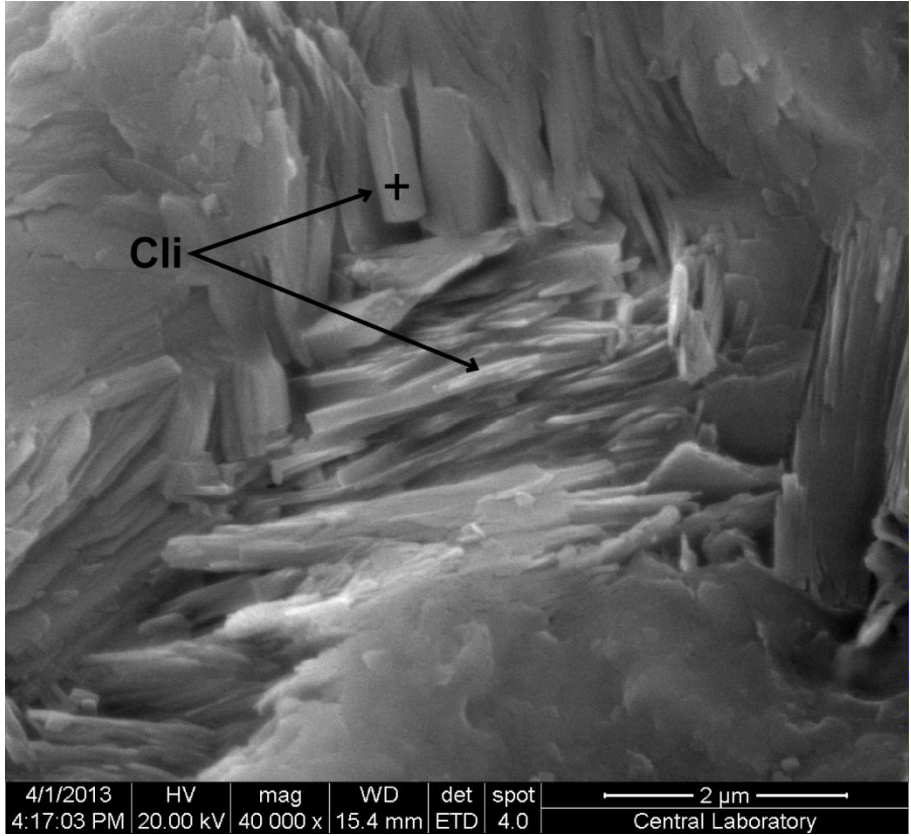


Figure 5.17 Scanning electron micrograph of clinoptilolite aggregate and corresponding EDX spectra (Sample: CLI-B, Cli: clinoptilolite).

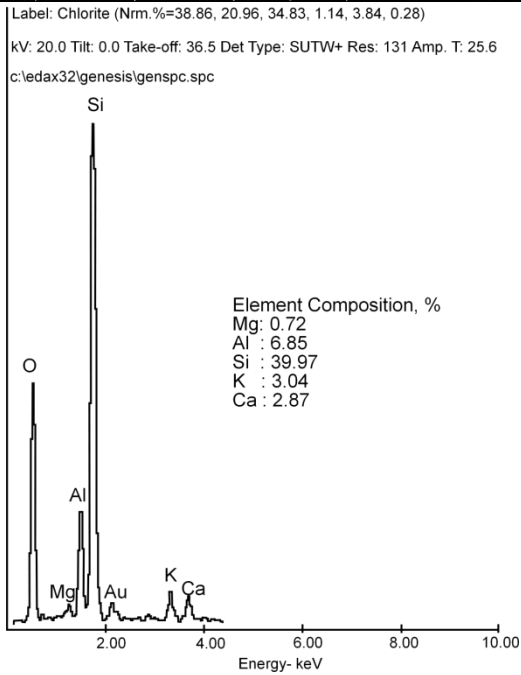


Figure 5.18 SEM image sample showing anhedral to subhedral clinoptilolite aggregates and corresponding EDX spot (Sample: CLI-B, Cli: clinoptilolite).

In nature, mordenite occurs as thin elongated fibers (Mumpton and Ormsby, 1978). In Figure 5.19, well-formed mordenite crystals are present as needles or fibers on the edge of pumice fragment. Image of sample also shows that mordenite crystals are formed as a consequence of direct alteration of volcanic glass. Identification of mordenite is based on morphology.

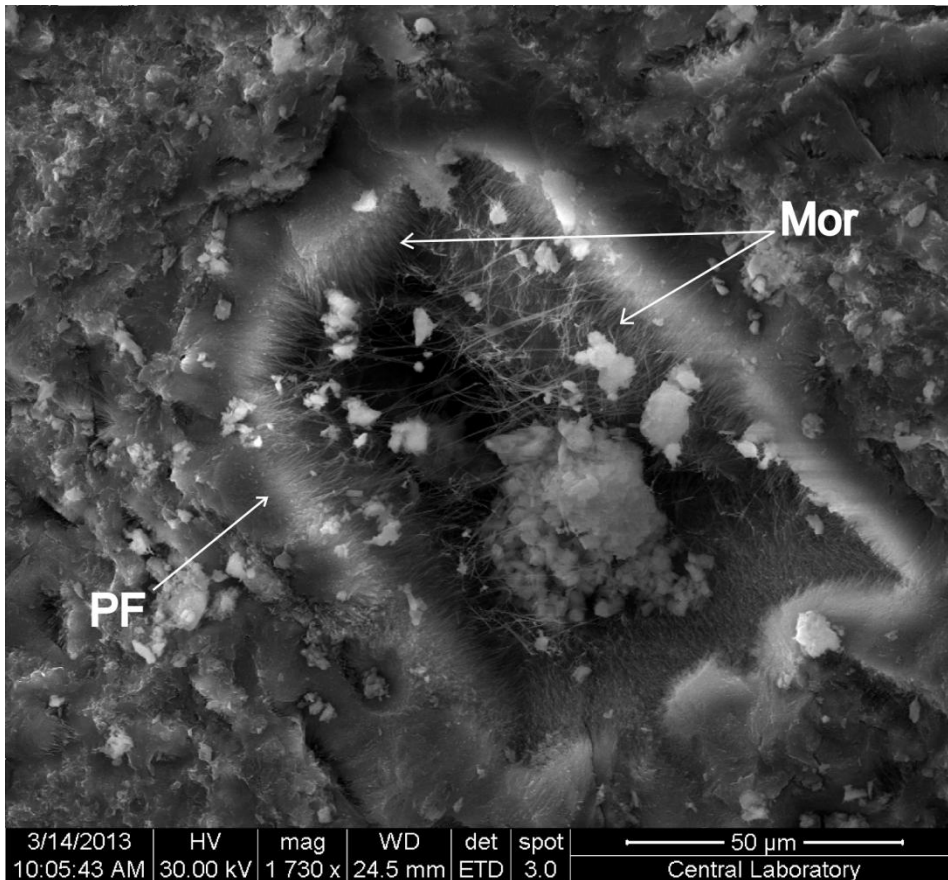


Figure 5.19 SEM image shows mordenite needles growing on the edge of the volcanic glass shard (Sample: MOR, Mor: mordenite PF: pumice fragment).

Figure 5.20 shows the higher magnification of mordenite of Figure 5.19. Mordenite needles/fibers, approximately 2 μm in diameter, are well presented.

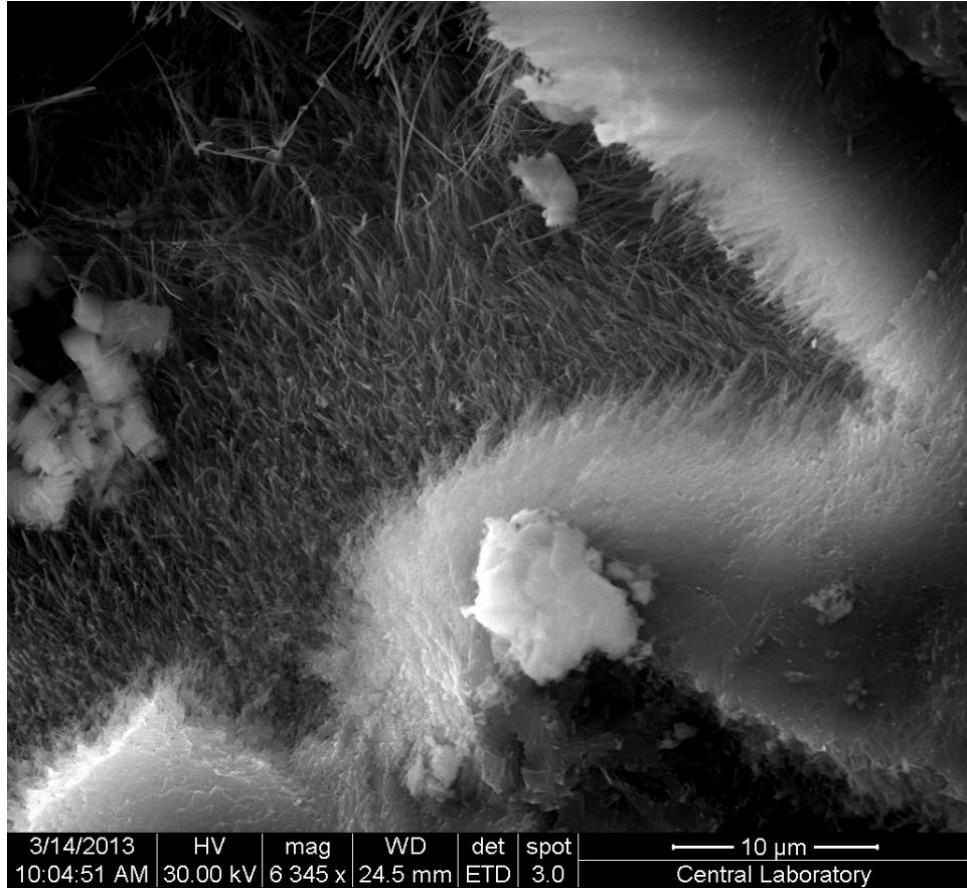


Figure 5.20 SEM image showing characteristic morphology of mordenite (Sample: MOR).

Figure 5.21 shows elongate needles/fibers of mordenite at higher magnification. Individual crystals of mordenite are 2-10 μ m in long and less than 0.2 μ m wide.

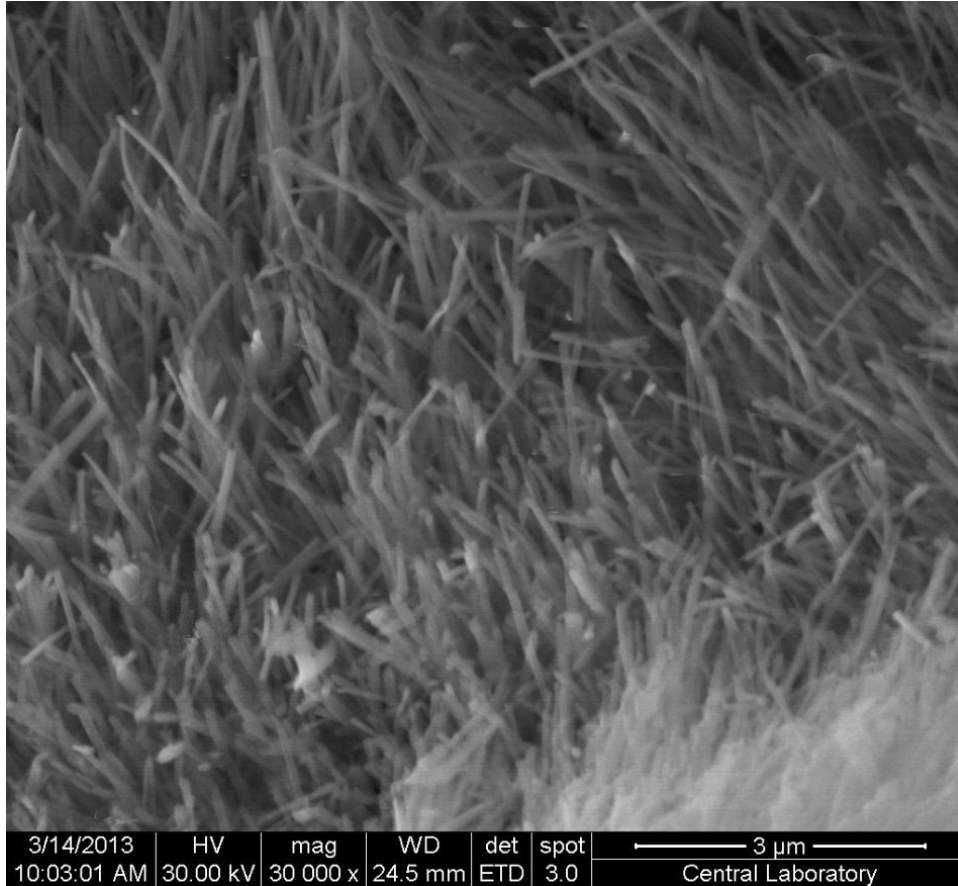


Figure 5.21 Scanning electron image of fibers of mordenite at high magnification (Sample: MOR).

In Figure 5.22, analcime occurs as cubo-octahedral crystal, which is $\sim 3 \mu\text{m}$ in diameter (Gottardi and Galli, 1985; Klein, 2002). Quartz exhibiting a trigonal trapezohedron crystal, a typical morphology for the quartz is seen on the left upper part of the image (Tröger, 1982). Smectite is known by its honeycomb arrangement and illustrated as well-formed crystals on the right corner of the image. Identification of analcime is based on morphology.

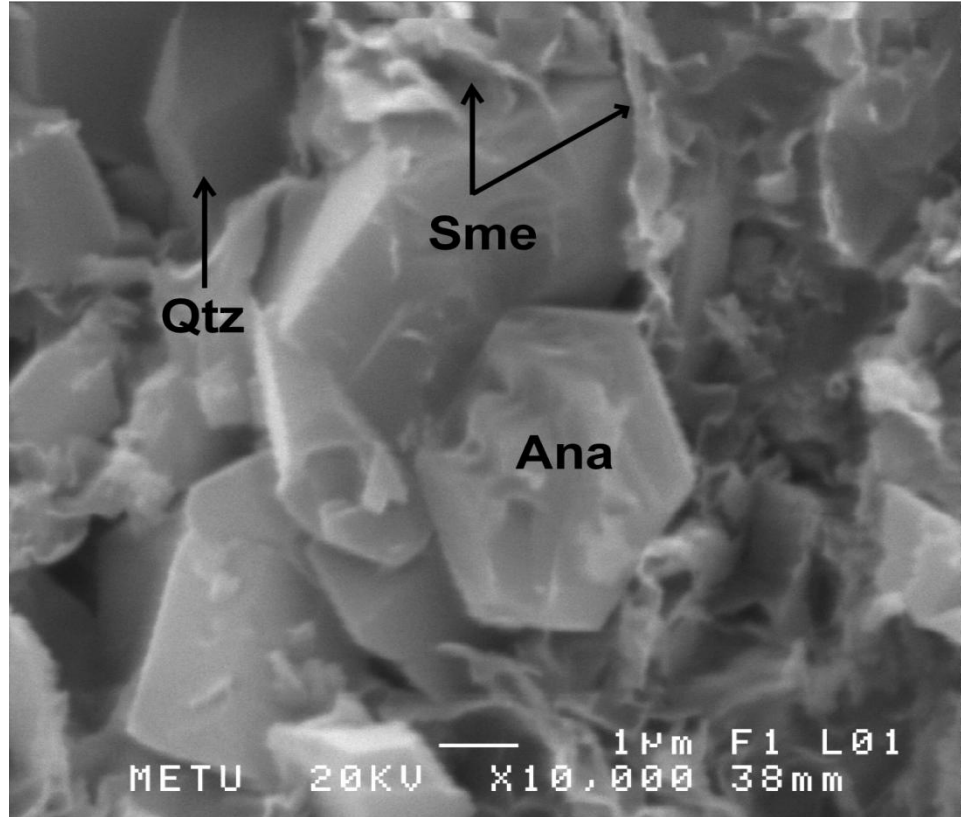


Figure 5.22 Scanning electron micrograph of cubo-octahedral analcime. Honeycomb smectite and quartz are also present (Sample ANA, Ana: analcime, Sme: smectite, Qtz: quartz).

5.2 Pozzolanic Reaction Evaluation

Pozzolanic activity of zeolite bearing tuffs was evaluated by thermogravimetric analysis (TG) and Fratini's test. Fratini's test is a quick method to understand whether the material is pozzolanic or not. Thermogravimetric method, on the other hand, gives quantitative results. Because Fratini test is a standard method, TG and Fratini's test was compared to see validity of TG method. Results of the experiments were presented below.

5.2.1 Thermogravimetric Analyses of Zeolitic Tuffs

TG was used in order to determine the amount of fixed lime ($\text{Ca}(\text{OH})_2$) present in the system, which determine the pozzolanic activity directly. Figure 5.23 presents the results of the thermogravimetric analysis on the hardened lime-tuff after curing for 3, 7, 28, 56, 90 and 180 days. The calculation method of the calcium hydroxide ($\text{Ca}(\text{OH})_2$) is described in section 7.3.1.1. Data are presented in form of plots, reporting the fixed lime percentage, which is a measure of the advancement of pozzolanic reaction. For all the pastes, it was noticed that the amount of fixed lime increases gradually with age and the pozzolanic reaction still proceed, as proved by the continuous increase of lime consumption. Also, it is worth noting that for all blended pastes while reaction progresses with time, the rate of reaction decreases especially after 28 days. The figure shows that clinoptilolite-rich tuffs are more reactive than the other zeolitic samples. In fact examining the thermogravimetric data point out that the pozzolanic activity follows this sequence:



CLI-G has the fastest lime consumption than all the other tuffs at the initial stages of the reaction, as can be deduced from the initial slope of the curves. In fact it is able to fix about 50% of the initial lime in only seven days, showing a high pozzolanic activity. The fixed lime values in seven days are 45.15%, 36.1%, 28.53% and 17.45% for the CLI-A, CLI-B, MOR and ANA, respectively. Even though the amount of fixed lime is different, the trend of the fixation of lime in CLI-A is the same as the CLI-G. Therefore, it can be concluded that the specific surface area which is significantly higher in CLI-G than CLI-A enhances the degree of reaction during initial period (before 3 days). As seen in Figure 5.23, the amount of fixed lime in CLI-B increases gradually at early hydration age but, after 90 days lime fixation remain nearly stable. Apparently, CLI-B does not has the same pozzolanic activity behavior with respect to CLI-G and CLI-A at long term hydration age. CLI-G and CLI-A comprise clinoptilolites with higher Si/Al ratio than CLI-B indicate that lime fixation seems to be mainly governed by Si/Al ratio at longer ages (Drzaj, 1978; Uzal et al., 2010; Mertens et al., 2009; Massazza, 1998). The lower pozzolanic activity of MOR can be explained by the lower zeolite content of mordenite and bearing tuff (Table 5.5). ANA shows the lowest fixed lime ability for all tested ages. However this situation was expected, as analcime with its denser crystal structure shows lower reactivity (Tsitsishvili, 1992). Since considerable amount of volcanic glass, which generates additional

effects on pozzolanic reaction in addition to zeolite was identified in MOR and ANA (Table 5.5), it was not preferred to correlate physical and chemical properties of mordenite and analcime. After 120 days of hydration, 78.67%, 76.47%, 58.26%, 50.51%, 37.67% of fixed lime is detected in CLI-G, CLI-A, CLI-B, MOR, ANA, respectively.

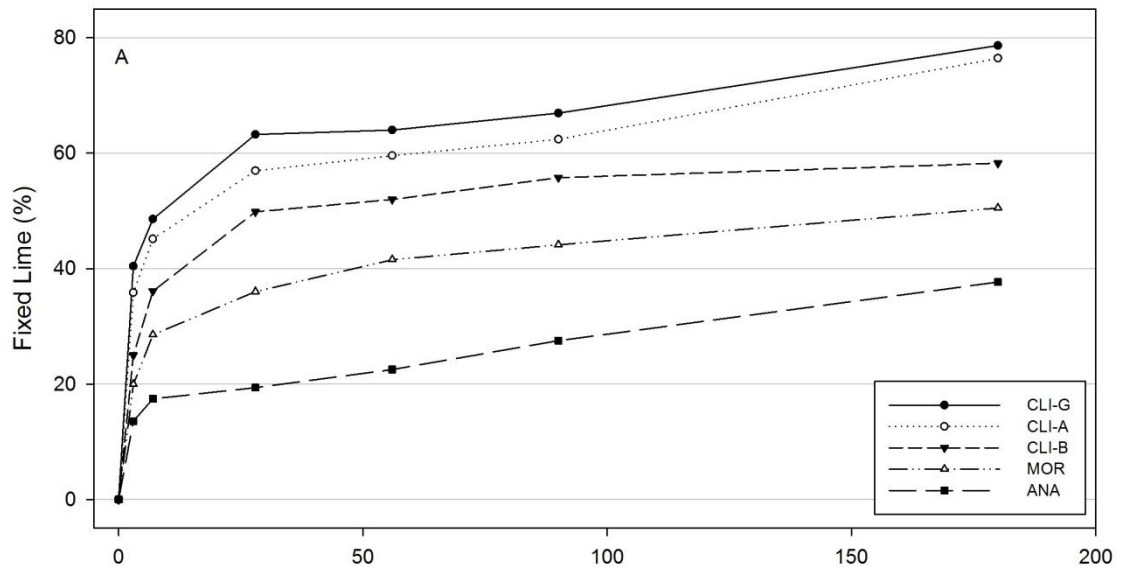


Figure 5.23 Amounts of fixed lime in zeolitic tuff-lime pastes.

5.2.2 Thermogravimetric Analyses of Exchanged Zeolitic Tuff

The cation content of the zeolites is an important parameter which influences the pozzolanic activity (Huizhen, 1992; Caputo et al., 2008; Mertens et al., 2009). Figure 5.24 shows the pozzolanic activity results of the sample CLI-B with comprehensively exchanged Na^+ , K^+ and Ca^{2+} . It is important to emphasize that all variables were considered to be constant except compositional difference for exchanged zeolitic tuff. The amount of fixed lime of monocationic tuff samples is nearly similar up to 28 days of hydration. But afterwards, the composition of exchanged zeolite start to affect pozzolanic reactivity as can be seen in Figure 5.24. At longer period (90 days), K^+ exchanged paste shows the best pozzolanic activity in terms of reacted lime. The higher pozzolanic activity of K^+ exchanged tuff at later ages could be explained by a higher pH of the pore solution. The pH of the pore solution is considered as an important parameter on pozzolanic reaction since a higher pH generates an increased solubility of silica (Urhan, 1987; Fraay et al., 1989). Distinctively, the pozzolanic activity of Na^+ -exchanged sample after 28 days progress very slowly when compared to the other exchanged samples. Although it was understood that type of cation content has an important effect on long term reactivity, the reason for the differences of the pozzolanic activity of samples including different cations is unclear.

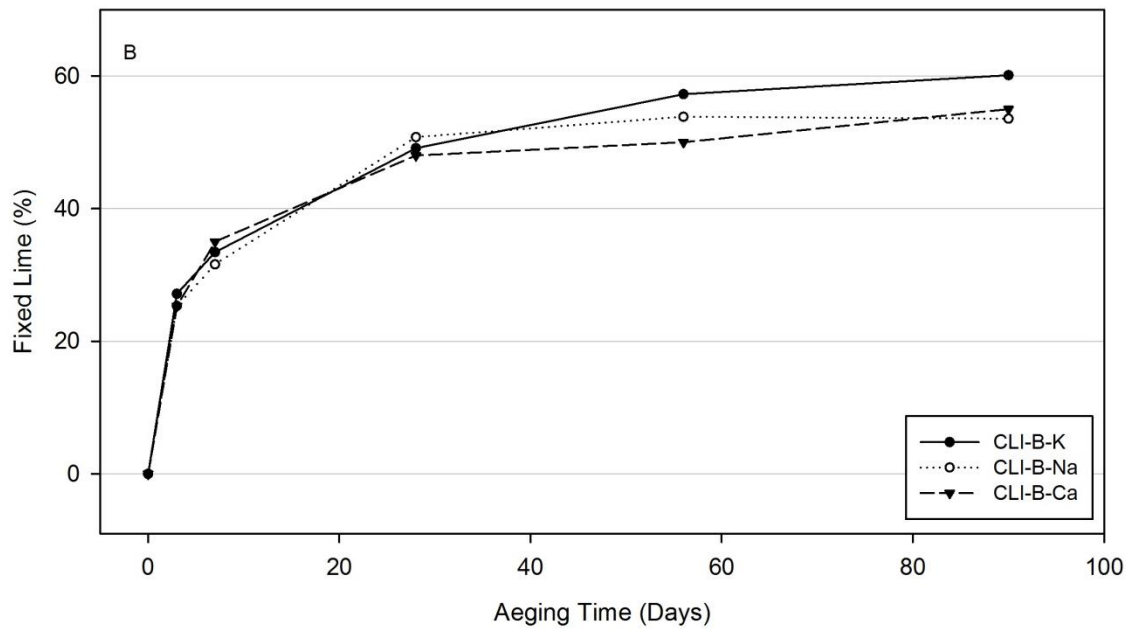


Figure 5.24 Amounts of of fixed lime in CLI-B exchanged with K^+ , Na^+ and Ca^{2+} cations-lime pastes.

5.2.3 Fratini's Test

Fratini's test is the fast chemical method to test pozzolanicity of material recognized in the European Standards (EN 196-5). The results of Fratini's test, representing the lime concentration of the solutions in contact with the blended cements are presented in Figure 5.25. Apart from ANA sample, all points fall below the $Ca(OH)_2$ solubility curve, indicating that contact solutions are found to be under-saturated in portlandite, which means that some of Ca^{2+} resulting from the pozzolanic activity was fixed by the zeolitic tuff. Therefore, it is possible to classify all the blended cements prepared with zeolitic tuffs as pozzolanic cements. Note that for the analcime-bearing sample, the Fratini's test is negative after 8 days, but positive after 15 days. The observed negative result of analcime at 8 days is undoubtedly due to the very dense nature of crystal structure.

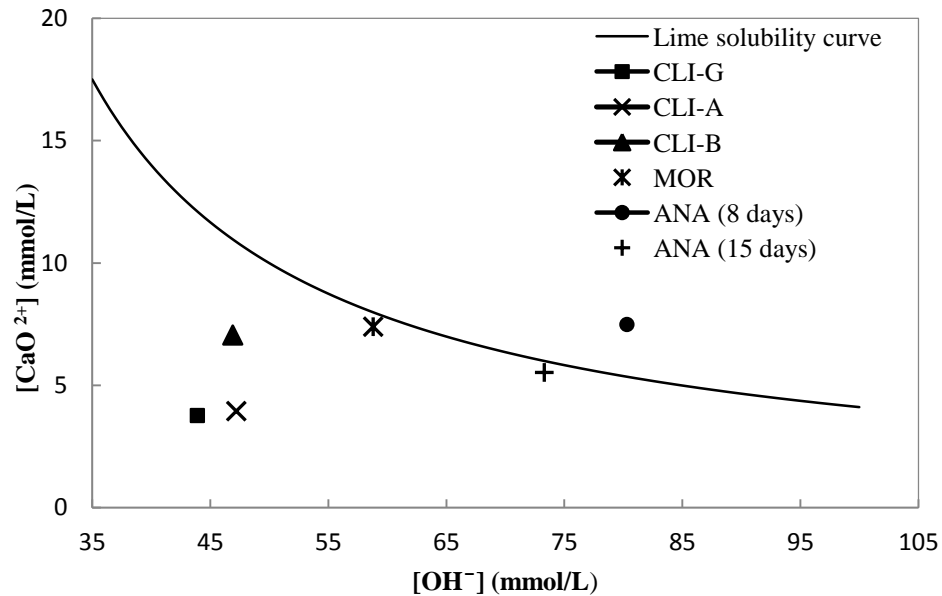


Figure 5.25 Results of Fratini's test to evaluate pozzolanicity of blended cements.

5.2.3.1 Comparison of Fratini's Test and Thermogravimetric Analysis

The pozzolanic activity of zeolitic tuffs was compared with the Fratini's test and the thermogravimetric method. Quantified Fratini's test results are shown in Table 5.6, which is calculated using equation 4.3 explained in chapter 7.3.1.3.1. Thus, quantitative assessment of Fratini's test also allows understanding not only whether the material is pozzolanic or not but also it allows to identify the degree of pozzolanicity like TG. As can be seen in Table 5.6, the Fratini's test gives identical pozzolanic activity distributions with thermogravimetric results. CLI-G is the most reactive pozzolan with 68.9% [CaO] reduction followed by CLI-A, CLI-B, MOR and ANA. In fact, ANA (8 days) gives greater [CaO] value than theoretical maximum [CaO] concentration as expected since it plots over the lime solubility curve from Fratini's test (Figure 5.25). As the negative value obtained from 8 days was not valid, ANA was excluded from correlation graph.

Table 5.6 Fratini's test results quantified using Equation 4.3.

Zeolitic tuffs	[OH] mmol l ⁻¹	[CaO] mmol l ⁻¹	Theoretical max. [CaO] mmol l ⁻¹	[CaO] reduction %
CLI-G	43.9	3.77	12.11	68.9
CLI-A	47.2	3.95	10.87	63.7
CLI-B	46.9	7.06	10.97	35.7
MOR	58.8	7.4	7.99	7.4
ANA (8 days)	80.3	7.49	5.36	-39.73
ANA (15 days)	73.3	5.53	6	7.9

After the calculation of the numerical values, the results were plotted on the correlation graph from Fratini's test after 8 days and thermogravimetric method after 7, 28 and 90 days (Figure 5.26). Comparison was performed with regard to the correlation coefficient (R^2), which is determined from regression analysis. The values near to zero indicate poor correlation whereas the values close to one prove high correlation. Since the correlation coefficients of three straight lines range from 0.97 to 0.99, it is deduced that there is significant correlation between the two test methods for pozzolanic activity. Since the Fratini test has a standard procedure (EN 196:5), this correlation also proves the validity of TG analysis.

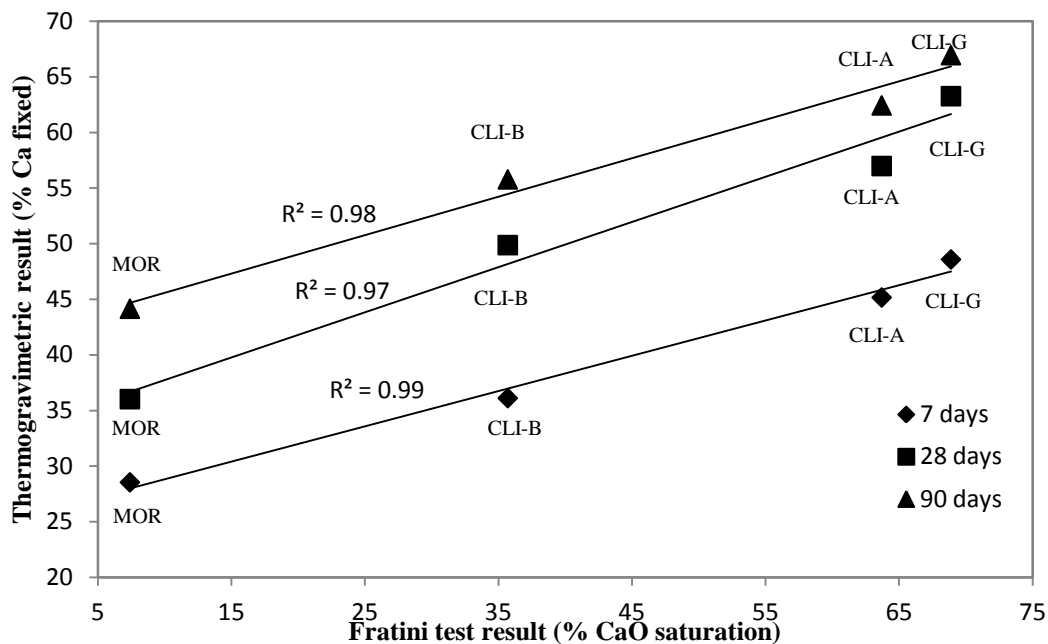


Figure 5.26 Correlation between pozzolanic activity of Fratini's test (8 days) and thermogravimetric analysis (7, 28 and 90 days).

5.2.4 Kinetic Analyses

The examination of the pozzolanic reaction kinetics was made by modified Jander Equation, which is one of the most commonly used models (Villar-Cocina, 2006).

The results of kinetic analyses were displayed by the plots of equation 4.2 using the fixed lime data obtained from thermogravimetric analysis (e.g. Shi and Day, 2000). Figure 5.27 shows the data from Figure 5.23. The slopes of the curves are the reaction grade N . The CLI-G and CLI-A samples show a similar trend of reaction kinetics with normalized slopes of 4.76 and 4.48, respectively. This means that the specific surface area, which is the main difference between two samples, has influence on the consumption of lime mainly during the initial period (before 3 days), whereas it did not affect reaction mechanism thereafter (Mertens et al., 2009). CLI-B, on the other hand, has different pozzolanic reaction behavior. The data is best represented by two steps. Between 3 and 28 days, the lower part of curve with a slope of 2.03 was determined. After that the upper part of the curve with a slope of 8.62 started. The higher reaction progress of CLI-B at longer ages is attributed to the lower Si/Al ratio. From this investigation, it can be concluded that Si/Al ratio has a powerful effect at longer dates (Drzaj et al., 1978; Mertens et al., 2009; Uzal et al., 2010; Massazza, 1998). Looking at the other zeolites, MOR displays two lines, one with a slope of 2.15 and the other with a slope of curve is 4.79. ANA shows only one trend with a slope of 4.16. The kinetic analysis according to the modified Jander equation indicated that only one process controlling the reaction mechanism was observed; the diffusion of reactants through a layer of dense reaction products (Phase III). Phase I and Phase II, however, were absent in all the samples. It was predicted from these data that they might have ended before 3 days of hydration.

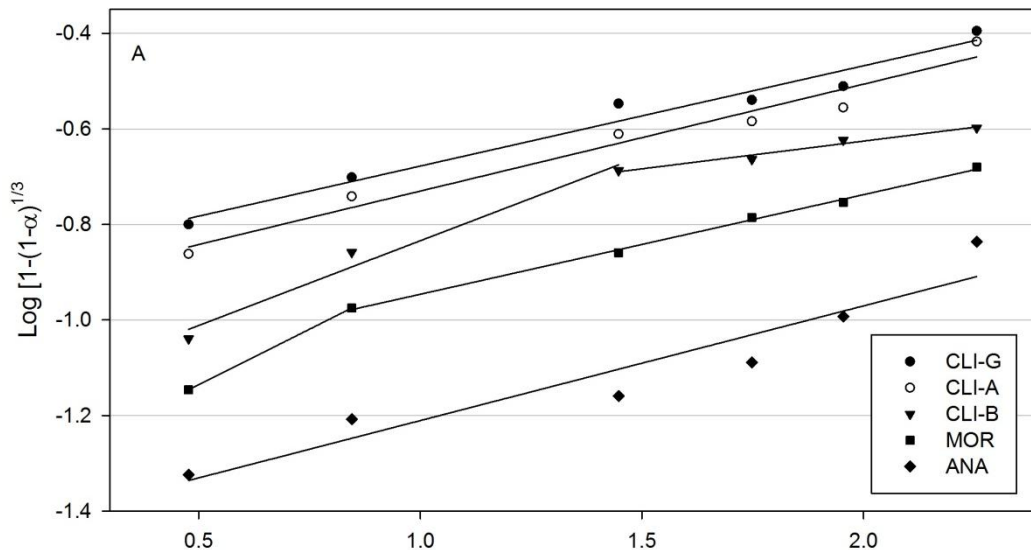


Figure 5.27 Pozzolanic reaction kinetics in zeolitic tuff-lime pastes.

Figure 5.28 shows the reaction kinetics of CLI-B exchanged with Na^+ , K^+ and Ca^{2+} cations. Reaction kinetic in the CLI-B- K^+ exhibits one trend with a slope of 3.36, CLI-B- Ca^{2+} and CLI-B- Na^+ , however, display two trends. The exchangeable cation content mainly influences the pozzolanic activity after 28 days of hydration. K^+ -exchanged sample displays the lowest reaction grade (N) and Ca^{2+} -exchanged one has slightly higher than K^+ . Na^+ -enriched sample, on the other hand, results in a clear increase of the reaction grade after 28 days. This means that the presence of K^+ in the system has a profound influence on the lime fixation capacity as the reaction advances. However, the behavior of pozzolanic reaction is significantly changed by introduction of Na^+ . Although the graph proves that the cation content is an important phenomenon on pozzolanic reaction at longer hydration ages, further research is needed to understand the way of effect on reaction mechanism.

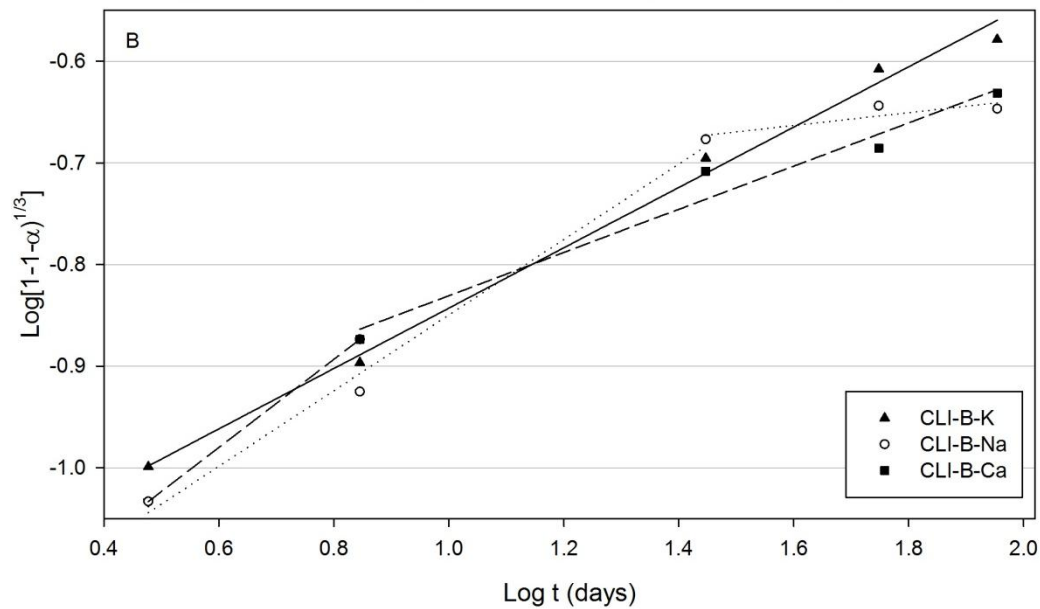


Figure 5.28 Pozzolanic reaction kinetics in CLI-B exchanged with K^+ , Na^+ and Ca^{2+} cations-lime pastes.

5.3 Reaction Products

The reaction products of pozzolanic activity are similar to that of products of hydrated Portland cement (Sersale, 1980; Massazza, 1998). According to Mehta and Monteiro (2006), reaction products are commonly CSH with small amounts of CAH.

5.3.1 XRD Analyses of Hardened Lime-Zeolite Pastes

Zeolitic tuff-lime hardened pastes were investigated by means of X-ray diffraction (XRD) analyses to determine the preexisting and new crystalline phases. Since intensities of diffraction peaks can yield significant information about the hydration, the peak heights were correlated in order to examine the progress of hydration from 3 days to 180 days. The degree of pozzolanic activity was further compared by peak heights of all blended cements at the same periods of hydration (180 days). Bulk material was used as reference material to see mineralogical changes.

Figure 5.29 shows the powder diffraction pattern of clinoptilolite-rich tuff (CLI-G) and corresponding blended cement hydrated for 3 days (CLI-G-R). Initially, clinoptilolite peaks (Treacy and Higgins, 2001) were identified by 2θ of 9.72, 11.12, 12.98, 17.27, 18.96, 22.37, 24.96, 25.94, 28.07, 30.00 and 31.93 with d -spacing of 9.09, 7.95, 6.81, 5.13, 4.67, 3.97, 3.56, 3.43, 3.17, 2.98 and 2.80 Å, respectively. Most intense peak of quartz (3.35 Å) near the clinoptilolite peak (3.33 Å) is hardly distinguished (JPDS, 1983). Besides, the peak of quartz with d -spacings at 2.13 Å overlaps with clinoptilolite's peak. Portlandite (Taylor, 1990) was identified by 2θ of 18.07, 28.65, 34.09, 47.10, 50.80 and 54.28 with d -spacing of 4.90, 3.11, 2.63, 1.93, 1.79 and 1.69 Å, respectively. The intensity of CSH (Taylor, 1990) peaks appeared at 3.04 and 1.85 Å. Hydrotalcite (Taylor, 1990) is determined by d -spacing at 7.59 Å. As can be seen in Figure 5.29, the intensity of diffraction peak of clinoptilolite markedly decreases when hydrated. The decreasing intensity of clinoptilolite peaks on XRD patterns confirms the dissolution and/or decomposition of clinoptilolite structure and participating pozzolanic reaction. The graph also indicates that the intensity of portlandite, CSH and hydrotalcite peaks appear after 3 days of curing.

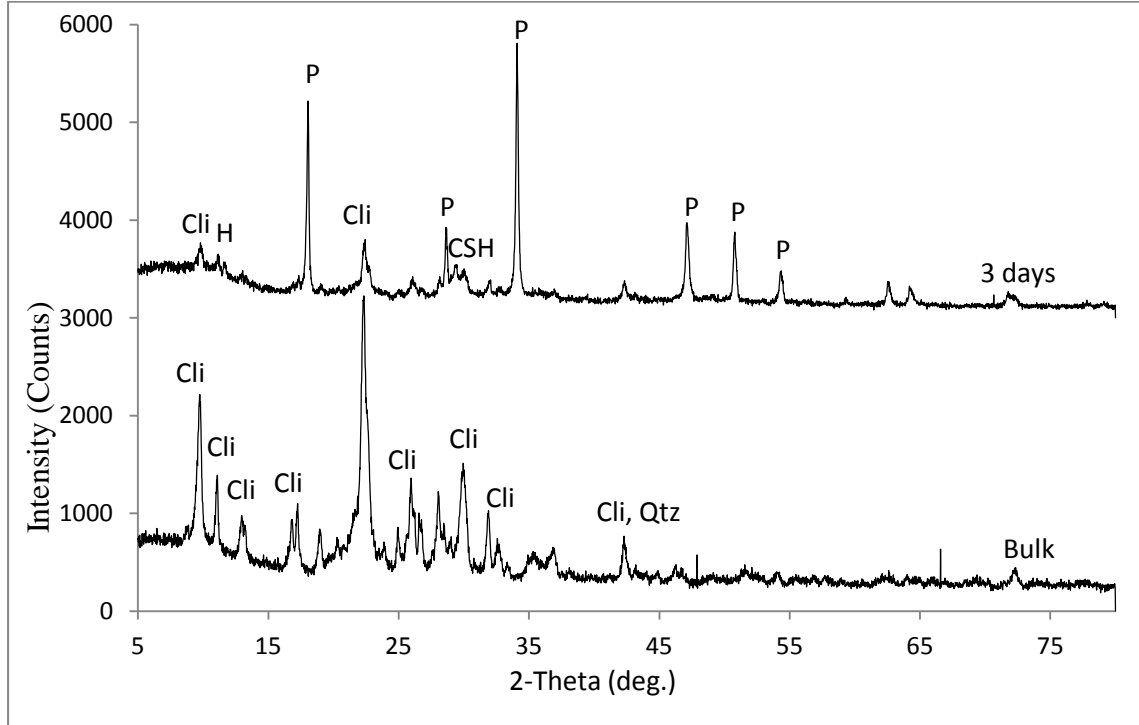


Figure 5.29 X-ray diffraction patterns of bulk material (CLI-G) and hardened paste (CLI-G-R at 3 days) (P: portlandite, Cli: clinoptilolite, H: hydrotalcite, Qtz: quartz).

Similar crystalline species in 2θ range were obtained from bulk material and corresponding blended cement pastes (3 days) of CLI-A (Figure 5.30a) and CLI-B (Figure 5.30b) samples. Clinoptilolite peaks can be easily differentiated from bulk material and distinctive reduction of the intensity of clinoptilolite peaks was also noticed. After 3 days of hydration, portlandite, hydrotalcite and CSH peak visible on the diffractogram. The similarity of XRD pattern for all clinoptilolite blended cements was expected because identical peak patterns are likely among the mixing of similar starting and lime phase content.

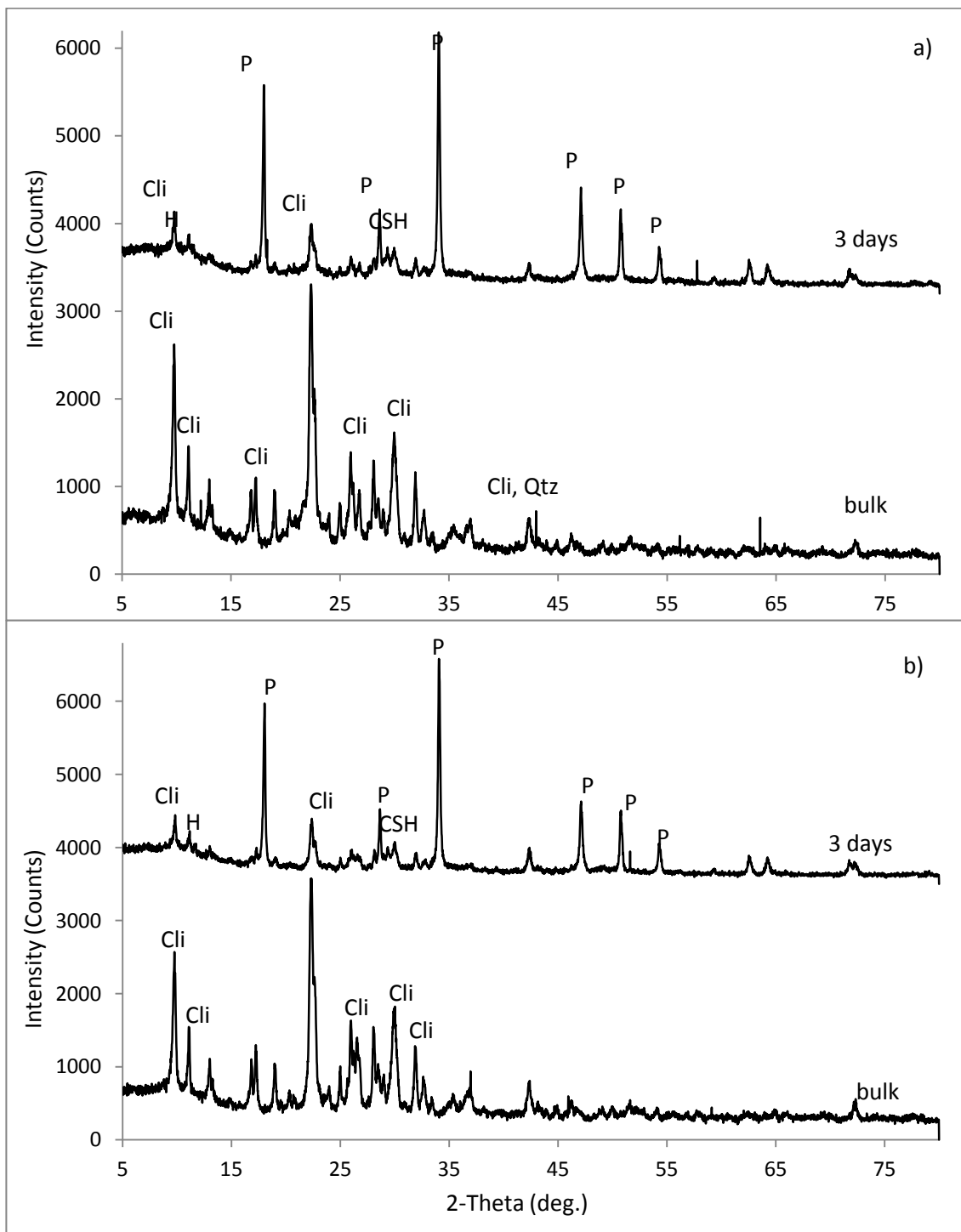


Figure 5.30 XRD patterns of a) CLI-A (bulk) and CLI-A-R (3 days), b) CLI-B (bulk) and CLI-B-R (3 days).

In Figure 5.31, the XRD patterns of bulk materials and corresponding hydrated blends at 3 days from MOR and ANA are presented as well. Mordenite reflections (d -spacing of 9.10, 4.53, 4.00, 3.47, 3.38, 3.23 and 2.90 Å with 2θ of 9.71, 19.57, 22.19, 25.63, 26.30, 27.60 and 30.82, respectively) are defined in the XRD pattern of bulk material (Figure 5.31a) (Treacy and Higgins, 2001). The hydrotalcite peak at 7.59 Å and the CSH ones at 3.03 Å are determined. Although some K-feldspar peaks (JPDS, 1983) overlap with diagnostic mordenite peaks (d -spacing of 6.59, 3.47 and 3.23), some of them (d -spacing of 3.79, 3.00 and 2.58 Å) differ. The peak of quartz with d -spacing at 4.25, 3.34 and 2.13 Å was also observed. The diffraction pattern of bulk material of ANA shows peaks at the d -spacing of 5.60, 4.85, 3.42, 2.92, 2.49, 2.22 and 1.74 Å, which were assigned to analcime (Figure 5.31b) (Treacy and Higgins, 2001). The characteristic peak of quartz was found at d -spacing of 3.34, 2.28, 2.13 and 1.82 Å. The most distinctive reflections of quartz were found in ANA. In addition, the d -spacing for K-feldspar was obtained at 3.80, 3.47, 3.23, 2.99 and 2.58 Å. The main peaks of K-feldspar (3.33 °A and 4.24 °A), on the other hand, overlaps with peaks of quartz.

The reduction of the intensity of mordenite and analcime peaks was also determined for these blends. Significant decrease in intensity of zeolite peaks at 3 days pattern is evidence that mordenite and analcime-bearing tuffs have a pozzolanic activity. There is in good agreement between the results of thermogravimetric and XRD analysis.

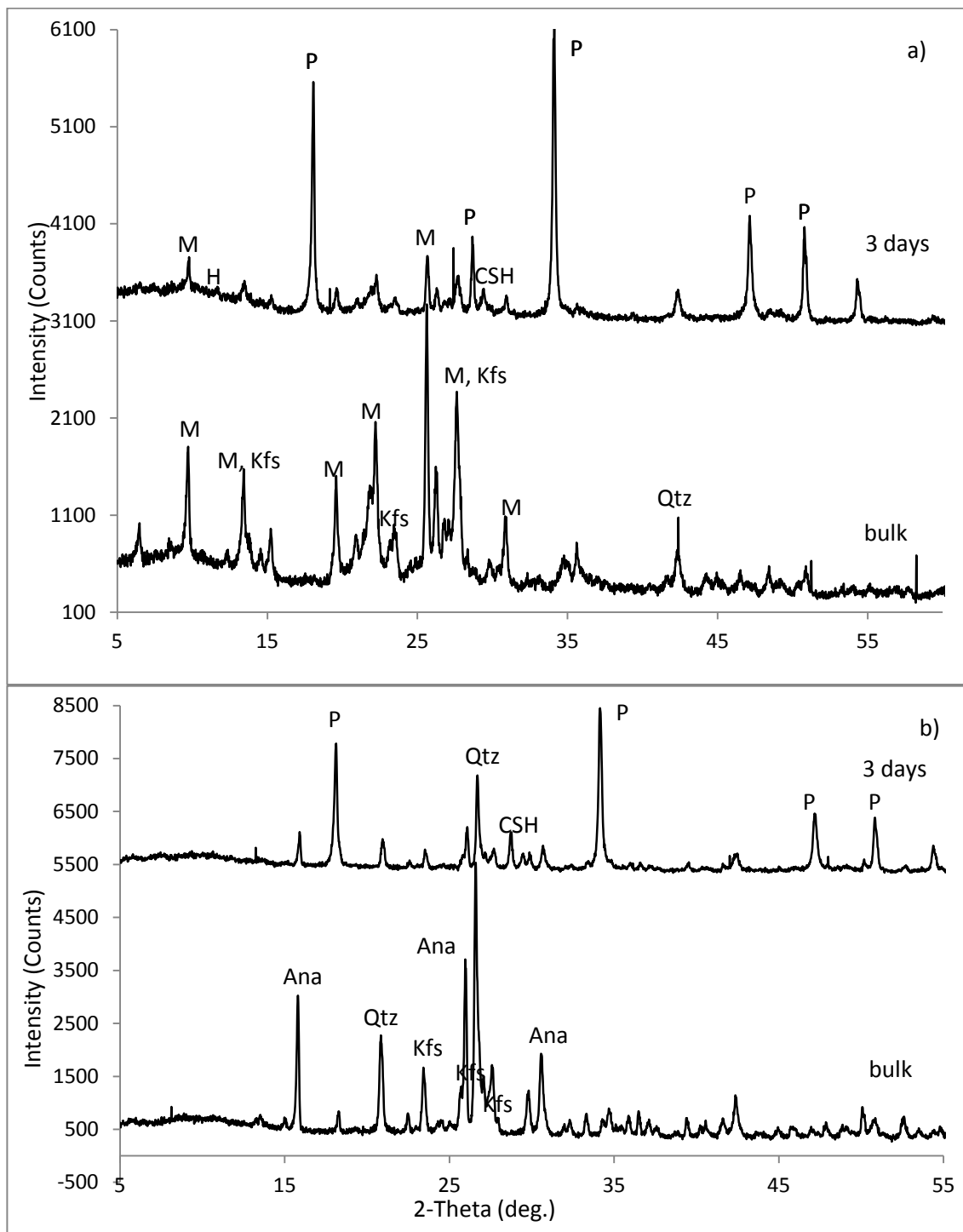


Figure 5.31 X-ray diffraction patterns and identified phases of a) MOR (bulk) and MOR-R (3 days), b) ANA (bulk) and ANA-R (3 days) (Mor: mordenite, Ana: analcime, Qtz: quartz).

Figure 5.32 presents the XRD patterns of the sample CLI-G-R at ages 3 days to 180 days. Figure 5.32 shows that the relative peak intensity of portlandite decreases gradually from the 3 days of hydration. This event is related to its consumption while the hydration goes on. The formation of CSH ($d = 3.04 \text{ \AA}$) which is the principal hydration product (Taylor, 1990; Massazza, 1998; Mehta and Monteiro, 2006) is detected in all samples even after 3 days of hydration. As the reaction advance, the intensity of diffraction peak of the CSH increases. A gradual increase of CSH peaks suggests a progression in crystallinity of CSH with ageing. It should be noticed that hydrotalcite type hydration product was also observed as a new crystalline phases for all pozzolanic reaction ages in all blended cements. Peak intensity of hydrotalcite generally is constant with time. An obvious reduction of the clinoptilolite peaks demonstrate the dissolution and/or decomposition of the clinoptilolite structure and the involvement of the zeolite phase in the pozzolanic activity (e.g. Perraki et al., 2005; Caputo et al., 2008; Uzal and Turanlı, 2012). Peak identification of C_4AH_13 (Taylor, 1990) is much difficult because of overlapping with clinoptilolite peak.

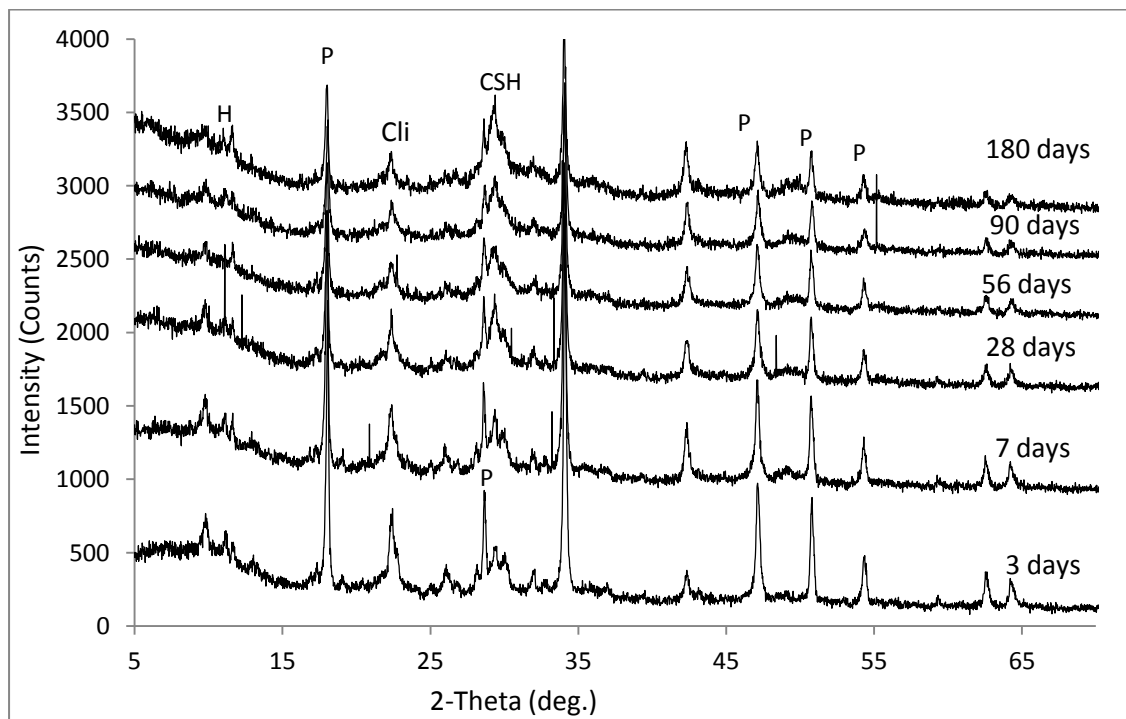


Figure 5.32 X-ray diffraction patterns and identified phases of the CLI-G-R at ages 3 days to 180 days (P: portlandite, Cli: clinoptilolite, H: hydrotalcite).

X-ray patterns on Figure 5.33 shows the same phase development taking place in CLI-A-R and CLI-B-R blends as CLI-G-R. Namely, the peak intensity of portlandite and clinoptilolite decrease while CSH peak increases during the ongoing hydration. The only difference between the three clinoptilolite blends is the peak height. In CLI-G-R, increase in crystallinity of CSH from 3 days to 180 days is better observed than CLI-A-R and CLI-B-R. Furthermore, the peak

intensity of clinoptilolite and portlandite in CLI-G-R are much weaker than those of CLI-A-R and CLI-B-R as hydration goes on. The differences of the peak intensities on the diffraction pattern are best expressed in Figure 5.34 which correlates powdered patterns of CLI-G-R, CLI-A-R and CLI-B-R pastes at the same hydration day (180 days).

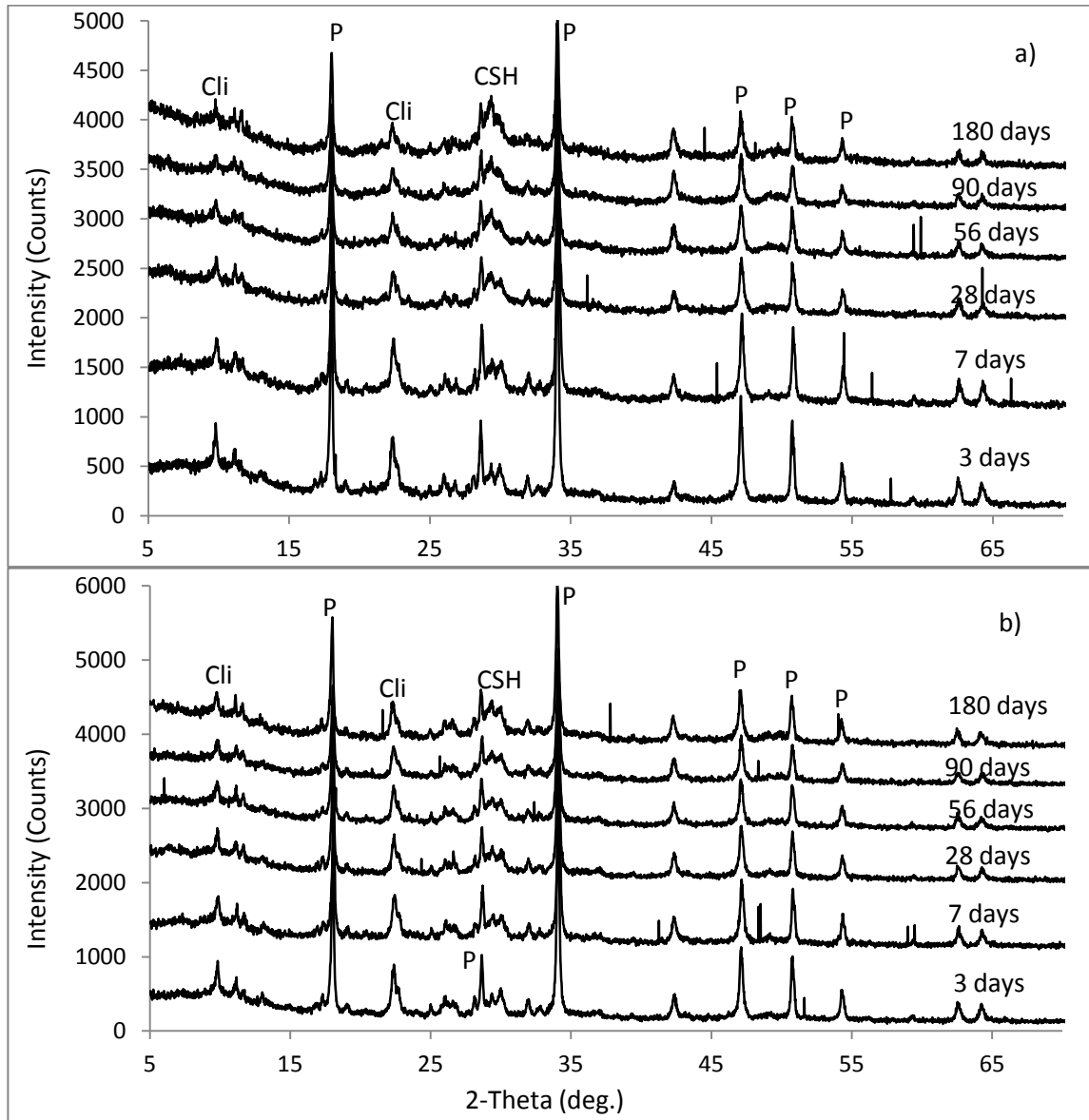


Figure 5.33 X-ray diffraction patterns and identified phases of the a) CLI-A-R, b) CLI-B-R at ages 3 days to 180 days (P: portlandite, Cli: clinoptilolite).

Figure 5.34 shows the best correlation peaks of three clinoptilolite blended pastes. CLI-G-R showed the highest consumption of portlandite and clinoptilolite. The intensity of the CSH related peak is the highest for the CLI-G-R than for the CLI-A-R and CLI-B-R.

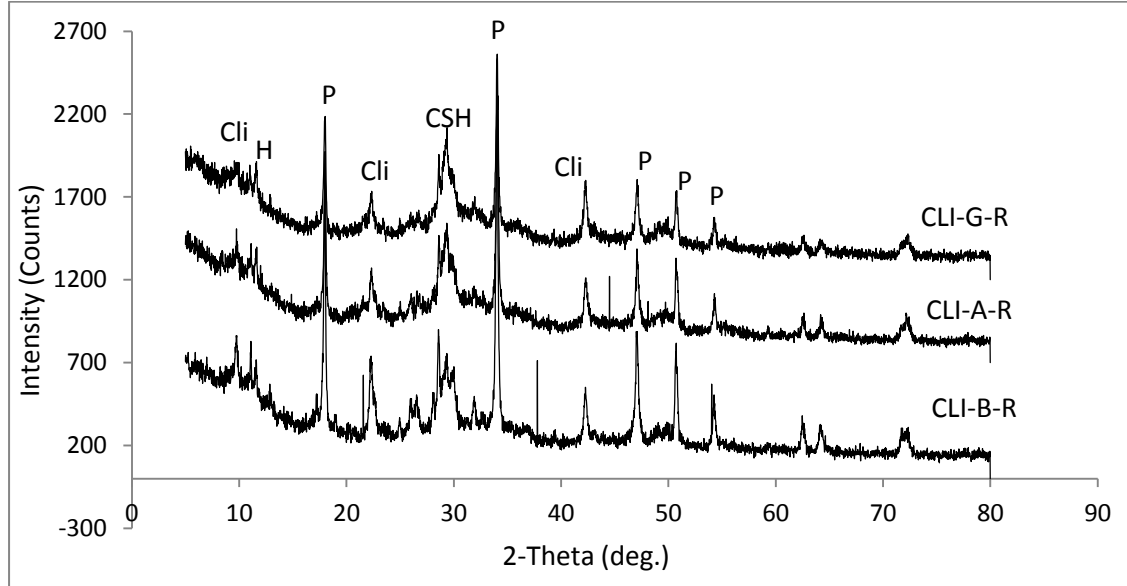


Figure 5.34 XRD patterns and identified phases of CLI-G-R, CLI-A-R and CLI-B-R at 180 days (P: portlandite, Cli: clinoptilolite, H: hydrotalcite).

In MOR-R and ANA-R blends, the very slight decline of zeolite and portlandite peak and slight incline of CSH peak are observed after 3 days age unlike clinoptilolite blends. This observation is compatible with the thermogravimetric data, which showed that clinoptilolite-rich blends are more reactive than mordenite and analcime blends. The diffraction peak of slight intensity at 8.2 Å (Taylor, 1990) of C_4AH_13 is observed in analcime and mordenite bearing pastes only after careful examination.

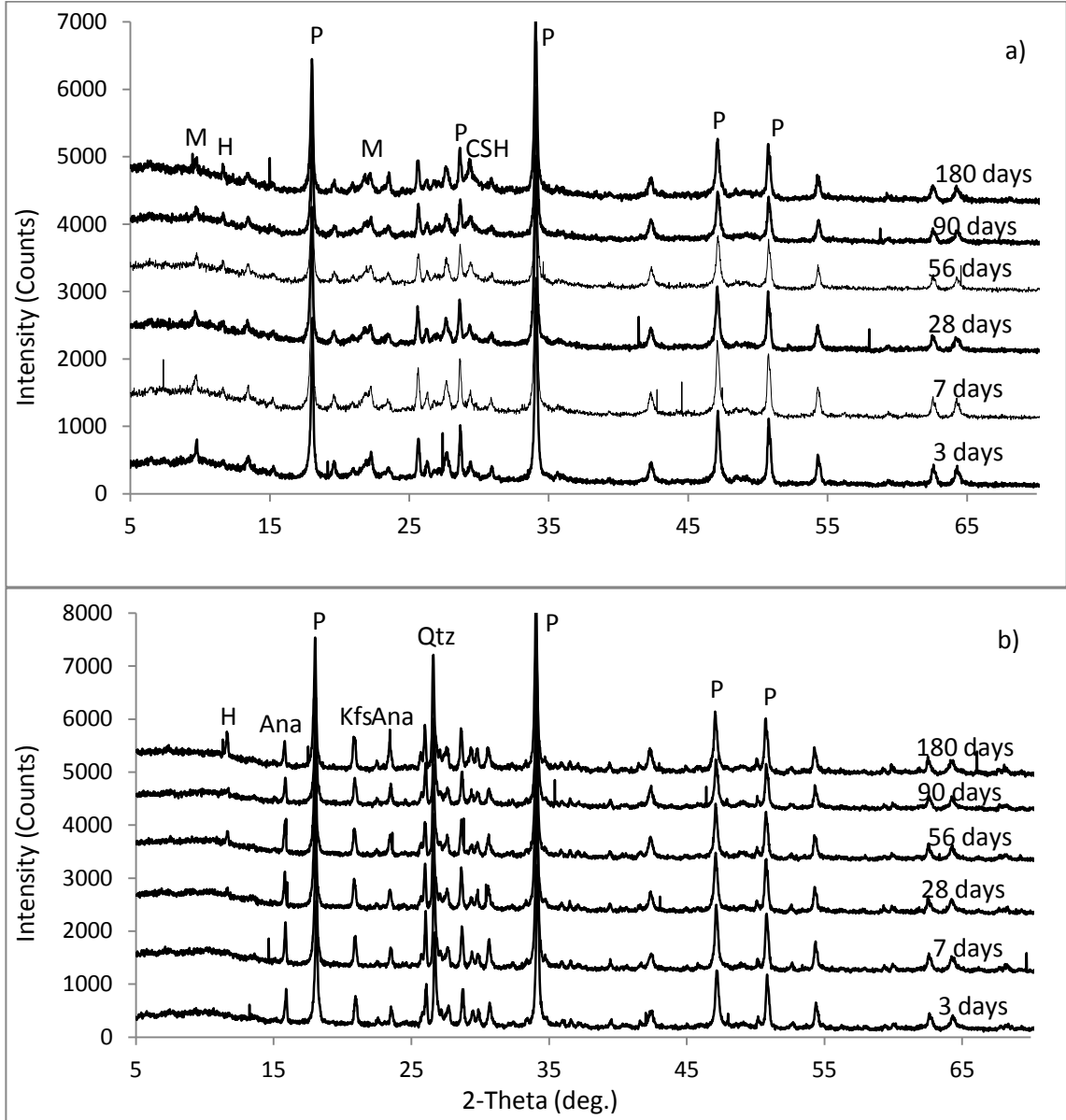


Figure 5.35 X-ray diffraction patterns and identified phases of the a) MOR-R, b) ANA-R at ages 3 days to 180 days (Mor: mordenite, Ana: analcime, P: portlandite, Kfs: K-feldspar).

The XRD patterns of the hardened lime-zeolite pastes at 180 days are given in the Figure 5.36. Although the nature of all phases is the same in the zeolite blends, the difference in the intensities of diffraction peaks was also observed in this figure. The diffraction peaks of clinoptilolite and portlandite in CLI-G-R, CLI-A-R and CLI-B-R are weaker and the peak corresponding to CSH is sharper than those of MOR-R and ANA-R, which confirms relatively higher reactivity than others as expected from the thermogravimetric analyses. Besides, it is

worth observing that the peaks of zeolite and portlandite are more evident on the patterns of MOR-R and ANA-R blends. In addition, detection of portlandite and zeolites at 180 days indicates that pozzolanic activity still continues in all pastes.

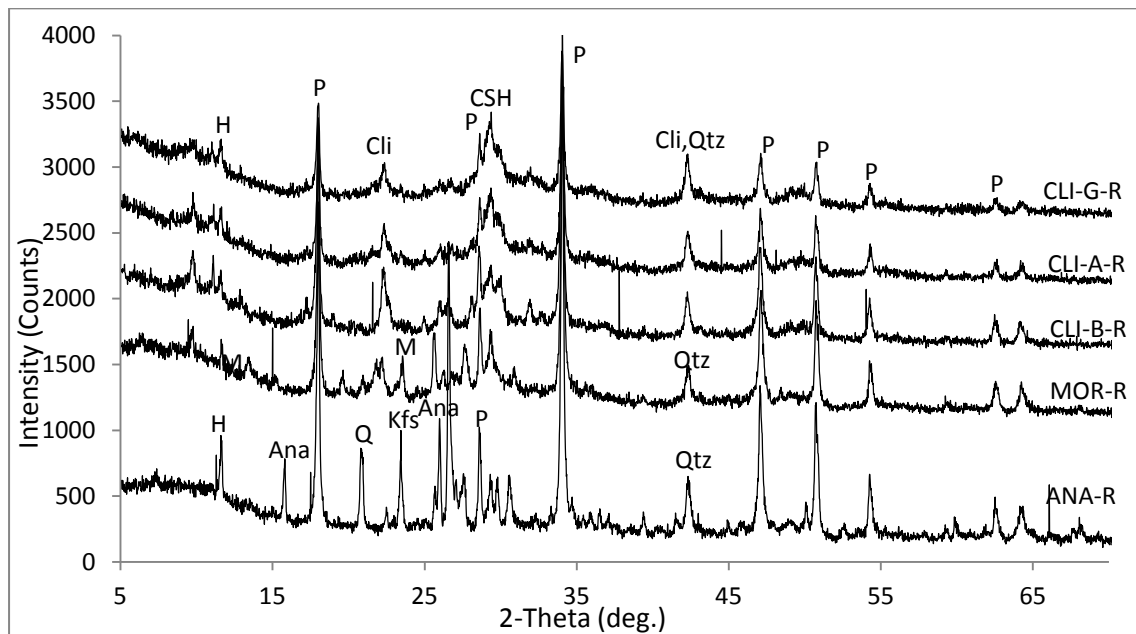


Figure 5.36 X-ray diffraction patterns and identified phases of the CLI-G-R, CLI-A-R, CLI-B-R, MOR and ANA samples at 180 days of hydration (H: hydrotalcite, Kfs: K-feldspar, Qtz: quartz, M: mordenite, Ana: analcime, P: portlandite).

5.4 FTIR Analyses of Hardened Lime-Zeolite Paste

In addition to XRD analyses, hydration products were identified by FTIR spectra. Besides, the evolution of spectral features and hydration process of hardened lime-zeolite pastes were monitored by applying the FTIR method from 3 days to 90 days. Bulk material was used as reference material to see mineralogical changes.

FTIR spectra of clinoptilolite are characterized by four groups of bands (Pechar and Rykl, 1985; Mozgawa, 2000). First area corresponds to the bands associated with lattice vibrations below 400 cm^{-1} . In the second area, bands are connected with pseudo-lattice vibrations of structural units ranged between $500\text{-}700\text{ cm}^{-1}$ (Mozgawa, 2000). The bands due to the internal Si-O-Si and Si-O-Al vibrations are observed in the range of $400\text{-}1200\text{ cm}^{-1}$. The last area in the FTIR spectrum of clinoptilolites is indicative for the presence of zeolitic water which is characteristic in the $1600\text{-}3700\text{ cm}^{-1}$ domain (Pechar and Rykl, 1985; Mozgawa, 2000, Wilson, 1994).

The qualitative FTIR spectra of bulk material (CLI-G) and corresponding hydrated blend at 3 days (CLI-G-R) have revealed the following aspects (Figure 5.37). The vibration band at 471 cm^{-1}

cm^{-1} is attributed to T-O bending mode. Band centered at 793 cm^{-1} is assigned to the stretching vibration of O-T-O group. The strongest peak at 1059 cm^{-1} is associated with the T-O stretching vibration. As stated before, the bands developed in the range between 1600 and 3700 cm^{-1} refer to water molecules in the channels of the zeolitic structure (Pechar and Rykl, 1985; Mozgawa, 2000, Wilson, 1994). The peak at 3628 cm^{-1} belongs to OH stretching mode, the peak at 3448 cm^{-1} belongs to hydrogen bonding and the peak at 1639 cm^{-1} belongs to bending mode of zeolite water. In Figure 5.37, the FTIR spectra of CLI-G-R for 3 days of curing are also presented. A sharp band at 3641 cm^{-1} is due to the O-H stretching vibration of the calcium hydroxide. Furthermore, new bands are observed at $\sim 1420 \text{ cm}^{-1}$ and 870 cm^{-1} are assigned to the presence of CaCO_3 . Significant reduction in the peak intensities of clinoptilolite is clearly observed, which again confirms the dissolution of zeolite structure and then involvement in the pozzolanic reaction (e.g. Perraki et al., 2003) as stated XRD analysis before.

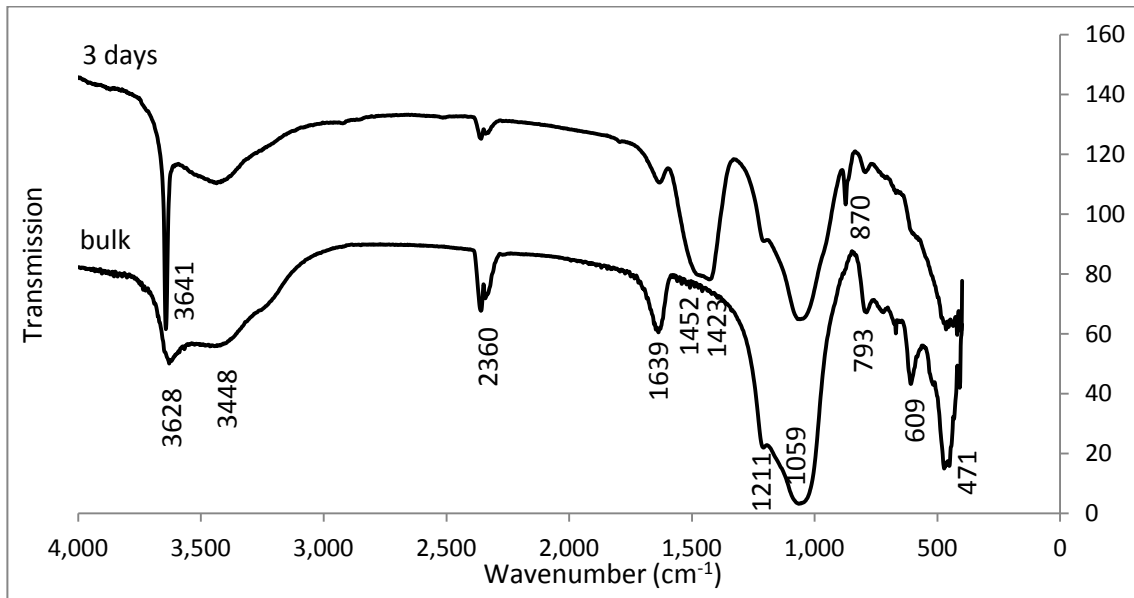


Figure 5.37 FTIR spectrum of bulk material (CLI-G) and corresponding blended paste at 3 days (CLI-G-R).

In Figure 5.38, the FTIR spectra of CLI-A, CLI-B and their corresponding blended pastes at 3 days of hydration are presented. The clinoptilolites exhibit characteristic bands at $\sim 470, 610, 780, 1050, 1635, 3440$ and 3625 cm^{-1} . The peak of calcium hydroxide appears at 3643 cm^{-1} . The vibrations at $\sim 1420 \text{ cm}^{-1}$ and 870 cm^{-1} are associated with the presence of CaCO_3 . The peaks which belong to the clinoptilolite decrease at the 3 days of hydration, indicating the decomposition of zeolite structure.

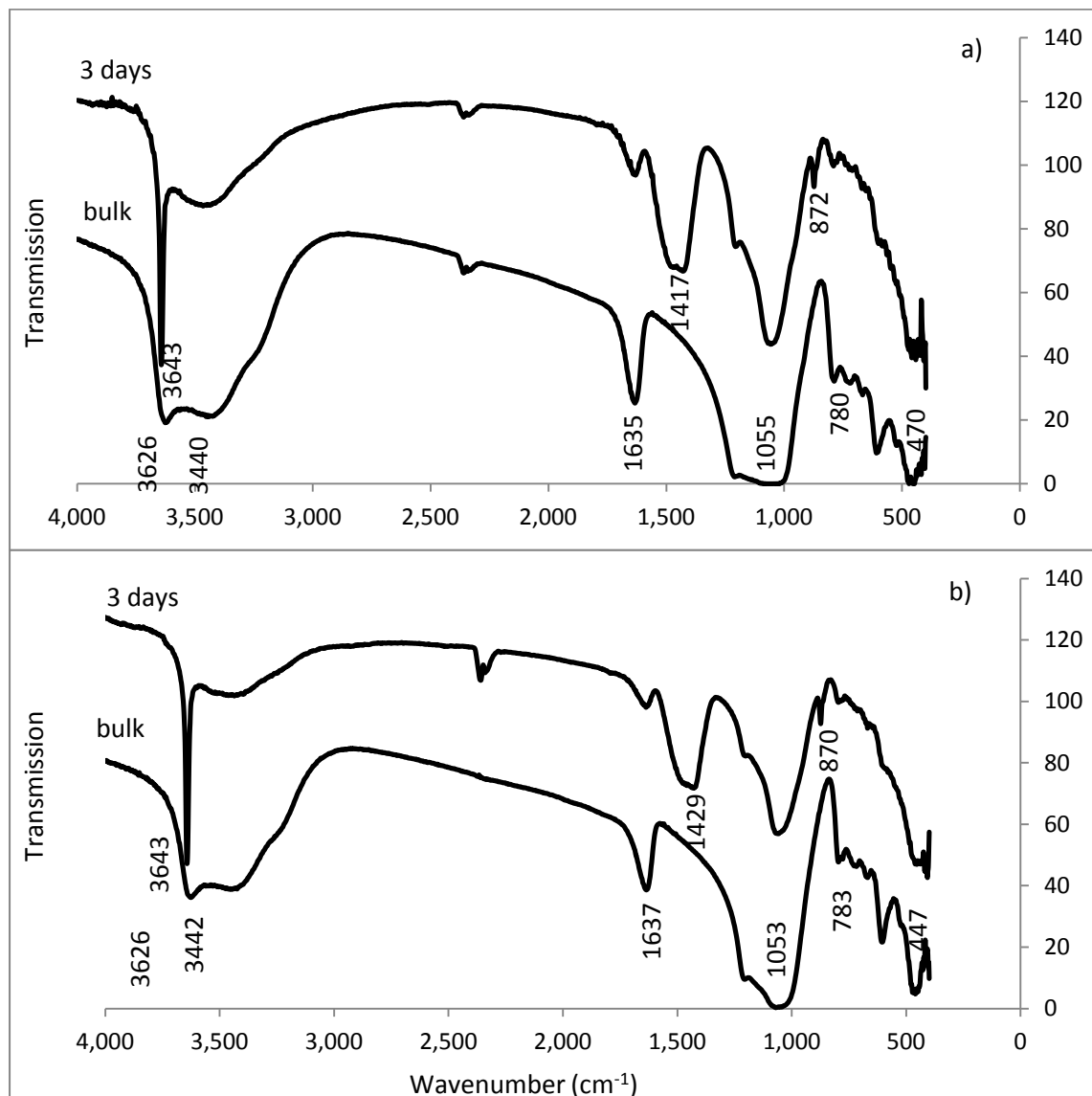


Figure 5.38 FTIR spectrum of a) bulk material (CLI-A) and corresponding blended paste at 3 days (CLI-A-R), b) bulk material (CLI-B) and corresponding blended paste at 3 days (CLI-B-R).

Figure 5.39 shows the FTIR spectrum of MOR and ANA. In the FTIR spectrum of mordenite, the presence of different types of rings in the structure causes lots of bands in the pseudo-lattice region which give rise to difficulties to assign the pseudo-lattice bands precisely (Mozgawa, 2001). From the spectrum, the band at 1041 cm⁻¹ corresponds to the asymmetric valence vibrations in SiO₄ tetrahedra (Korkuna et al., 2006; Dutta and Twu, 1991). A spectral band at 1630 cm⁻¹ reflects the deformation vibration of absorbed water. The bands at 3429 cm⁻¹ and 3637 cm⁻¹ are attributed to the vibrations of the O-H-O stretching and stretching vibrations of Si-O(H)-Al, respectively (Korkuna et al., 2006). Analcime shows the vibration bands at about

1024 cm^{-1} , 723 cm^{-1} , 619 cm^{-1} , 451 cm^{-1} referring to the Si-O asymmetric stretching vibration, Si-O symmetric stretching, double ring and T-O bending vibrations, respectively (Breck, 1974). The peaks at 1622 cm^{-1} and 3622 cm^{-1} are related to the OH bending deformation and free OH stretching vibration of water, respectively (Breck, 1974; Mozgawa, 2001; Mozgawa et al, 1999).

As determined in clinoptilolite blended pastes, the peak of calcium hydroxide ($\sim 3640 \text{ cm}^{-1}$) and the presence of CaCO_3 ($\sim 1420 \text{ cm}^{-1}$ and 870 cm^{-1}) appeared after 3 days of hydration. Similar decreases in the intensities of vibrations of zeolite peaks were also detected for MOR and ANA samples.

The FTIR patterns of the lime-zeolite pastes for 3, 7, 28, 56 and 90 days are shown from Figure 5.40 to Figure 5.44. Upon examination of peaks with increasing age of hydration occurring in the FTIR spectra of all samples, it was observed that:

a) the reduction and gradual narrowing of the band corresponding to the clinoptilolite at about 1050 cm^{-1} as a consequence of destruction and involving of zeolite structure in the pozzolanic reaction,

b) slight decline in the intensity of the bands at 1041 and 1024, corresponding mordenite and analcime respectively, indicates lower dissolution of zeolite structure and therefore lower pozzolanic reaction than clinoptilolite blended pastes,

c) relative intensity of the peak at 3640 cm^{-1} due to OH band from $\text{Ca}(\text{OH})_2$ is gradually decreasing with hydration age which confirms the consumption of lime and enhancement of pozzolanic activity,

d) characteristic peak at 970 cm^{-1} due to CSH become evident after 7 days for clinoptilolite blends, indicating formation of hydration product,

e) the peak of CSH in MOR-R is clear after 28 days and it is not seen in ANA-R,

f) presence of $\text{Ca}(\text{OH})_2$ and clinoptilolite at the 90-days hydration indicate proceeding of pozzolanic reaction,

g) even though the FTIR results presented in this chapter are in general agreement with XRD results, it can be said that XRD is more sensitive method to examine hydration products than FTIR method.

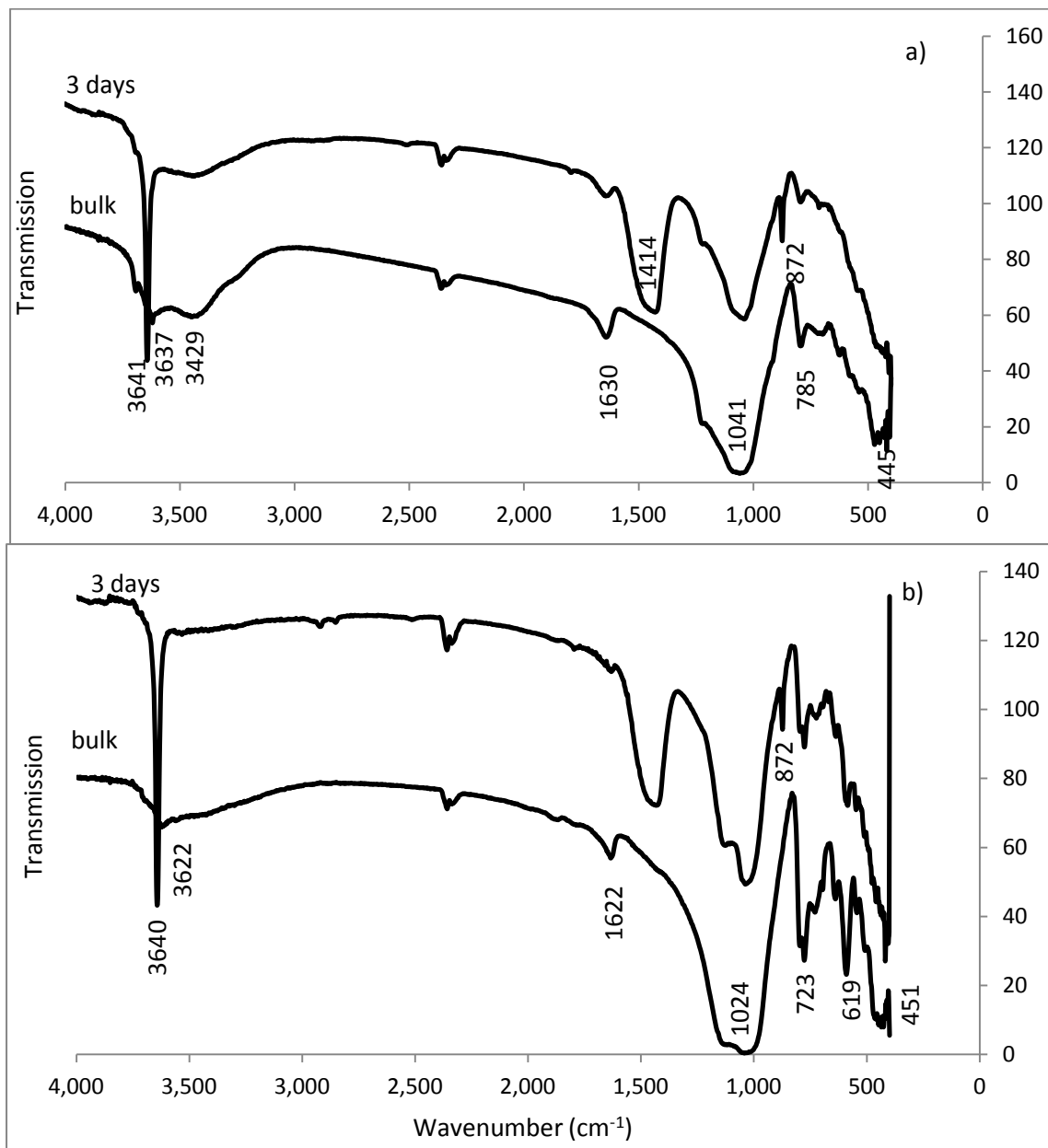


Figure 5.39 FTIR spectrum of a) bulk material (MOR) and corresponding blended paste at 3 days (MOR-R), b) bulk material (ANA) and corresponding blended paste at 3 days (ANA-R).

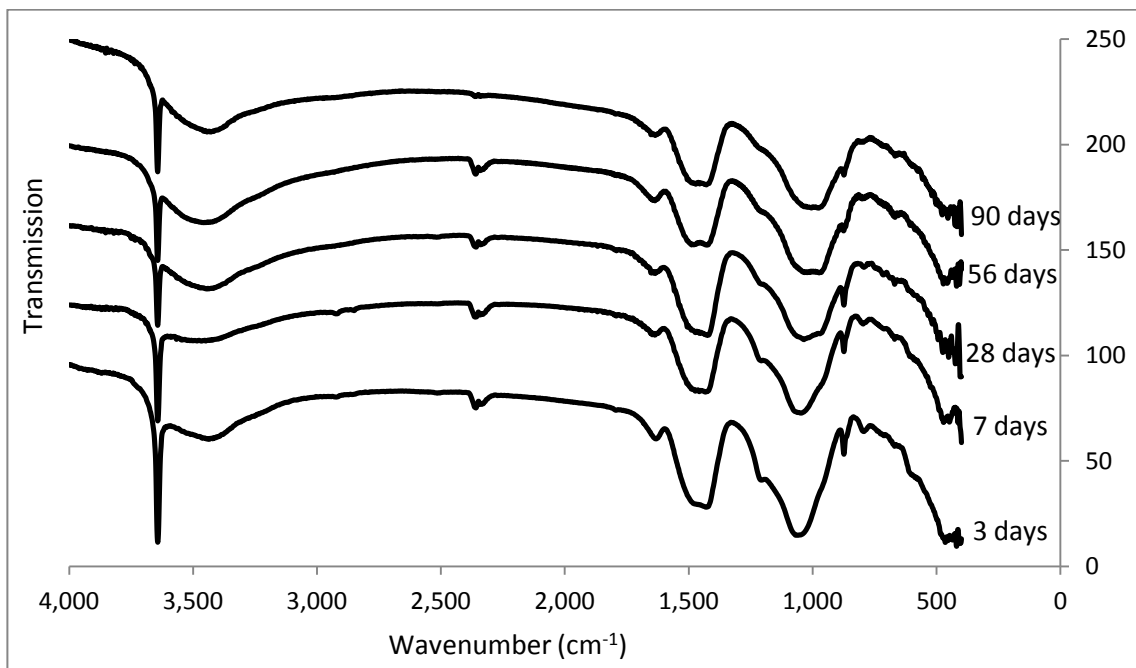


Figure 5.40 FTIR spectra of CLI-G-R/lime pastes after 3, 7, 28, 56 90 days.

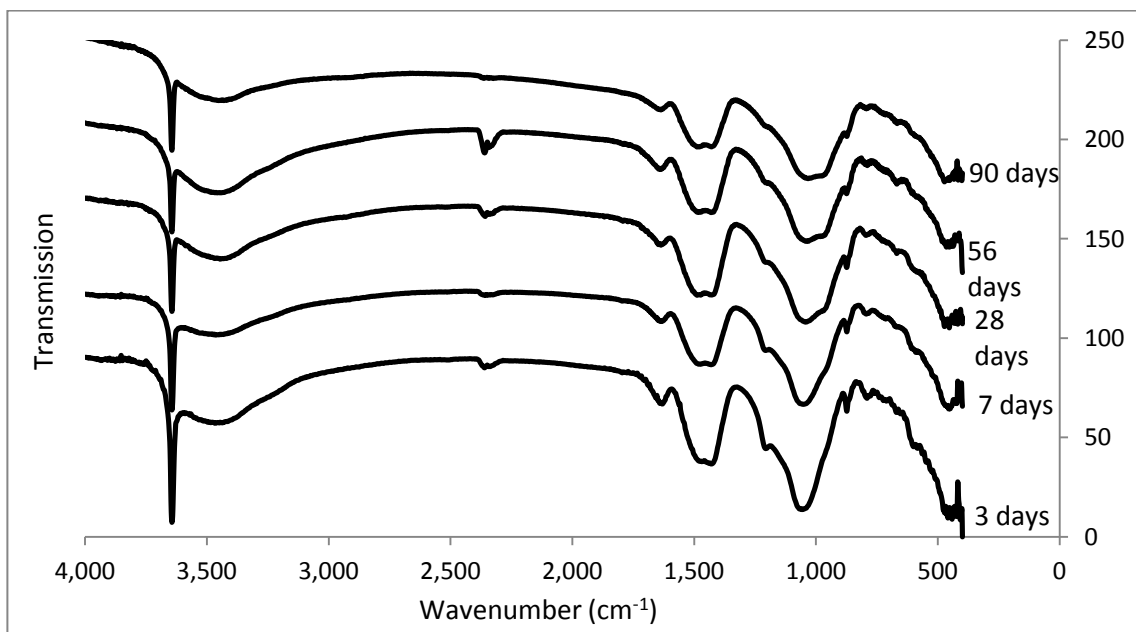


Figure 5.41 FTIR spectra of CLI-A-R/lime pastes after 3, 7, 28, 56 90 days.

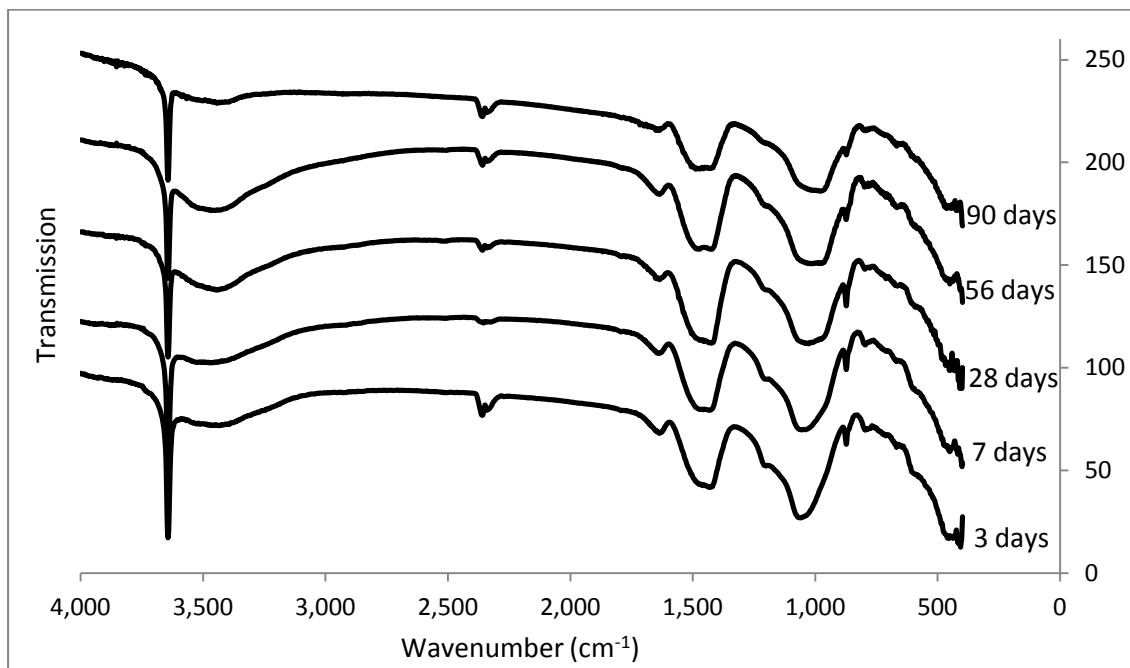


Figure 5.42 FTIR spectra of CLI-B-R/lime pastes after 3, 7, 28, 56 90 days.

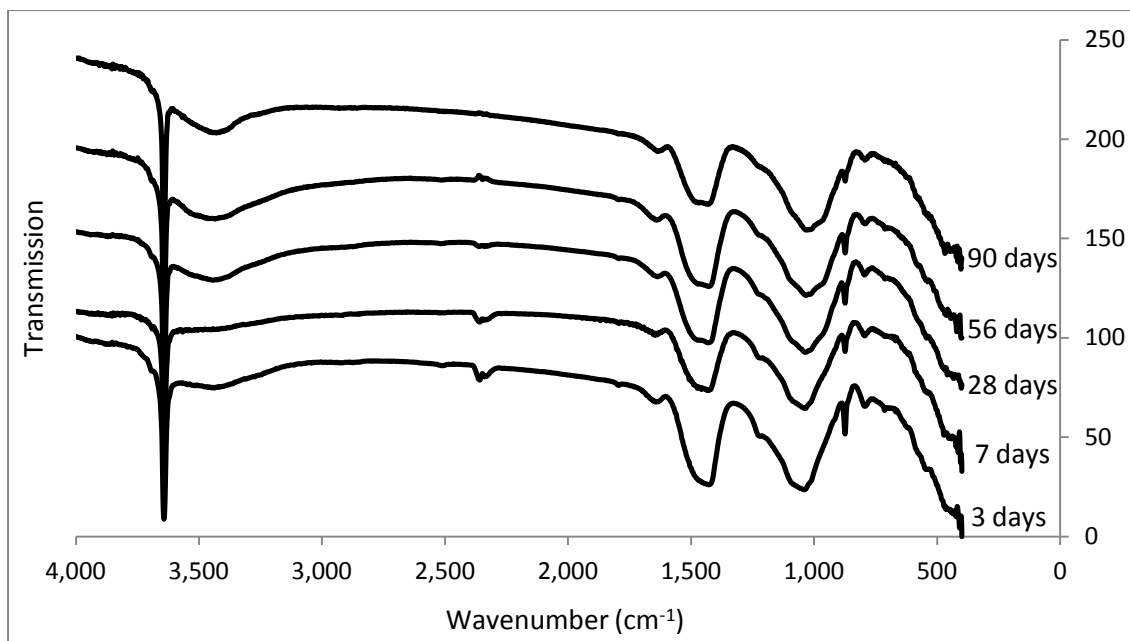


Figure 5.43 FTIR spectra of MOR-R/lime pastes after 3, 7, 28, 56 90 days.

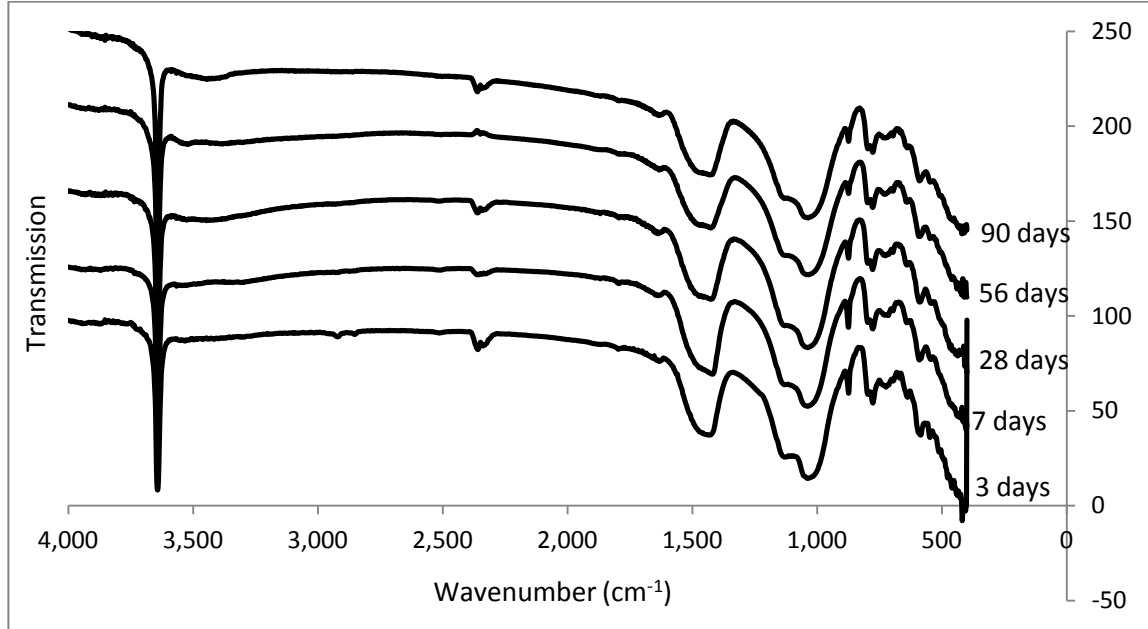


Figure 5.44 FTIR spectra of ANA-R/lime pastes after 3, 7, 28, 56 90 days.

5.5 Compressive Strength Analyses

The results of the mechanical test of the blended and control cements at 7, 28, 56 and 90 days are shown in Figure 5.45. All blended cements exhibit lower compressive strength than the control Portland cement mortar at 7 days of age. This result is typical for supplementary cementitious materials (SCMs), which often reduce the initial strength development (Massazza, 1998). From the literature (Massazza, 1998), it is also known that the compressive strength of the pozzolanic cement may become comparable or even higher than those of the corresponding reference cement at longer ages as seen in Figure 5.45. After 28 days of hydration, MOR acquired almost the same and CLI-G and CLI-B obtained higher compressive strength than the reference Portland cement mortar (Figure 5.45). From the Figure 5.45, it can be said that CLI-B provides a clear strength improvement compared to the control Portland cement. As seen from Figure 5.45, although compressive strength of CLI-G at 28 and 56 days of hydration is higher than that of control cement paste, it display nearly the same result at 90 days. At 28 days, compressive strength values of ANA are lower than those found other blended mortars. But at longer hydration days, the values of CLI-A and ANA are very close to each other.

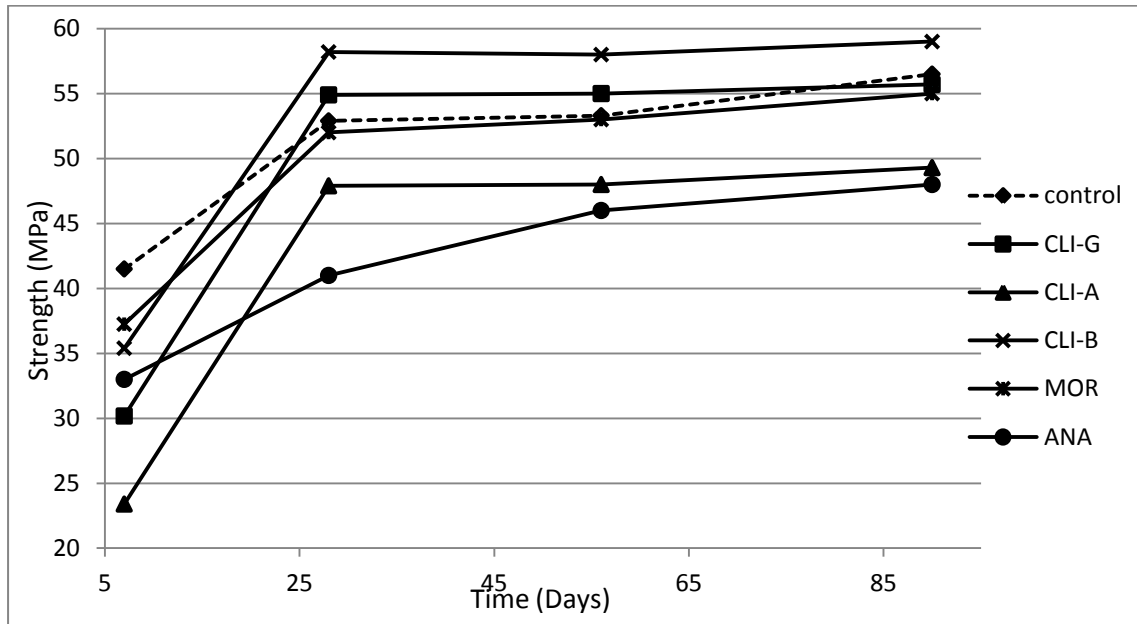


Figure 5.45 The compressive strength of blended cements at 7, 28, 56, 90 days.

The results of compressive strength test are summarized in Table 5.7. In order to provide the same workability of the blended cements, the flow test was performed. Water requirement and water/cementitious (w/cm) ratio are also given in Table 5.7 together with strength activity index (SAI).

Table 5.7 Compressive strength test results of the zeolite blended and control cement mortar.

Days	Compressive Strength					
	Control	CLI-G	CLI-A	CLI-B	MOR	ANA
7	41.5	30.18	23.4	35.4	37.25	33
28	52.9	54.9	47.9	58.2	52	41
56	53.3	55	48	58	53	46
90	56.5	55.7	49.3	59	55	48
w/cm	0.484	0.548	0.578	0.514	0.504	0.496
Water requirement	100	113	119	106	104	102
Days	Strength Activity Index					
	Control	CLI-G	CLI-A	CLI-B	MOR	ANA
7	100	72.72	56.39	85.30	89.76	79.52
28	100	103.78	90.55	110.02	98.30	77.50
56	100	103.19	90.06	108.82	99.44	86.30
90	100	98.58	87.26	104.42	97.35	84.96

The effect of pozzolanic material on mechanical strength depends on a number of factors (Massazza, 1998). Therefore, a combination of more than one parameter (e.g. particle size, water requirement, mineralogical effect, specific surface area, microstructural effect etc.) affecting mechanical behavior should be considered while interpreting compressive strength data.

At 28 days curing age, the compressive strengths of CLI-G and CLI-A are 54.9 MPa and 47.9 MPa, whereas that of the CLI-B is 58.2 MPa. Normally it is expected that the higher lime fixation capacity of pozzolanic material causes the higher strength development. But, zeolite blended cements with high lime fixation capacity did not always perform high compressive strength. For example CLI-G, which has a fixed lime, which is 21.17% higher than that of CLI-B at 28 days, provided a strength about 5.67% lower than that of CLI-B at 28 days. Also CLI-A which has higher lime fixation capacity than CLI-B produces lower compressive strength. Another example is that although the lime consumption of CLI-A is higher than MOR from the thermogravimetric analysis, MOR exhibits stronger mechanical behavior at all ages. In literature the reverse relationship between lime fixation and strength is also observed (Massazza, 1998; Uzal et al., 2010). For this reason, we can conclude that there are also other influential parameters that affect the strength of mortar. It is assumed that the difference in grain size might be brought about divergent strength results. The mechanical behavior of the supplementary cementitious materials (SCMs) is increased by the finer grained size (Sersale, 1980; Massazza, 1998). But, it is being reported in literature that if the fineness of pozzolan exceeds a certain limit, the strength of pozzolanic mortar can decrease rather than increase (Giergiczny and Werynska, 1989; Massazza, 1998). In fact, grain size is associated with water requirement, which affect workability of mixture. It is known that if the amount of water is less, the strength of the mixture is higher (Sersale and Frigione, 1985; Poon et al., 1999). From the Table 5.7, it can be seen that the water requirement and thus water to cement ratio of CLI-A is highest. It is important to remark that w/c ratio of CLI-A is higher than the maximum value, which is proposed as 115% by ASTM C 618. Consequently, it is thought that the higher water requirement of CLI-A and thus higher water to cement ratio (Table 5.7) can results lower compressive strength than expected.

It is known that mixing of pozzolan in cement brings about the microstructural modifications (Massazza 1998). Mehta (1981) showed that a clear decrease in the pores greater than 1000 Å may occur, when pozzolanic material is added in the cement. Uzal and Turanlı (2012) also examined the microstructure of clinoptilolite blended pastes and concluded that the pore size distribution of hardened cement has powerful effect on strength. Diamond (2000) stated that the microstructure of concrete is strongly related with the water to cement ratio and the composition of supplementary cementitious material (SCM). In the next chapter (Chapter 8.6), scanning electron microscopic examinations applied to determine the microstructure of hardened cements shows that the mortars of CLI-G and CLI-B exhibit denser matrix than CLI-A (Figure 5.46, 5.54). In addition, Figure 5.58 shows that the microstructure of CLI-A is more porous than MOR. Therefore, it was deduced that MOR, which has lower w/c ratio enables the generation of dense microstructure which, in turn, gives way to a higher compressive strength. Certainly such

improvement of microstructure is also related with composition of pozzolan, which may explain the higher strength of CLI-B (74% clinoptilolite) compared with MOR (20% mordenite). In overall terms it can be said that there is a limit for w/c ratio, to improve the microstructure of hardened cement. In order to diminish the effect of w/c ratio superplasticizers is suggested. It is important to point out that CLI-A would have performed higher strength result in case of having low w/c ratio. This can be achieved by short grinding time, which provides lower energy consumption. To conclude, the main parameters to be accepted, for obtaining higher mechanical strength, are water to cement ratio, which finally determine porosity of hardened cement and pozzolanic activity of SCMs.

Water requirement seems to be related not only specific surface area but also grain size as stated by Uzal and Turanlı (2007). It is important to note that water requirement of CLI-A is higher than CLI-G although BET specific surface area of CLI-G is higher than CLI-A. Therefore higher water requirement of CLI-A is associated with its finer grain size distribution. It is worth noting that CLI-B has lowest water to cement ratio and highest strength considering all clinoptilolite blends.

Considering the affect of composition; in regard to the quantity and quality of phases, it was observed that mineralogy of bulk samples has a significant effect on mechanical behavior (e.g. Massazza, 1998). It is known that the presence of volcanic glass may play an important role on improvement of the mechanical strength (Kitsopoulos and Dunham, 1996). When quantitative XRD results of CLI-B are examined, it is noticed that CLI-B includes considerably higher amount of volcanic glass (18.24%) than CLI-G (6.4%). Therefore, the higher compressive strength of CLI-B can be ascribed to a combination of physical and mineralogical parameters. From these results, it can be observed that the compressive strength of MOR is comparable to the control mixture after 7 days (Figure 5.45). The high strength results of MOR are attributed to the presence of not only quality of zeolite (mordenite) but also volcanic glass. Incorporation of mordenite was reported to produce high compressive strength in literature (Fragoulis et al., 1997). The higher volcanic glass content of MOR (31%) could be resulted in high compressive strength than expected. But why CLI-B or MOR, which include higher volcanic glass cannot fix higher lime from thermogravimetric analysis remains obscure.

5.6 Microstructure of Hydrated Cement Pastes

In this chapter, the analyses performed on the microstructure of the hardened cement pastes using scanning electron microscopy (SEM) equipped with energy dispersive X-ray analysis (EDX) and electron microprobe analysis (EPMA) on the crushed pieces and the polished thin sections, respectively, will be evaluated.

The hydration products present in hydrated cement pastes consist predominantly of calcium silicate hydrate (CSH) and calcium hydroxide, together with smaller amounts of Afm and Aft phases (Mehta and Monteiro, 2006). CSH is produced by hydration of clinker constituents (C_3S

and C_2S). As hydration occurs in the cement matrix, the microstructure begins to develop. The resulting hydrated cement phases crystallize on/near the cement grains which bring about solid mass with time.

5.6.1 SEM Analyses of Hardened Cement

The structure of hydrated cement pastes on a micro scale at the end of 28 days of hydration was examined. Fractured surfaces of clinoptilolite, mordenite and analcime blended hardened cements examined by SEM give information about the relative density of pastes, texture of the samples, crystals of bulk minerals and/or reaction products and their morphologies. A comparison was made between the hardened cements at the same magnifications. The composition of the hydrated phases was semi-quantitatively analyzed with the EDX analysis. Although EDX analyses give valuable information about chemistry, one must be careful in the case of small phases, to prevent the contributions from surrounding phases.

The general microstructure of CLI-G-R and CLI-B-R are shown in Figure 5.46 which stated relatively dense microstructure of hydrated cement matrix. CLI-A-R, on the other hand, displays a more loose matrix. MOR-R and ANA-R display completely different microstructures when compared to the other pastes. However, at this magnification, it is difficult to distinguish the hydration products.

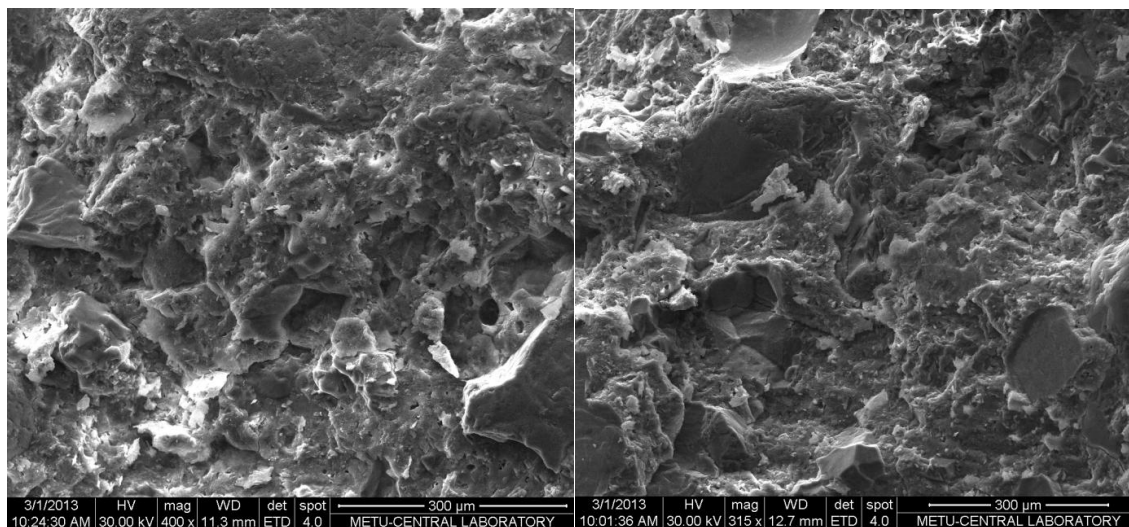


Figure 5.46 Scanning electron micrographs showing general microstructure of a) CLI-G-R, b) CLI-B-R at low magnification.

In Figure 5.47, non-reacted cement grain (alite) having a characteristic polygonal morphology (Campbell, 1986), approximately 1 μ m in diameter, is identified from CLI-B-R. Furthermore,

there are thin films of CSH coating the surface of hardened cement as well as spongy CSH developed in the cavities.

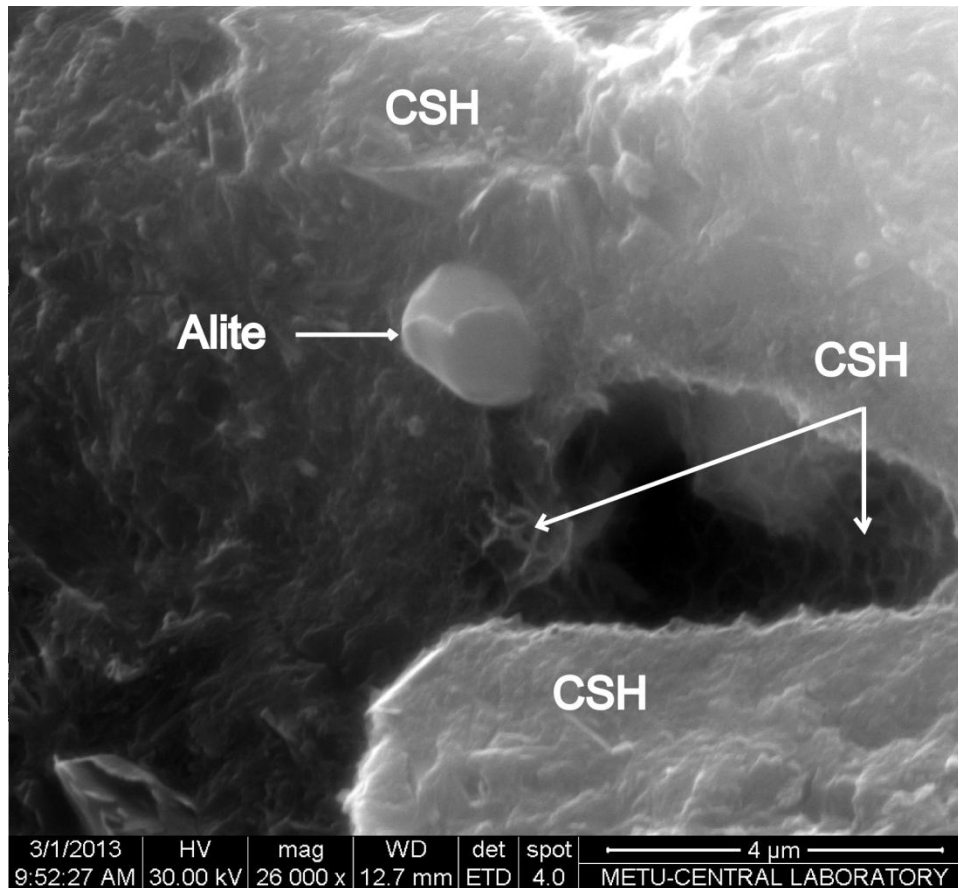


Figure 5.47 Scanning electron micrograph showing the characteristic polygonal morphology of cement grain (alite), CSH coating and sponge-like CSH found in the cavity (Sample: CLI-B-R).

The morphology of non-reacted and partly reacted round clinker (belite) grains (Campbell, 1986) range from 0.5 to 2.5 μm in diameter is observed from Control-R sample with a scanning electron microscope (Figure 5.48). Some belite crystals (upper right and upper left) start to hydrate. Semi-quantitative chemical composition determined by using EDX spectrometer is also presented in Figure 5.48. Belite crystals were found in small quantities. The reason that belite crystal remains non-reacted even at 28 days, might be unmixed part of blend.

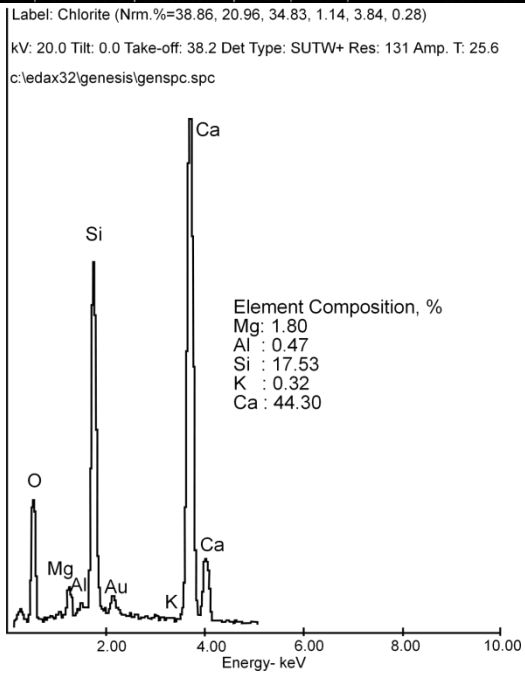
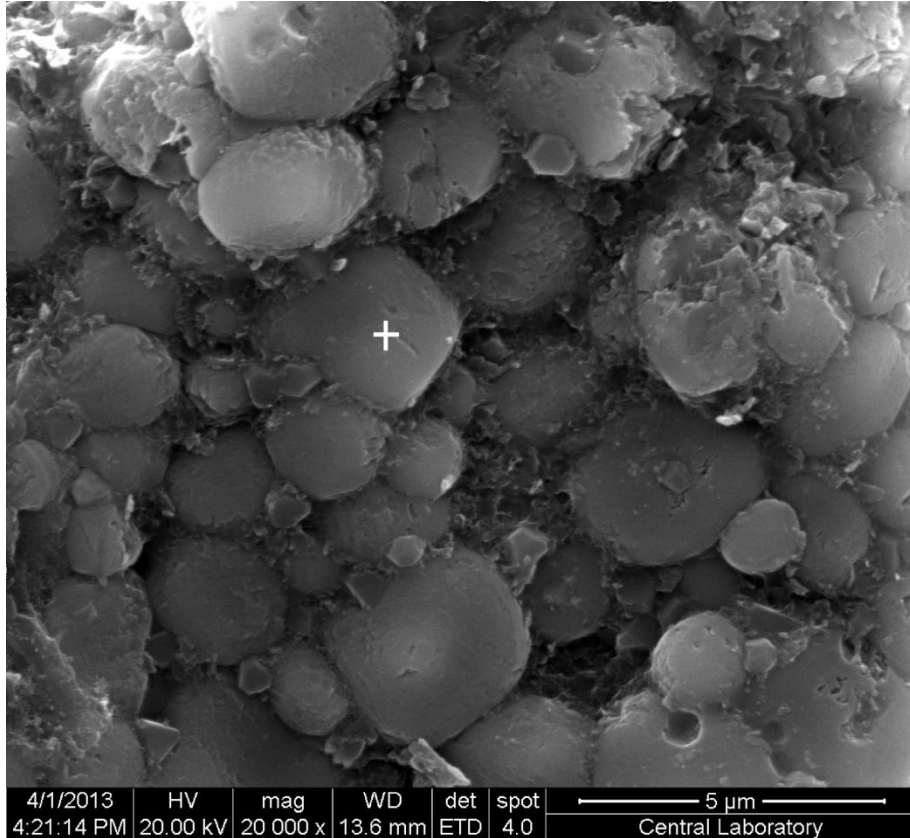


Figure 5.48 Scanning electron micrograph displaying round belite crystals and corresponding EDX spectra of belite (Sample: Control-R).

Figure 5.49 shows hydrated minerals crystallizing as hexagonal plates identified by scanning electron microscopy and corresponding EDX spectra. EDX analysis suggests strong peaks of Ca, Al, Si elements. The morphology and high content of designated elements indicate the presence of gehlenite hydrate (C_2ASH_8), also known as stratlingite. Gehlenite hydrated was detected only in ANA-R in very small quantities compared with the other phases.

The main hydration product of the pozzolanic activity is calcium silicate hydrate (CSH) (Mehta and Monteiro, 2006). As it can be seen on the scanning electron images (Figure 5.50, 5.51, 5.52, 5.53), the CSH phase presents different morphologies and sizes. In the Figure 5.50, CSH crystals can be easily differentiated by branched fibrous morphology (Diamond, 1976; Scrivener, 2004). Corresponding EDX analysis of CSH is given in Figure 5.50 which contains two main elements, Ca and Si. Some CSH fibers radiate out from the region of remnant cement grains well seen in right part of the image. Needle-like or prismatic crystals 1-4 μm in diameter are too small to be resolved by EDX method. These crystals over CSH bundles are considered as mordenite.

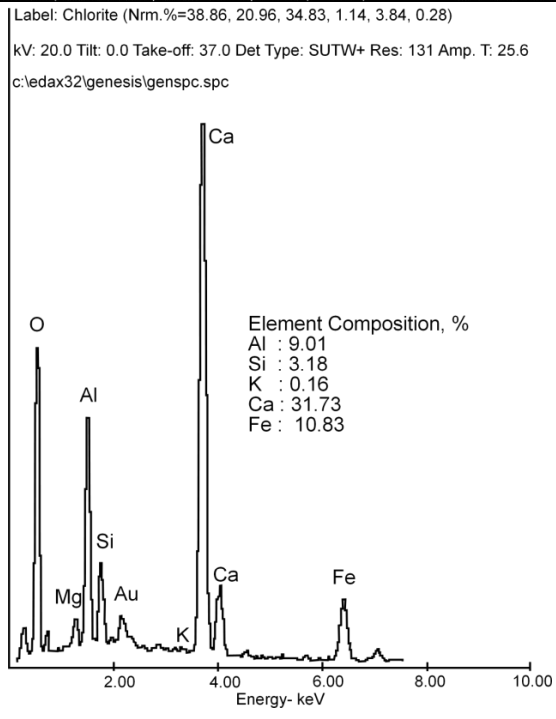
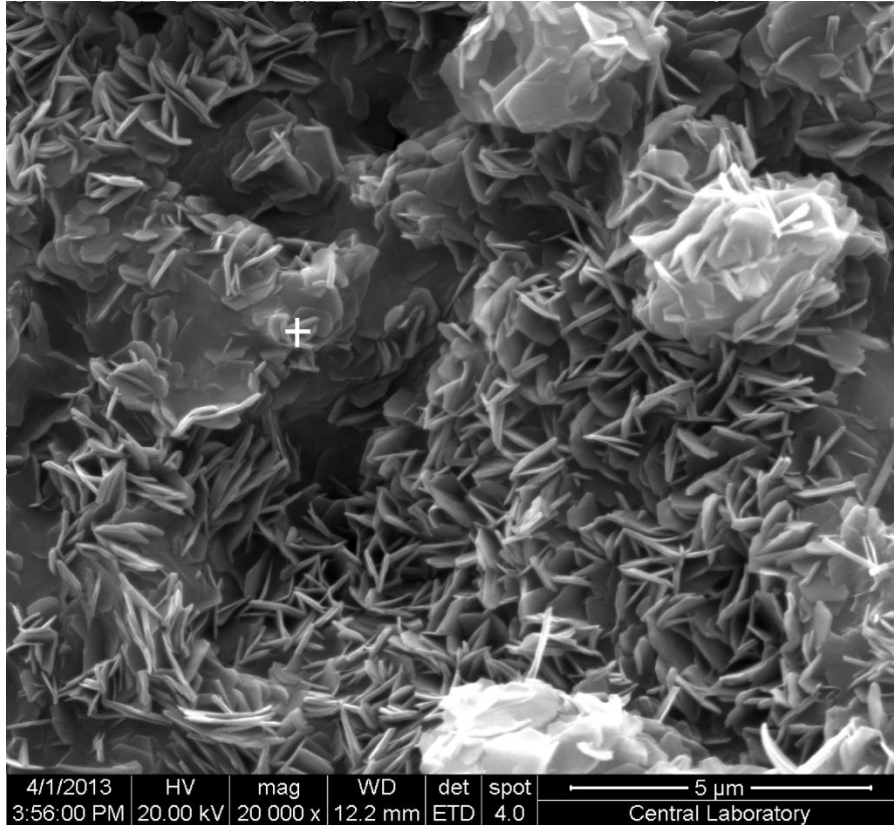


Figure 5.49 Scanning electron micrograph of gehlenite hydrate and corresponding EDX analysis (Sample: ANA-R).

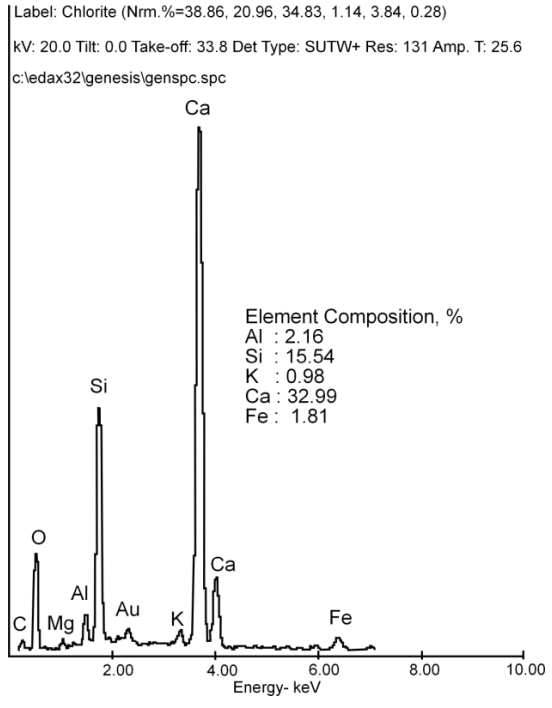
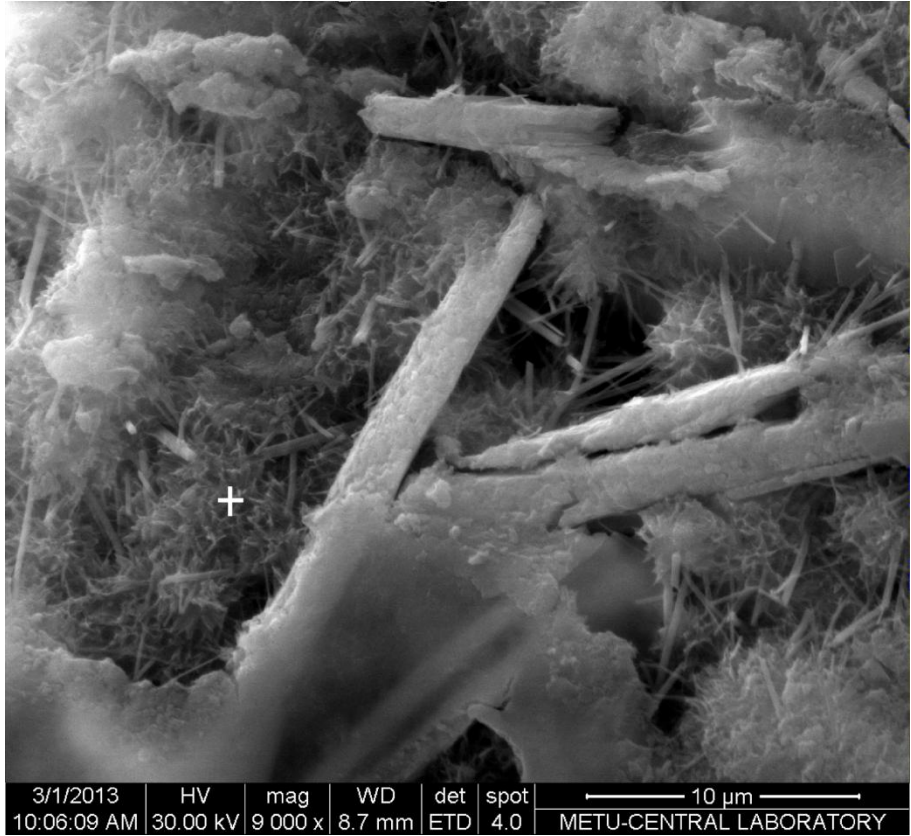


Figure 5.50 SEM image displaying branched fibrous CSH and mordenite needles and corresponding EDX spectra of the CSH (Sample: MOR-R).

The Figure 5.51 also shows the branched morphology of CSH crystals radiating out to the edges from the center of residual particles of cement grains in ANA-R. This morphology is very similar to the MOR-R.

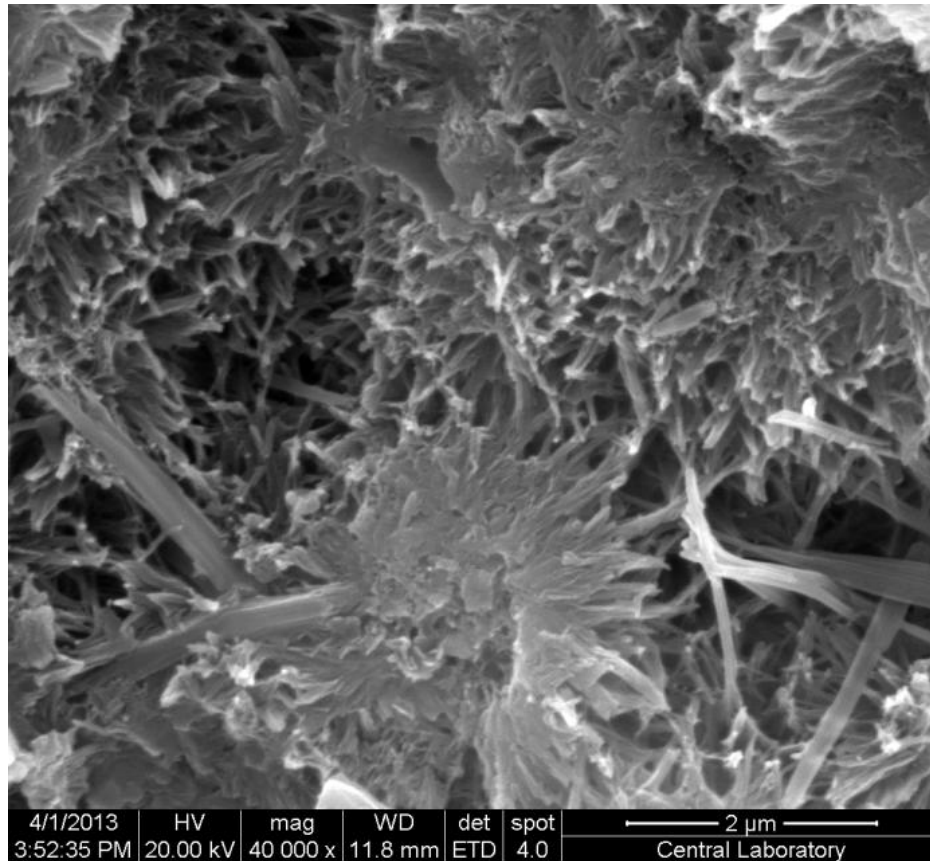


Figure 5.51 Scanning electron image of CSH radiate outward from the remnant cement particles (Sample: ANA-R).

In the Figure 5.52, the morphology of the CSH is characterized by sponge-like crystals (Diamond, 1970). The differences from MOR-R and ANA-R samples are that the CSH in CLI-A-R is not radiating from the center. Besides, there are many prismatic clinoptilolite crystals enclosed by CSH.

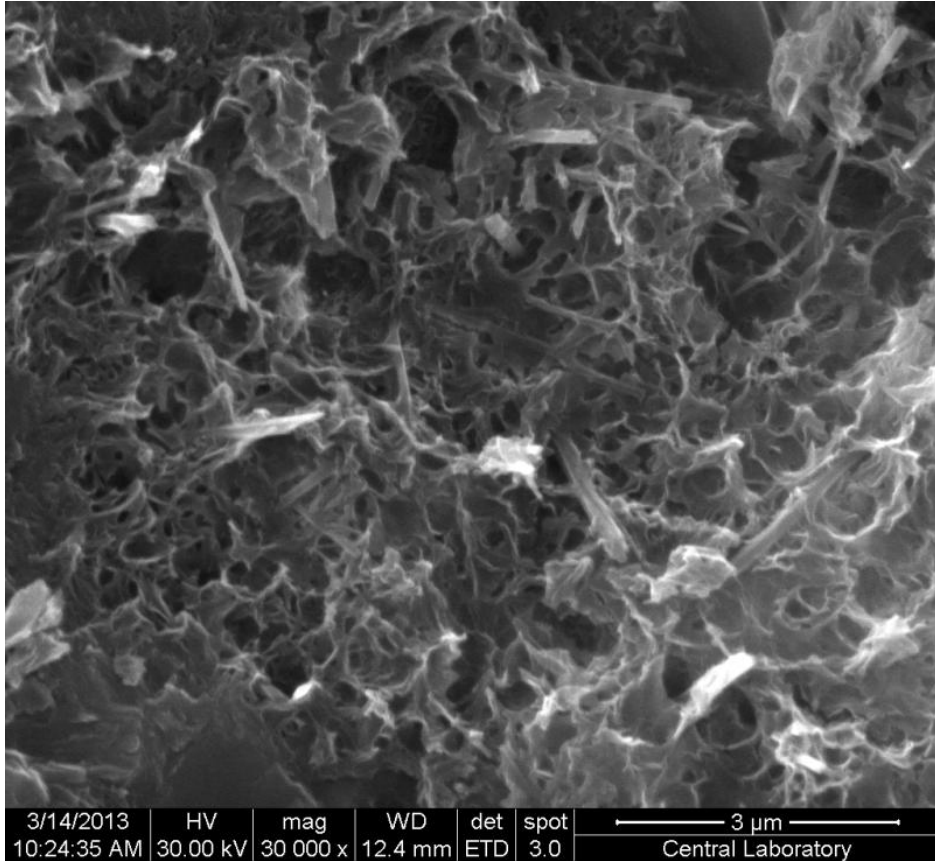


Figure 5.52 Scanning electron image of CSH and prismatic clinoptilolite crystals (CLI-A-R).

There are also thin porous CSH coatings developed on surface of hydrated matrix. Similar morphology was also observed on the sample of CLI-B-R (Figure 5.53).

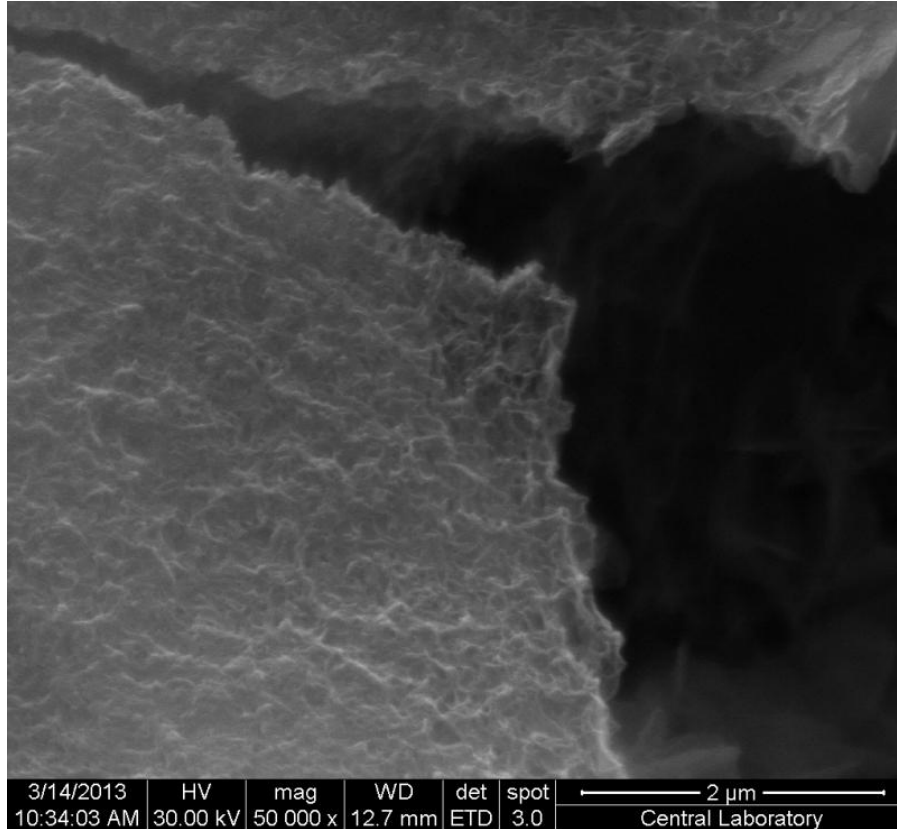


Figure 5.53 Scanning electron image illustrating thin porous CSH coatings (CLI-G-R).

Figure 5.54 shows the general appearance of crushed surface of three clinoptilolite, one mordenite and one analcime blended cement pastes at higher magnification. CLI-G-R and CLI-B-R have massive appearance than CLI-A-R. CLI-G-R has a porous CSH coating on the surface. CSH phase of sponge-like morphology was observed for CLI-A-R. Composite mass of denser CSH are observed on the surface of matrix in CLI-B-R. These CSH coating appears nonporous at this magnification. Figure 5.54c also exhibits that the microstructural development of CLI-B-R is much more uniform. The bundles of CSH found in MOR-R are shown radiating outward from the center of residual particles of cement grains. Besides, there are mordenite needles over CSH bundles (Figure 5.54d). ANA-R, on the other hand, represents formless texture in general (Figure 5.54e).

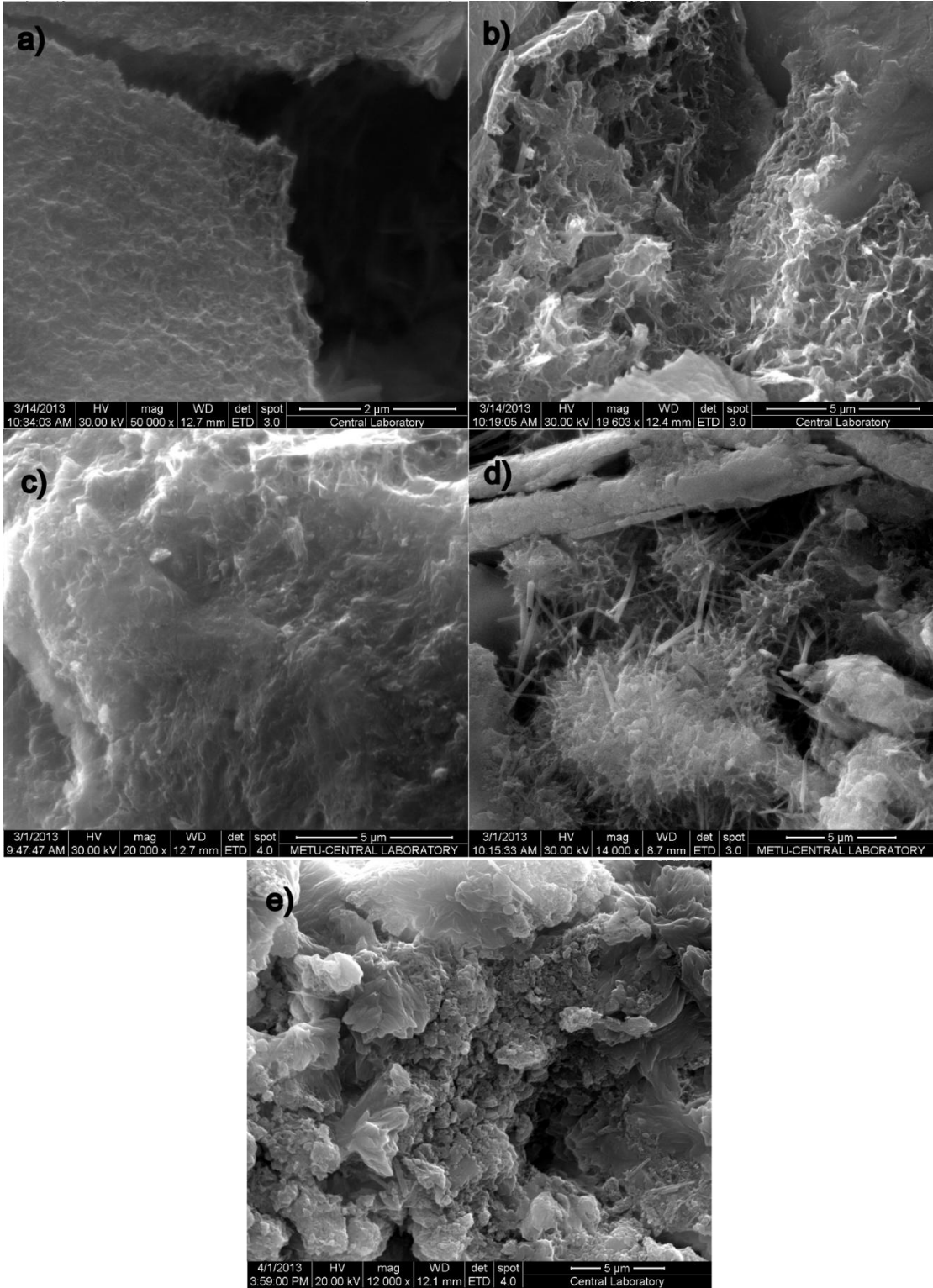


Figure 5.54 Scanning electron micrographs of a) CLI-G, b) CLI-A, c) CLI-B, d) MOR, d) ANA.

Figure 5.55 shows the scanning electron microscope image of CLI-G-R, CLI-A-R and CLI-B-R at similar magnification and corresponding EDX analyses. It was noticed that all hardened cements include prismatic/platy crystals, which are partly embedded in the cement matrix. After semi-quantitative chemical characterization by EDX, the relative peak height of Ca, Al, and Si elements are displayed. Based on the morphology of crystals and EDX results, it was considered that prismatic/platy crystals are partially reacted clinoptilolites. There are two minerals at the right side of the Figure 5.55a. Even though they have different morphology, one has prismatic morphology and the other one has platy morphology, the EDX spectrum contains the same elements and same peak height. Clinoptilolites retaining in some parts outside from matrix are easily distinguishable, while some others have already been covered by cement matrix. In addition, EDX spectrum of CLI-G (Figure 5.55a) has higher Ca and lower Si, Al peaks with regard to EDX spectrums of CLI-A and CLI-B (Figure 5.55b, 5.55c). This means that clinoptilolites in CLI-G are more reacted than CLI-A and CLI-B.

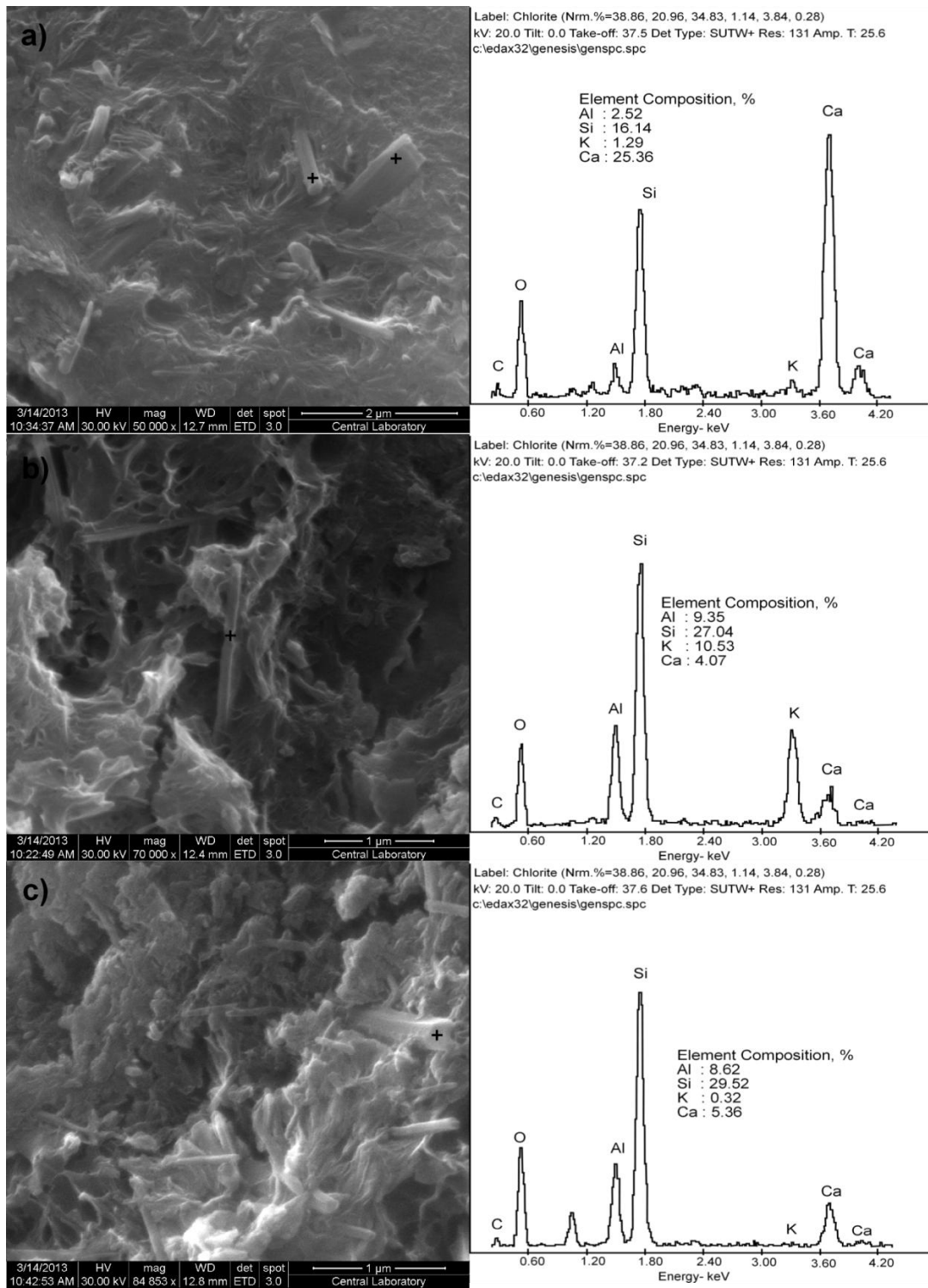


Figure 5.55 SEM-EDX characterization of hardened cement pastes after 28 days of curing; prismatic clinoptilolites in the a) CLI-G, b) CLI-A, c) CLI-B and corresponding EDX spectrums.

Figure 5.56 shows the two prismatic clinoptilolite crystals embedded in the matrix. At first sight, it is difficult to differentiate the bottom one from the matrix since this clinoptilolite is completely covered by surrounding hydrated matrix. There is also sponge-like CSH well seen at the lower right part of the image.

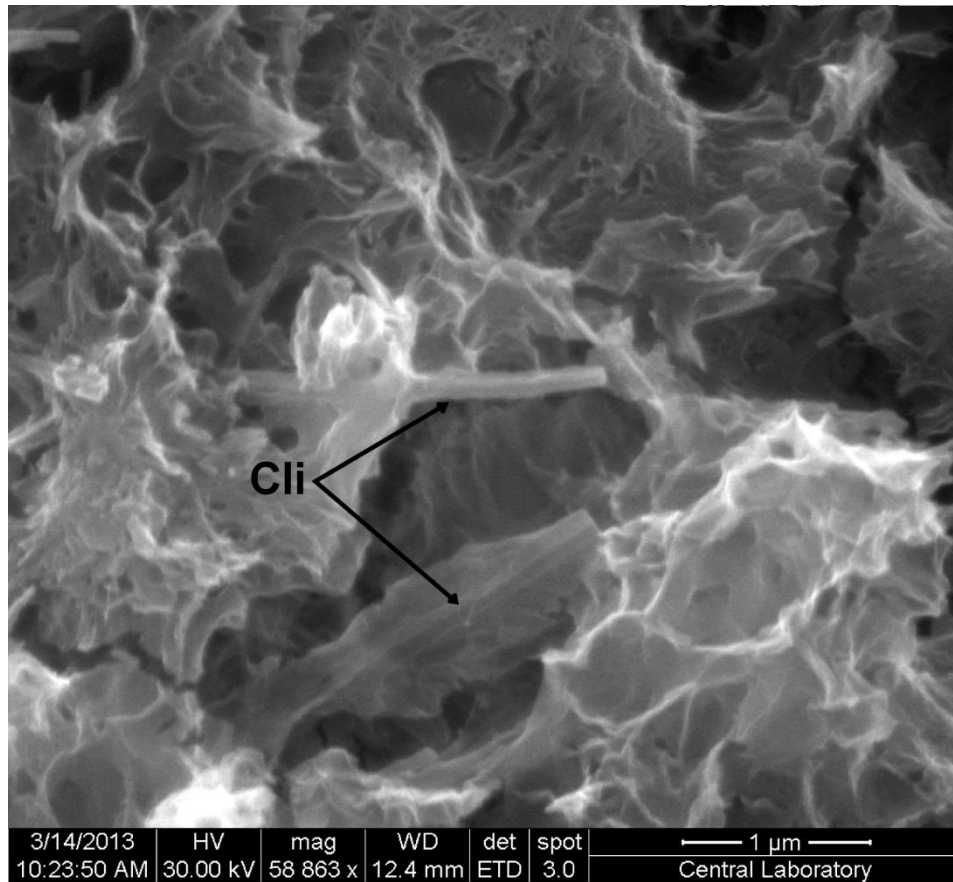


Figure 5.56 SEM image of clinoptilolites embedded in the cement matrix (Sample: CLI-A-R, Cli: clinoptilolite).

5.6.2 Quantitative Electron Microprobe Analyses of Hardened Cement

Hardened cement pastes at 28 days of hydration were examined chemically by microprobe analysis. While all hardened cement pastes were investigated, typical area was presented in the figures. Point analysis was performed on partly reacted zeolitic tuff grains, cement particles as well as random selection of areas across the matrix. The results of some point analyses are excluded because of possible mixing of the phases. The results are shown in Table 5.8.

Table 5.8 Electron microprobe analysis of hardened cement (wt %).

	CLI-G	CLI-G	CLI-G	CLI-G	CLI-G	CLI-A	CLI-A	CLI-B	CLI-B	CLI-B	CLI-B	CLI-B	CLI-B	MOR	MOR	ANA	ANA
	cli	cli	matrix	CSH	CSH	cli	matrix	ferrite	C3A	cli	cli	cli	matrix	mor	matrix	ana	matrix
	1	2	3	4	5	6	7	8	9	10	11	12	13	14	15	16	17
SiO ₂	61.70	57.06	47.13	23.20	29.30	58.45	27.99	1.35	4.56	66.21	63.87	64.80	16.91	65.51	23.76	59.73	29.21
Al ₂ O ₃	10.54	10.20	5.60	7.06	5.95	10.50	6.18	24.63	26.83	12.94	12.50	12.23	3.45	9.72	3.96	21.54	7.94
Fe ₂ O ₃	0.13	0.17	1.39	1.94	2.02	0.07	1.27	20.92	9.82	0.06	0.11	0.07	0.49	0.03	1.07	0.08	1.99
MgO	1.20	1.18	1.64	1.29	1.76	1.03	1.12	1.85	2.45	1.05	0.99	0.96	1.70	0.17	0.81	0.01	1.59
CaO	9.54	11.31	21.98	28.87	28.30	10.77	23.49	48.00	54.50	4.22	5.08	4.55	40.27	7.06	33.23	0.33	20.85
Na ₂ O	0.22	0.25	0.49	0.77	0.84	0.37	0.97	0.07	0.51	0.24	0.12	0.31	0.22	1.15	1.76	10.57	1.18
K ₂ O	3.30	3.23	1.90	2.26	2.58	4.01	2.38	0.07	0.19	2.20	1.47	3.14	0.60	3.52	1.43	0.26	2.87
SrO	0.00	0.01	0.03	0.00	0.00	0.15	0.05	0.01	0.11	0.16	0.10	0.00	0.10	0.00	0.30	0.06	0.01
MnO	0.13	0.03	0.64	0.60	0.57	0.20	0.65	2.89	0.57	0.00	0.05	0.00	0.48	0.02	0.64	0.00	0.62
BaO	0.21	0.21	0.00	0.10	0.00	0.18	0.20	0.22	0.01	0.17	0.15	0.06	0.13	0.01	0.15	0.00	0.00
Total	86.97	83.66	80.80	66.10	71.33	85.74	64.30	100.00	99.54	87.25	84.43	86.13	64.36	87.18	67.12	92.57	66.25
LOI	13.03	16.33	19.20	33.89	28.67	14.26	35.70	0.00	0.45	12.74	15.57	13.86	35.64	12.82	32.87	7.42	33.74
Na	0.16	0.19	0.37	0.57	0.63	0.28	0.72	0.05	0.38	0.18	0.09	0.23	0.16	0.85	1.30	7.84	0.87
Mg	0.73	0.71	0.99	0.78	1.06	0.62	0.68	1.12	1.48	0.64	0.59	0.58	1.02	0.10	0.49	0.10	0.96
Sr	0.00	0.01	0.02	0.00	0.00	0.13	0.04	0.01	0.09	0.14	0.09	0.00	0.09	0.00	0.26	0.05	0.01
Mn	0.10	0.03	0.49	0.47	0.44	0.15	0.49	2.24	0.44	0.00	0.03	0.00	0.40	0.01	0.49	0.00	0.50
K	2.74	2.68	1.58	1.88	2.14	3.33	1.97	0.06	0.16	1.83	1.22	2.60	0.50	2.93	1.19	0.21	2.38
Al	5.58	5.40	2.97	3.74	3.15	5.56	3.27	13.03	14.20	6.85	6.61	6.47	1.83	5.14	2.10	11.40	4.20
Si	28.84	26.67	22.03	10.85	13.70	27.32	13.09	0.63	2.13	30.95	29.86	30.29	7.90	30.62	11.11	27.92	13.66
Ba	0.19	0.19	0.00	0.09	0.00	0.16	0.18	0.20	0.01	0.15	0.13	0.06	0.11	0.01	0.14	0.00	0.00
Fe	0.09	0.12	0.98	1.36	1.42	0.05	0.89	14.63	6.87	0.04	0.08	0.05	0.35	0.02	0.75	0.05	1.39
Ca	6.82	8.09	15.71	20.63	20.22	7.70	16.79	34.30	38.95	3.02	3.63	3.25	28.78	5.05	23.75	0.24	14.90
O	41.73	39.58	35.68	25.74	28.57	40.44	26.17	33.74	34.85	43.48	42.09	42.59	23.24	42.45	25.55	44.85	27.40
Ca/Si	0.22	0.71	1.90	1.90	1.47	0.28	1.28	54.42	18.29	0.10	0.12	0.11	3.64	0.16	2.14	0.01	1.09

Figure 5.57 was taken from 28 days old clinoptilolite-blended cement paste (CLI-G-R) at low magnification (x200) and it shows the general microstructures of hardened paste. Three different phases are differentiated in the hydrated material as can be seen from Figure 5.57. The brightest areas are of non-hydrated and/or partially hydrated cement grains which their compositions determined by point analysis (Table 5.8). The largest grains with certain boundaries consist almost wholly of grains of sand used and those of the regions occupied by the medium size partially hydrated grains with ambiguous border are clinoptilolite-rich tuff grains. The residual part forms the matrix. Micro cracks are also present in all hardened cement pastes (Figure 5.57). Similar textural features were observed for other clinoptilolite blended hardened cement pastes.

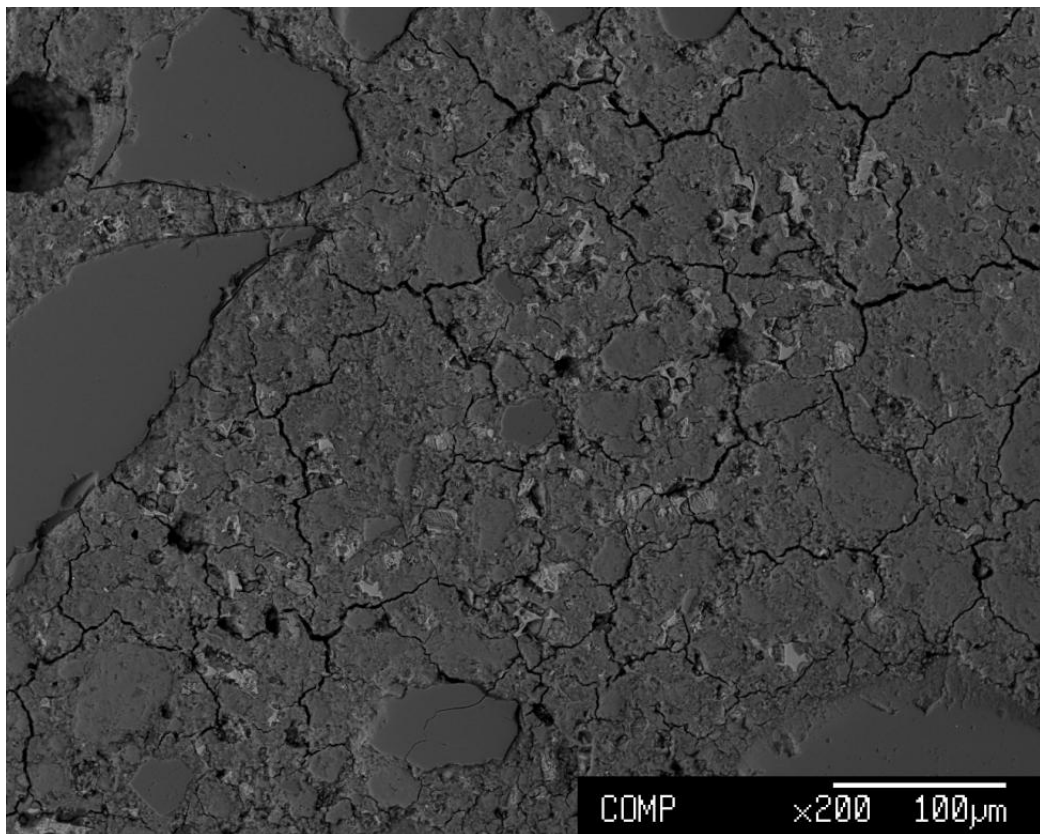


Figure 5.57 Backscattered electron image of cement paste showing general microstructure (Sample: CLI-G-R).

Figure 5.58 demonstrates that CLI-A and MOR blended cements nearly at the same magnification. It can be seen CLI-A has porous microstructure than MOR.

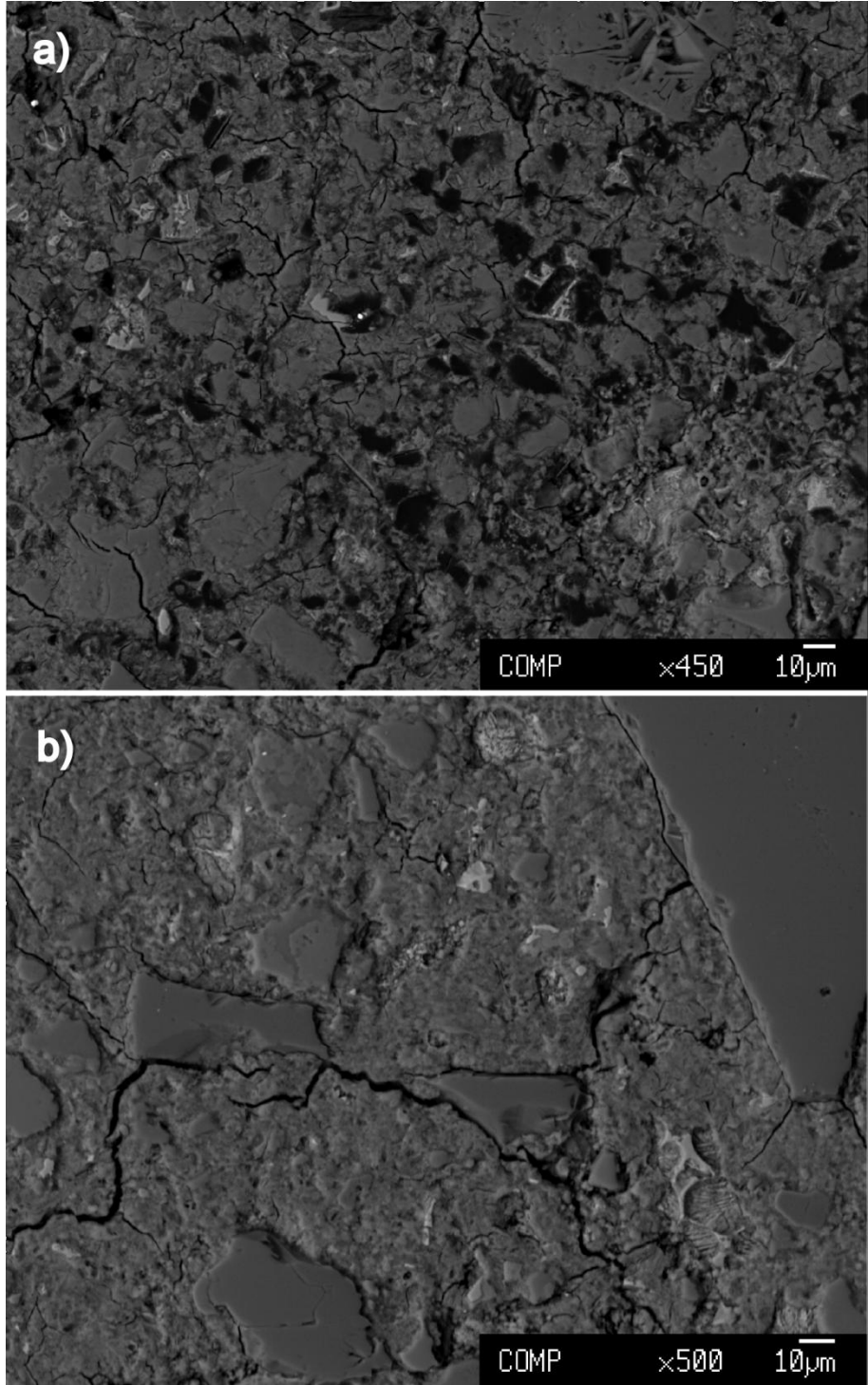


Figure 5.58 Backscattered electron image of a) CLI-A, b) MOR.

Backscattered electron image of CLI-B-R paste at x1.100 magnification is shown in Figure 5.59. General appearance is similar to that CLI-G-R paste. Phases on this area can be clearly identified

using the electron microprobe analysis. As a result of point analysis (labeled as 8 in Figure 5.59 and Table 5.8), non-reacted cement grain was detected as ferrite phase by the point analysis revealed 24.63 wt% of Al_2O_3 , 48 wt% CaO and 20.92 wt% Fe_2O_3 , which is in agreement with the results of ferrite phase obtained by Taylor (1990).

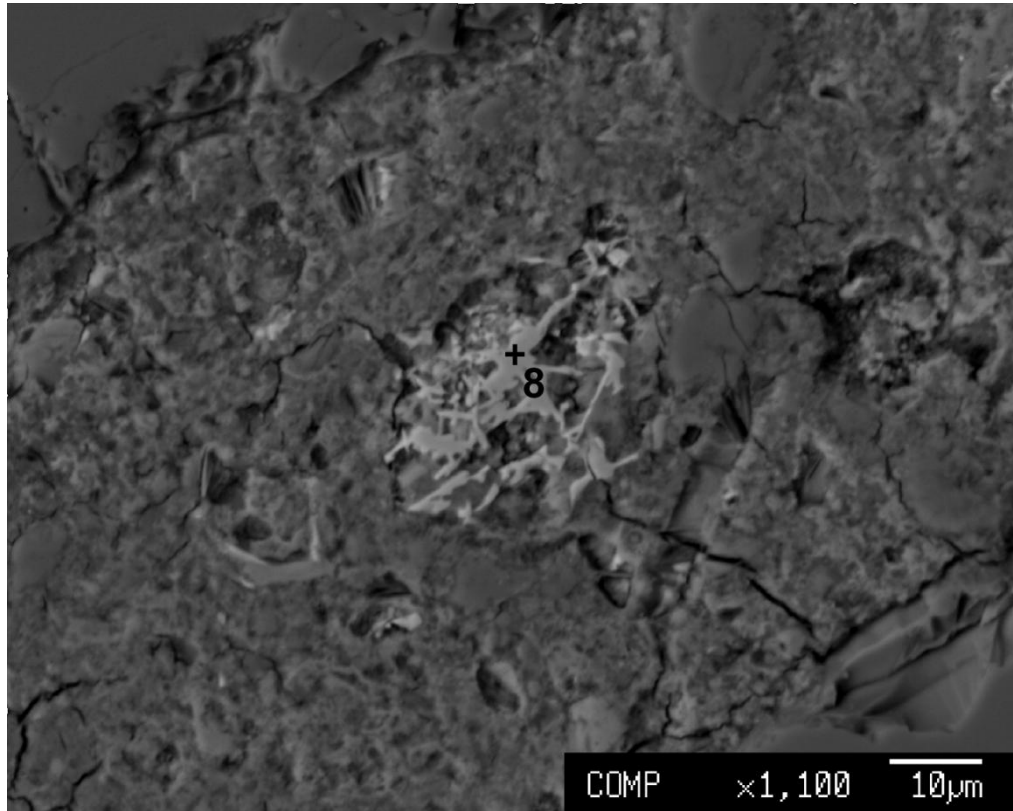


Figure 5.59 Backscattered image of blending cement paste showing the ferrite phase (Sample: CLI-B-R).

Figure 5.60 also shows the bright cement particle taken from CLI-B-R paste. The presence of non-hydrated cement particle is determined by the point analyses (labeled as 9 in Figure 5.60 and Table 5.8) showing 54.5 wt% of CaO , 26.83 wt% of Al_2O_3 which indicate the aluminate phase (C_3A). These point analysis are consistent with the results given by Taylor (1990). Similar clinker phases have been observed for all other samples. Micro cracks and sand grains also are detected in Figure 5.60.

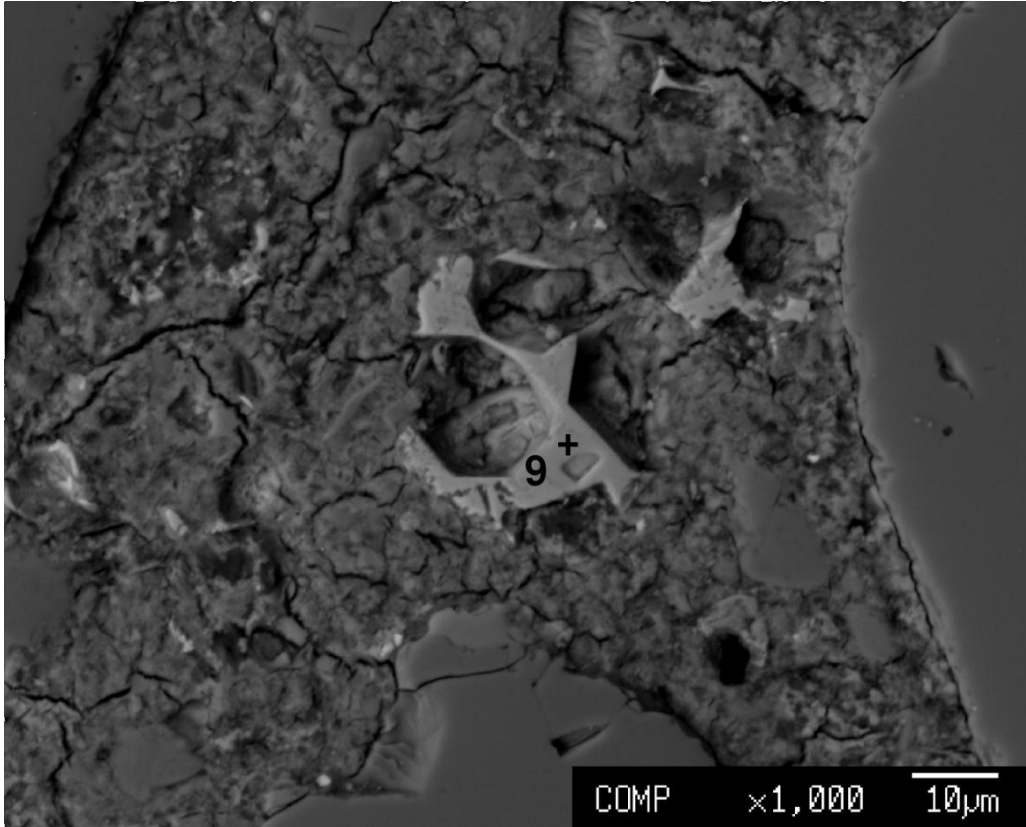


Figure 5.60 Backscattered image of blending cement paste showing the aluminite phase (Sample: CLI-B-R).

Electron microprobe analyses of hardened cement paste provide significant information on the compositional characterization and evolution of hydrated phases especially reacted zeolites. For this reason, in order to see compositional differences and evolutions, clinoptilolite crystals were analyzed from inner to outer zone, later the matrix near the crystal was processed. The results are interpreted and correlated with clinoptilolites from bulk material.

The points (labeled as 1 and 2 in Figure 5.61a and Table 5.8) indicates partially reacted clinoptilolite-rich tuff sample with increasing Ca content (6.82, 8.09, respectively) and decreasing Si content (28.84, 26.67, respectively) from center to edge for CLI-G-R. The third point (labeled as 3 in Figure 5.61a) identify matrix with high Ca^{2+} content (15.71). The same procedure was repeated for CLI-B-R sample. Three spots were taken from clinoptilolite-rich tuff (labeled as 10, 11 and 12). One spot (labeled as 13) was taken from the matrix near tuff (Figure 5.61c). The results showed that Ca content comparatively increases and Si content decreases from center to the both edges, which proof dissolution of clinoptilolite found in tuff grain and pozzolanic reaction with Ca ions as stated previously by Uzal and Turanlı (2012). The fourth point (labeled as 13 in Figure 5.61c) identify matrix with very high Ca content (28.78).

As a result of the examination of all points it was concluded that Ca, Si and Al are almost evenly distributed in clinoptilolite-rich tuff grains while they are unevenly distributed throughout the matrix designating the mixed hydration products in the matrix. Nevertheless it can be said that Ca content of CLI-B-R in matrix is higher than Ca contents of CLI-G-R and CLI-A-R in the matrix. Average weight percentages of Ca is 7.46% for CLI-G, 7.7% for CLI-A, 3.3 for CLI-B; Si is 27.76 for CLI-G, 27.32% for CLI-A, 30.36 for CLI-B; Al is 5.49 for CLI-G, 5.56% for CLI-A and 6.64% for CLI-B. Higher Ca and lower Si and Al values in the CLI-G-R and CLI-A-R than in the CLI-B-R proves the higher extent of reaction for Gördes and Aliğa clinoptilolites.

Dissolution of zeolite structure was further proved by chemical correlation of non-reacted zeolites from bulk analysis and reacted zeolites from hardened cement. Si^{4+} and Al^+ values in reacted zeolites except analcime are less than Si and Al values of zeolites measured from bulk analysis, while Ca in reacted zeolite crystal are between 3,02 and 8,09%. This demonstrates an increased Ca content in comparison with bulk analyses. The diminishing of Si and Al elements is attributed to a gradual dissolution of zeolite structure. In the hardened paste of CLI-G-R, Ca/Si molar ratios of CSH produced by cement hydration are 1.48 and 1.90 with minor content of Na, Fe, Al, K, Mg (Table 5.8). These values coincide with data reported in literature which has given 1.5-1.9 (Mielenz, 1950; Lea, 1988; Sersale and Frigione, 1985; Massazza and Costa, 1977).

As can be seen in Figure 5.61, the border of analcime-bearing tuff grain (Figure 5.61e) in micrograph is more easily distinguishable, but those of the clinoptilolite-rich and mordenite-bearing grains are not (Figure 5.61a, b, c, d). Less visible phase boundaries is presumably due to the fact that particles of clinoptilolites and mordenite are more hydrated with respect to analcime.

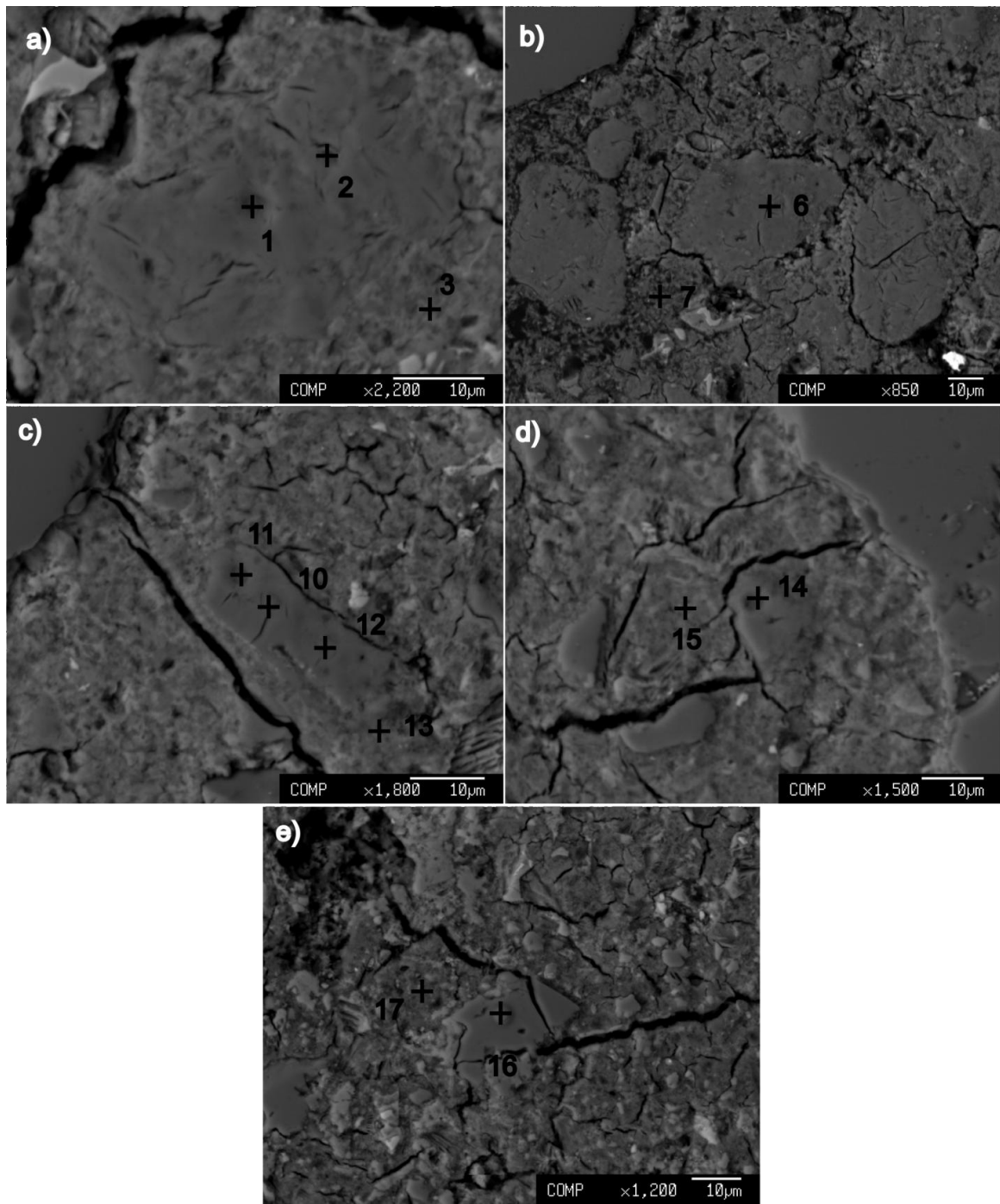


Figure 5.61 Backscattered electron images of a) CLI-G-R, b) CLI-A-R, c) CLI-B-R, d) MOR-R, e) ANA-R cement pastes.

CHAPTER 6

DISCUSSION

When pozzolans are properly selected, they will have improved advantages on the physical and mechanical aspects of the resulting concrete (Malhotra and Mehta, 1996; Sersale, 1992). Similarly, with improved knowledge of the material characteristics, the estimation of material efficiency is increasing. Therefore, characterization of pozzolan is a crucial step in selection of raw material and manufacture of cement.

In the current study, a thorough characterization of the zeolitic tuffs was performed by electron microprobe, cation exchange capacity, quantitative XRD, BET specific surface area and grain size analysis. Electron microprobe analyses showed that zeolite in CLI-G is chemically very similar to that of CLI-A. Clinoptilolite in CLI-B, on the other hand, includes lower Si/Al ratio than other clinoptilolites (Table 5.3). The analysis revealed that CECs of CLI-G, CLI-A and CLI-B are 1.75 meq/g, 1.78 meq/g and 1.72 meq/g, respectively (Table 5.4). Concerning CECs, the difference of cation exchange capacity effect on pozzolanic activity is negligible since they have similar CECs. Quantitative mineralogical composition (XRPD) of zeolitic tuffs is summarized in Table 5.5. The main phase of CLI-G, CLI-A and CLI-B is clinoptilolite, which is about 80%. Since quantity of zeolite in clinoptilolite-rich tuff is very similar, the difference of the mineralogical effect on pozzolanic activity is also negligible. MOR and ANA, on the other hand, appeared to contain less zeolites (27.3% and 20.3%, respectively). The presence of insignificant amount of smectite (4.6%) and kaolinite (5.7%) is also relevant. It is important to note that each sample also includes volcanic glass especially high in quantity in MOR and ANA, which could have a role on pozzolanic activity. Hence, it was not preferred to correlate physical and chemical properties of MOR and ANA.

By mixing lime with zeolitic tuffs, the pozzolanic activity has been investigated by Fratini's test and thermogravimetric method. Although Fratini's test is a quick standard method, it only allows to determine whether the material is pozzolanic or not. Thermogravimetric method, however, gives quantitative results. According to Fratini's test all zeolitic tuff-lime pastes gave positive results (Figure 5.25). After thermogravimetric method, the pozzolanic activity follows the sequence from highest to lowest; CLI-G>CLI-A>CLI-B>MOR>ANA (Figure 5.23). After assessing pozzolanic activity of materials, two common test methods for determining pozzolanic activity were compared in order to understand whether Fratini's test and thermogravimetric method correlate with each other or not. The numerical Fratini's test results show identical pozzolanic activity with thermogravimetric method, which again follows the sequence from highest to lowest; CLI-G>CLI-A>CLI-B>MOR>ANA (Table 5.6). In addition, significant correlation between the two test methods for pozzolanic activity was determined on the

correlation graph (Figure 5.26). Consequently, it can be said that these tests correlate well with each other and therefore provide certain assessment of pozzolanic activity.

The examination of the pozzolanic reaction kinetics was made by modified Jander Equation. According to Figure 5.27, CLI-G and CLI-A samples show a similar trend of reaction kinetics. Mineralogical and chemical characteristics of CLI-G are very similar to the CLI-A. The main difference between these two is physical, namely BET specific surface area, which is higher in CLI-G than CLI-A (Table 5.1). Even though the amount of lime fixation is different at 3 days of hydration for CLI-G and CLI-A, they display similar trend during the whole reaction. This means that the specific surface area has influence on the consumption of lime mainly during the initial period (before 3 days), whereas it did not affect (Figure 5.27) reaction mechanism thereafter (e.g. Mertens et al., 2009). CLI-B, on the other hand, has different pozzolanic reaction behavior. The higher reaction progress of CLI-B at longer ages is attributed to the lower Si/Al ratio. The kinetic analysis according to the modified Jander equation indicated that only one process controlling the reaction mechanism was observed; the diffusion of reactants through a layer of dense reaction products (Phase III). Phase I and Phase II, however, were absent in all the samples. It was predicted from these data that they might have ended before 3 days of hydration.

According to kinetic analysis of CLI-B exchanged with Na^+ , K^+ and Ca^{2+} cations, the exchangeable cation content mainly influences the pozzolanic activity after 28 days of hydration (Figure 5.28). K^+ -exchanged sample shows the best pozzolanic reaction, Ca^{2+} -exchanged one has slightly lower pozzolanic reaction than K^+ . Na^+ -enriched sample, on the other hand, displays the lowest reaction. This means that the presence of K^+ in the system has a profound influence on the lime fixation capacity as the reaction advances. The behavior of pozzolanic reaction is, on the other hand, significantly changed by introduction of Na^+ . This result confirms Mertens et al. (2009)'s findings that K^+ -exchanged sample has low reaction exponent, Na^+ -exchanged one has the highest exponent of reaction and Ca^{2+} -exchanged sample has an exponent of reaction in between them. In addition, Uzal and Turanlı (2012) stated that higher lime reactivity of GZ than that of BZ is attributed to the major cation content of zeolites. Lower pozzolanic activity of BZ than GZ was explained by Ca-rich composition of BZ. Although the present and previous studies (Mertens et al., 2009; Uzal and Turanlı, 2012) prove that the cation content is an important phenomenon on pozzolanic reaction, further research is needed to understand the way of effect on reaction mechanism.

Zeolitic tuff-lime hardened pastes were investigated by means of X-ray diffraction (XRD) and Fourier transform infrared spectroscopy (FTIR) analysis to determine the preexisting and new crystalline phases. The reason for performing both XRD and FTIR is comparison of two analytical methods. The peaks of zeolites, portlandite and CSH were observed in both XRD and FTIR analysis. But, the peaks of hydrotalcite were only observed with XRD analysis. The intensity of diffraction peak/bands of zeolites markedly decreases when hydrated on both methods (Figures 5.29 – 5.44). The decreasing intensity of zeolite peaks/bands confirms the dissolution and/or decomposition of zeolite structure and participating pozzolanic reaction. The

graph of XRD indicates that the intensity of portlandite, CSH and hydrotalcite peaks appear after 3 days of curing for all zeolitic tuff-lime pastes. CSH peak on FTIR analysis, on the other hand, appears after 7 days for clinoptilolite-rich tuff-lime pastes (Figures 5.40, 5.41, 5.42), after 28 days of hydration for mordenite-bearing tuff-lime pastes (Figure 5.43) and the band of CSH is not seen in ANA-R (Figure 5.44). Therefore it can be stated that XRD is more the sensitive method than the FTIR method for examining hydration products.

Compressive strength analysis of the blended and control cements at 7, 28, 56 and 90 days are shown in Figure 5.45. All blended cements exhibit lower compressive strength than the control Portland cement mortar at 7 days of age. This result is typical for supplementary cementitious materials (SCMs), which often reduce the initial strength development (Massazza, 1998). After 28 days of hydration, MOR acquired almost the same and CLI-G and CLI-B obtained higher compressive strength than the reference Portland cement mortar (Figure 5.45). Mechanical performances follows from highest to lowest CLI-B>CLI-G>MOR>CLI-A>ANA. In fact, CLI-B provides a clear strength improvement compared to the control Portland cement. As can be seen from the results of compressive strength analysis (Chapter 5.5), characterization of raw material is an incontrovertible step for understanding the pozzolanic activity of material before analysis. Despite this, the conditions of preparation of mortars are also very important. Therefore, the field performance of pozzolanic materials is very important to find the best physical conditions (grain size or w/c ratio) of SCMs before using at constructional application.

Hardened cement pastes at 28 days of hydration were examined chemically by microprobe analysis in order to examine elemental evaluations of zeolites. Ca^{2+} content of clinoptilolites in CLI-G, CLI-A and CLI-B (unreacted tuff) (Table 5.3) are 1.41%, 1.49% and 1.52%, respectively. Ca^{2+} content of clinoptilolites in CLI-G-R, CLI-A-R and CLI-B-R (reacted tuff) ranges from 3,02% to 8,09%. Furthermore, Si and Al values in reacted zeolites except analcime are less than Si and Al values of zeolites measured from bulk analysis. Therefore, dissolution of zeolite structure and participating pozzolanic reaction was also proved by microprobe analysis. A similar result was determined by Ortega et al. (2000) that the microprobe analysis of clinoptilolite indicates elevated Ca content compared to the unreacted zeolite. As a result of point analysis of clinoptilolite-rich tuff grains, increasing Ca content and decreasing Si content were observed from center to edge (Figure 5.61). This indicates that dissolution of zeolite found in tuff grain and pozzolanic reaction with Ca ions as stated previously by Uzal and Turanlı (2012).

The sample specification of experimental methods is shown in Table 5.9.

Table 5.9 The sample specification of experimental methods.

	ICP-OES	Quantitative XRD	Particle size	BET Specific Surface Area	Blaine Surface Area	Electron Microprobe Analysis (EMPA)	Thermogravimetric Analysis (TG)	Fratini's Test	Kinetic Analysis	Compressive Strength	X-ray Diffraction (XRD)	Scanning Electron Microscopy (SEM)	Fourier Transform Infrared Spectroscopy (FTIR)
CLI-G	+	+	+	+	+	+	+	+	+	-	+	+	+
CLI-A	+	+	+	+	+	+	+	+	+	-	+	+	+
CLI-B	+	+	+	+	+	+	+	+	+	-	+	+	+
MOR	+	+	+	+	+	+	+	+	+	-	+	+	+
ANA	+	+	+	+	+	+	+	+	+	-	+	+	+
CLI-B-Na ⁺	+	-	-	-	-	-	+	-	+	-	-	-	-
CLI-B-K ⁺	+	-	-	-	-	-	+	-	+	-	-	-	-
CLI-B-Ca ²⁺	+	-	-	-	-	-	+	-	+	-	-	-	-
CLI-G-R	-	-	-	-	-	+	-	-	-	+	-	+	+
CLI-A-R	-	-	-	-	-	+	-	-	-	+	-	+	+
CLI-B-R	-	-	-	-	-	+	-	-	-	+	-	+	+
MOR-R	-	-	-	-	-	+	-	-	-	+	-	+	+
ANA-R	-	-	-	-	-	+	-	-	-	+	-	+	+

CHAPTER 7

CONCLUSIONS AND RECOMMENDATIONS

The pozzolanic reactions of different types of natural zeolites and their reaction products have been examined.

From the mineralogical, physical and chemical analysis, following conclusions can be drawn. CLI-G offers the largest specific surface area. The BET surface area of the CLI-B is smaller than those of CLI-G and CLI-A. CLI-A has the smallest grain size distribution. Electron microprobe analyses showed that zeolite in CLI-G is chemically very similar to that of CLI-A. Clinoptilolite in CLI-B, on the other hand, includes high amounts of K^+ and lower Si/Al ratio than other clinoptilolites. CLI-G and CLI-A have the highest CEC and ANA has the lowest CEC value. The main phase of CLI-G, CLI-A and CLI-B is clinoptilolite, with minor amounts of feldspar, quartz and biotite. MOR and ANA, on the other hand, appeared to contain less zeolites, and considerably higher feldspar and volcanic glass.

CLI-G is the most reactive pozzolan than all the other tuffs. It is able to fix about 50% of the initial lime in only seven days, showing a high pozzolanic activity. The pozzolanic activity follows the sequence with decreasing amount CLI-G, CLI-A, CLI-B, MOR, ANA, respectively based on the TG analysis.

It is concluded from the results that the specific surface area enhances the degree of reaction during initial period (before 3 days). But it did not affect the reaction mechanism thereafter (e.g. Mertens et al., 2009; Uzal et al., 2010). From the results, it can be concluded that Si/Al ratio has a powerful effect at longer dates (e.g. Drzaj et al., 1978; Mertens et al., 2009; Uzal et al., 2010; Massazza, 2001). With regard to reacted lime, K^+ exchanged paste shows the best pozzolanic activity at longer reaction dates.

The kinetic analysis followed by Jander equation showed that only one process is controlling the reaction mechanism, which is the diffusion of reactants through a layer of dense reaction products.

According to Fratini's test it is possible to classify all blended cements as pozzolanic cements and there is significant correlation between the results of Fratini's test and thermogravimetric analysis ($R^2= 0.97-0.99$).

There is no considerable difference observed for all blended pastes in terms of crystalline hydration product. However, the peak heights are different. The intensity of diffraction peak of

zeolites markedly decreases and the decreasing intensity of zeolite peaks on XRD patterns confirms the dissolution and/or decomposition of zeolitic structure and participating pozzolanic reaction (e.g. Perraki et al., 2005; Caputo et al., 2008; Uzal and Turanlı, 2012). The relative peak intensity of portlandite decreases gradually from the 3 days of hydration. This event is related to its consumption while the hydration continues. As the reaction advances, the intensity of diffraction peak of the CSH increases. A gradual increase of CSH peaks suggests a progression in crystallinity of CSH with ageing. CLI-G-R showed the highest consumption of portlandite and clinoptilolite. The intensity of the CSH related peak is the highest for the CLI-G-R compared with the CLI-A-R and CLI-B-R, which is in good agreement with thermogravimetric results.

The consumption of portlandite and zeolite are also observed from the FTIR analysis. Significant reduction in the peak intensities of zeolite is clearly observed, which again confirms the dissolution of zeolite structure and then involvement in the pozzolanic reaction (e.g. Perraki et al., 2003) as stated by XRD analysis. The relative intensity of the peak at 3640 cm^{-1} due to OH band from $\text{Ca}(\text{OH})_2$ is gradually decreasing with hydration age, which again confirms the consumption of lime and enhancement of pozzolanic activity. The characteristic peak of CSH became evident after 7 days for clinoptilolite blends, indicating formation of hydration products.

Determination of characterization of raw material and then lime fixation capacity of paste yield critical results about the rate of pozzolanic reaction. However, literature (e.g. Uzal, 2007) and the current study indicate that there is no useful correlation between fixed lime value and compressive strength. For example, CLI-G and CLI-A react with lime more readily than CLI-B, but CLI-B contributes to a significant improvement of the mechanical resistance of the mortar at 28 days of hydration. Therefore we can conclude that lime fixation data from thermogravimetric analysis do not alone allow a prediction of compressive strength results for every time. At the end of this interpretation, it can be said that the evaluation of pozzolanic activity of zeolitic tuffs by mechanical point of view depends on physical, mineralogical, chemical parameters of pozzolan, which result in lime fixation ability and the physical parameters connected to the preparation of the mixture, which are closely related to each other.

At 28 days of hydration, the mechanical resistance of CLI-G, CLI-A, CLI-B, MOR, ANA and control mortars are 54.9 MPa, 47.9 MPa, 58.2 MPa, 52 MPa, 41 MPa and 52.9 MPa, respectively. According to the results of compressive strength analyses, CLI-B provides clear strength improvement, which is approximately 10% higher than that of control Portland cement at 28 days. In addition, CLI-G and MOR have good strength results, which indicate clear potential economic importance. Analysis showed that CLI-A needs more water to produce mortars of the same workability, which result in lower compressive strength. According to authors, if appropriate w/cm ratio is set, CLI-A can also be used for constructional purposes. Therefore, if zeolitic tuffs from Aliğa region are also used for production, it is suggested to use superplasticizer in order to control consistency. To conclude, all zeolitic tuffs from western Turkey are suitable for manufacturing in cement production as an additive. Mechanical

performances follows from highest to lowest CLI-B>CLI-G>MOR>CLI-A>ANA. Low cost, energy efficiency and reduction in CO₂ emission makes cement production by blended zeolitic tuff is very promising. But, the effect of blended cement with zeolitic tuffs must also be investigated directly on concrete production as future work. Further investigation can also be made on blended cement mixing with different kind of natural zeolites in the same mortar and concrete. Use of zeolitic tuff samples exchanged with K⁺, Na⁺ and Ca²⁺ cations in compressive strength analysis is another recommended topic which can be investigated.

REFERENCES

- Adams, J., Dollimore, D. and Griffiths, D.L. 1993. Thermal analytical investigation of ancient mortars from Gothic churches. Proceeding of the Tenth International Congress on Thermal Analysis. Journal of Thermal Analysis 40 (1), 275-284.
- Adams, J., Dollimore, D. and Griffiths, D.L. 1993. Thermal analytical investigation of ancient mortars from Gothic churches. Proceeding of the Tenth International Congress on Thermal Analysis. Journal of Thermal Analysis 40 (1), 275-284.
- Aitcin, P.C. Binders for durable and sustainable concrete. First Edition, published by Taylor and Francis Group Ltd, New York, 2008, pages, 500.
- Akay, E. and Erdogan, B. 2004. Evolution of Neogene calc-alkaline to alkaline volcanism in the Alağa-Foca region (West Anatolia, Turkey). Journal of Asian Earth Sciences 24, 367-387.
- Akyürek, B. and Soysal, Y. 1978. Geology of the Kırkağaç-Soma (Manisa), Savaş tepe-Korum-Ayvalık (Balıkesir), Bergama (İzmir) Region, General Directorate of Mineral research and Exploration (MTA), Report no: 6432.
- Albayrak, M. 2008. Batı Anadolu, Trakya, Kapadokya Yöresi Zeolitleri Mineralojik Veri Kitabı, MTA Rapor No:11053, Ankara, 204s.
- Albayrak, M. 2010. Manisa (Gördes) bölgesi zeolitlerinin mineralojik, kimyasal ve teknolojik incelenmesi. Kibited 1(4), 273-285.
- Albayrak, M. and Özgüner, A. M. 2013. Geology and diagenesis of a zeolitic Foça Tuff Unit deposited in a Miocene phreatomagmatic lacustrine environment (Western Anatolia). Turkish Journal of Earth Sciences 22, 1-21.
- American Society for Testing and Materials (ASTM) C-125, Standard terminology relating to concrete and concrete aggregates, 2007.
- Armbruster, T. and Gunter, M. E. 2001. Crystal structures of natural zeolites. In D.L. Bish and D.W. Ming (eds) *Natural Zeolites: Occurrence, Properties, Applications*. Reviews in Mineralogy and Geochemistry; Vol. **45**, Washington, D.C., 1-67.
- ASTM C 109 test method for compressive strength of hydraulic cement mortars (using 2-in or 50-mm cube specimens), Am Soc Test Mater, 2005.
- ASTM C 109, Test Method for Compressive Strength of Hydraulic Cement Mortars (Using 2-in. or 50-mm Cube Specimens), American Society for Testing and Materials, 2005.

- ASTM C 618. 2005. Standard Specification for Fly Ash and Raw or Calcined Natural Pozzolan for Use as a Mineral Admixture in Portland Cement Concrete, American Society for Testing and Materials.
- ASTM C618. Standard Specification for fly ash and raw or calcined natural pozzolan for use as a mineral admixture in Portland cement concrete.
- Ataman, G. 1977. Batı Anadolu zeolit oluşumları. *Yerbilimleri* 7, 9-14.
- Baronio, G., Binda, L. and Lombardini, N. 1997. The role of brick pebbles and dust in conglomerates based on hydrated lime and crushed bricks, *Construction and Building Materials* 11 (1), pp. 33-40.
- Barrer, R.M. 1982. *Hydrothermal Chemistry of Zeolites*. Academic Press. London. 360 pp.
- Bish, D. L. and Howard, S. A. 1988. Quantitative phase analysis using the Rietveld method. *J. Appl. Cryst.* 21, 86-91.
- Blezard, R.G. 1998. The history of Calcareous Cements, in: P.C. Hewlett (Ed.), *Lea's Chemistry of Cement and Concrete*, London: Arnold, p. 6-23.
- Bogue, R.H. 1952. *La chimie du ciment Portland*, Paris: Eyrolles.
- Borsi, S., Ferrara, C., Innocenti, F. and Mazzudi, R. 1972. Geochronology and petrology of recent volcanics of Eastern Aegean Sea. *Bulletin of Volcanology*, 36, 473-496.
- Bottale, M.G., Caputo, D. and Colella, C. 1998. Measurement of the cation exchange capacity of a natural zeolite: a preliminary approach. Pp. 31 - 36 in: *Proceedings of the IV Convegno Nazionale Scienza e Tecnologia delle Zeoliti* (E. Fois and A. Gamba, editors). Cernobbio (Como) Italy, September 1998.
- Breck, D.W. 1974. *Zeolite Molecular Sieves*. Wiley. New York. 529-536.
- Brunauer, S., Emmett, P.H. and Teller, E. 1938. Adsorption of gases in multimolecular layers. *Journal of the American Chemical Society* 60, 309-319.
- Buhrke, V.E., Jenkins, R., Smith, D.K. 1998. *Preparation of specimens for X-ray fluorescence and X-ray diffraction analysis*. 2nd edition. John Wiley & Sons, New York. 333p.
- Campbell, D.H. 1999. *Microscopical examination and interpretation of Portland cement and clinker*. 2nd edition. Portland Cement Association.

- Canpolat, F., Yılmaz, K., Köse, M. M., Sümer, M. and Yurdusev, M. A. 2004. Use of zeolite, coal bottom ash and fly ash as replacement materials in cement production. *Cement and Concrete Research* 34, 731-735.
- Caputo, D., Liguori, B. and Colella, C. 2008. Some advances in understanding the pozzolanic activity of zeolites: the effect of zeolite structure. *Cement and Concrete Composites*; 30:455–62.
- Çelik, E., Ayok, F. and Demir, N. 1999. Phosphate mineralization in Ayvacik-Kucukkuyu (Canakkale Province). General Directorate of Mineral Research and Exploration Open File Report No: 10228.
- Cerri, G., Langella, A., Pansini, M. and Cappelletti, P. 2002. Methods of determining cation exchange capacities for clinoptilolite-rich rocks of the Logudoro region in northern Sardinia, Italy. *Clays and Clay Minerals* 50 (1), 127-135.
- Chung, F.H. 1974. Quantitative interpretation of X-ray diffraction patterns of mixtures. I. Matrix-flushing method of quantitative multicomponent analysis. *Journal of Applied Crystallography* 7, 519–525.
- Colella, C., de' Gennaro, M, and Aiello, R. 2001. Use of zeolitic tuff in the building industry. *In: Bish, D.L. and Ming, D.W. (eds.) Natural Zeolites: Mineralogy, Occurrence, Properties, Applications, Reviews in Mineralogy & Geochemistry, Mineralogical Society of America, Vol. 45, Washington, D.C., 551-587.*
- Colleparidi, M., Baldini, G., Pauri, M. and Corradi, M. 1978. The effect of pozzolanas on the tricalcium aluminate hydration, *Cement and Concrete Research* 8 (6), 741-751.
- Cook, D. J. 1986. Natural pozzolanas, in: R.N. Swamy (Ed.), *Cement Replacement Materials*, Surrey University Press, pp. 200.
- Coombs, D. S., Alberti, A., Armbruster, T., Artioli, G., Colella, C., Galli, E., Grice, J.D., Liebau, F., Mandarino, J.A., Minato, H., Nickel, E.H., Passaglia, E., Peacor, D.R., Quartieri, S., Rinaldi, R., Ross, M., Sheppard, R.A., Tillmanns, E. and Vezzalini, G. 1998. Recommended nomenclature for zeolite minerals: report of the subcommittee on zeolites of the International Mineralogical Association, Commission on New Minerals and New Names. *European Journal of Mineralogy* 10, 1037-1081.
- Diamond, S. 1976. Cement paste microstructure: an overview at several levels. Hydraulic cement pastes: their structure and properties, *Proceedings of a conference at Sheffield University, Cement and Concrete Association, Wexham Springs, 1-30.*

- Diamond, S. 1970. Application of Scanning Electron Microscopy to the Study of Hydrated Cement. Third Annual Scanning Electron Microscope Symposium , Chicago, pp. 385-392.
- Diamond, S. 2000. Mercury porosimetry: an inappropriate method for the measurement of pore size distributions in cement-based materials. Cement and Concrete Research 30, 1517-1525.
- Donatello, S., Tyrer, M. and Cheeseman, C. R. 2010. Comparison of test methods to assess pozzolanic activity. Cement and Concrete Composites 32, 121-127.
- DPT (Devlet Planlama Teskilatı). (1996). Madencilik Özel İhtisas Komisyonu Endüstriyel Hammaddeler Alt Komisyonu-Diger Endüstri Mineralleri Çalışma Grubu Raporu, <http://ekutup.dpt.gov.tr/madencil/sanayiha/oik480c1>.
- Draffin, J.O. 1943. A brief history of lime, cement, concrete and reinforced concrete'. University of Illinois Bulletin 40, 5-38.
- Drzaj B, Hocevar S. and Slokan M. 1978. Kinetics and mechanism of reaction in the zeolitic tuff-CaO-H₂O systems at increased temperature. Cement and Concrete Research 8,711-20.
- Dutta, P.K. and Twu, J. 1991. Influence of framework silicon/aluminum ratio on the Raman spectra of faujasitic zeolites. Journal of Physical Chemistry 95 (6), 2498-2501.
- EN 196/5. 1994. Anonymous, *Methods of testing cement: Pozzolanicity test for pozzolanic cement*, EN 196/5, European Committee for Standardization: Bruxelles, Belgium, 10 pp.
- Ercan, T. Dinçel, A. Metin, S. Türkecan, A. and Günay, E. 1978. Usak Yöresindeki Neojen Havzalarının Jeolojisi, Türkiye Jeoloji Kurumu Bülteni, c. 21, 97-106.
- Ercan, T., Çevikbaş, A., Günay, E., Ateş, M., Can, B., Küçükayman, A. ve Erkan, M. 1984c, Bigadiç çevresinin (Balıkesir) jeolojisi ve magmatik kayaçların petrolojisi. Türkiye Jeoloji Kurultayı 1984, Bildiriler kitabı, 75-85.
- Ercan, T., Günay, E., Çevikbaş, A., Ateş, M., Küçükayman, A., Can, B. ve Erkan, M. 1984. Bigadiç çevresinin (Balıkesir) jeolojisi, magmatic kayaçların petrolojisi ve kökensel yorumu. MTA Derleme Rapor No: 7601, Ankara.
- Ercan, T., Satır, M., Steinitzi G., Dora, A., Sarıfakıoğlu, E., Adis, C., Walter, H.J. and Yıldırım, T. 1995. Features of the Tertiary volcanism in Biga peninsula, Gokceada, Bozcaada ve Tavşan islands (NW Anatolia). Mineral Research and Exploration Bulletin, 117, 55-86.

- Esenli, F. 1992. Gördes çevresindeki Neojen serilerinin ve zeolitleşmenin jeolojik, mineralojik ve jeokimyasal incelenmesi. Doktora Tezi, İTÜ Fen Bil. Enst., İstanbul, 209s.
- Esenli, F. and Özpeker, I. 1994. Gördes çevresindeki Neojen havzanın zeolitik diyajenezi ve hoylandit-klinoptilolitlerin mineralojisi. 46. Türkiye Jeoloji Kurultayı, Ankara, Bildiri Özleri, 63.
- Faujas De Saint-Fond, B. 1778. Recherches sur les volcans éteints du Vivarais et du Velay, avec un discours sur les volcans brulans, des memoires analytiques sur les schorls, la zeolite, le basalte, la pouzzolane, les laves & les differentes substances qui s'y trouvent engagees, &c. Cuchet, Grenoble et Paris. 460 pp.
- Felder-Casagrande, S., Wiedemann, H.G. and Reller, A. 1997. The calcinations of Limestone: Studies on the past, the present and the future of a crucial industrial Process'. Journal of thermal Analysis 49, 971-978.
- Fick, A. 1855. Uber diffusion, Poggendorff's Annalen der Physik und Chemie, 94 59-86.
- Fisher, R. V. and Schmincke, R. V. 1984. Pyroclastic rocks. Springer-Verlag, Berlin, 472 pp.
- Fraay, A.L.A., Bijen, J.M. and de Haan, Y.M. 1989. The reaction of fly ash in concrete. A critical examination. Cement and Concrete Research 19, 235-246.
- Fragoulis, D., Chaniotakis, E. and Stamatakis, M. G. 1997. Zeolitic tuffs of Kimolos island, Aegean Sea, Greece and their industrial potential, Cement and Concrete Research 27(6), 889-905.
- Fratini, N. 1949. Researches on hydrolysis lime in cement pastes. – Part I. (in Italian); Annali di Chimica (Rome), 39, pp. 41-49.
- Giergiczny Z. and Werynska A. 1989. Influence of fineness of fly ashes on their hydraulic activity. In: Malhotra, VM ed. Proceedings of the 3rd International Conference on Fly Ash, Silica Fume, Slag, and Natural Pozzolans in Concrete, Trondheim. American Concrete Institute Special Publication 114; vol. I: 97-115.
- Göktaş, F. 1996. Gördes Neojen Havzasının Jeolojisi, MTA Derleme Rapor No: 9931, Ankara.
- Goldstein, J.I., Newbury, D.E., Echlin, P., Joy, D.C., Fiori, C.E. and Lifshin, E. 1981. Scanning electron microscopy and X-ray microanalysis. Plenum Press, New York, 401pp.

- Göncüoğlu, M.C., Dirik, K. and Kozlu, H. 1997. General characteristics of pre-Alpine and Alpine Terranes in Turkey: Explanatory notes to the terrane map of Turkey. *Annales Geologiques des Pays Helleniques* 37, 515-536.
- Gottardi, G. 1978. Mineralogy and crystal chemistry of zeolites. In L.B. Sand and F.A. Mumpton (eds) *Natural Zeolites: Occurrence, Properties, Use*. Pergamon Press, Elmsford, New York, 31-44.
- Gottardi, G., and Galli, E., 1985. *Natural Zeolites*. Springer-Verlag, 409 p. Berlin, Germany.
- Güleç, A. and Tulun, T. 1997. Physico-chemical and petrographical studies of old mortars and plasters of Anatolia. *Cement and Concrete Research* 27 (2), 227-234.
- Hay, R. L. 1978. Geologic occurrence of zeolites: in *Natural Zeolites: Occurrence, Properties, Use*, L. B. Sand and F. A. Mumpton, eds., Pergamon Press, Elmsford, New York, 135-143.
- Hay, R.L. and Sheppard, R.A. 2001. Occurrence of zeolites in sedimentary rocks: An overview. In D.L. Bish and D.W. Ming (eds) *Natural Zeolites: Occurrence, Properties, Applications*. *Reviews in Mineralogy and Geochemistry*; Vol. 45, Washington, D.C., 217-234.
- Helvacı, C. and Alaca, O. 1991. Geology and mineralogy of the Bigadiç borate deposits and vicinity. *Mineral Res. Expl. Bull.*, 113, 31-63.
- Hill, R. J. and Howard, C. J. 1987. Quantitative phase analysis from neutron powder diffraction data using the Rietveld method. *J. Appl. Cryst.* 20, 467-474.
- Huizhen, L. 1992. Effect of structure and composition on reactivity of zeolite-tuff used as blending material of portland cement. *Proceedings of the 9th International Congress on the Chemistry of Cement*, Nat. Council for Cement and Building Materials, New Delhi, India, Vol. 3, 128-134.
- Idorn, M.G. 1997. *Concrete progress from Antiquity to the third millennium*, Telford, London, ISBN 0-7277-2631-5, pp 330.
- İnci, U. 1984. Stratigraphy and organic material contents of Demirci ve Burhaniye bituminous shales. *Bulletin of the Geological Society of Turkey*, 5, 27-40.
- Jander, W. 1927. Reactins in the solid state at high temperature. *Z. Anorg. Allge. Chem.* 163 (1-2), 1-30.

- Janotka, I. and Krajci, L. 2003. Utilization of natural zeolite in Portland cement of increased sulphate resistance, ACI Special Publications 221, 223-229.
- Janotka, I., Ray, A. and Mojumdar, S.C. 2004. Acid and sulfate resistance of Portland cement - natural zeolite mortar. In Proc 8th CANMET/ACI International Conference on Fly Ash, Silica Fume, Slag and Natural Pozzolans in Concrete, Las Vegas, p. 639–652.
- JCPDS (Joint Committee of Powder Diffraction Standards). 1983. International Centre for X-ray powder diffraction.
- Kaya, O. and Savaşçın, M.Y. 1981. Petrologic significance of the Miocene volcanic rocks in Menemen, west Anatolia. *Aegean Earth Sciences* 1, 45–58.
- Kingery, W.D. 1980. Social needs and ceramics technology. *Ceramic Bulletin* 59 (6), 598-600.
- Kitsopoulos, K. P. and Dunham, A. C. 1996. Heulandite and mordenite-rich tuffs from Greece: a potential source for pozzolanic materials. *Mineral. Deposita* 31, 576-583.
- Klein, C., 2002. The 22nd Edition of the Manual of Mineral Science (after J. D. Dana). John Wiley and Sons, Inc., New York, 641 pp.
- Kondo, R., Lee, K. and Daimon, M. 1976. Kinetics and mechanism of hydrothermal reaction in lime-quartz-water systems. *Journal of the Ceramic Society (Japan)* 84 (11), 573-578.
- Korkuna, O., Lebeda, R., Skubiszewska-Zieba, J., Vrublevs'ka, T., Gun'ko, V.M. and Ryzkowski, J. 2006. Structural and physicochemical properties of natural zeolites: clinoptilolite and mordenite. *Microporous and Mesoporous Materials* 87, 243-254.
- Kosanovic, C., Bronic, J., Subotic, B., Smit, I., Stubicar, M., Tonejc, A., Yamamoto, T. 1993. Mechanochemistry of zeolites: Part 1 Amorphization of zeolites A and X and synthetic mordenite by ball milling. *Zeolites* 13, 261-268.
- Lea, F. M. 1998. *Lea's Chemistry of Cement and Concrete*, 3rd ed., Arnold, London.
- Lengeranlı, Y., Baykul, A., Sun, A., Işın, R., Metli, F., Aşar, M., Türkbileği, H, Tan, T. ve Lorient, A.J. 1774. *Memoire sur une decouverte dans L2aer de batir*. Paris.
- Lucas, A. 1968. *Ancient Egyptian materials and industries*. London, 1934. Analysis of ancient Egyptian lime mortars (Roman period) and gypsum mortars are given in this work. 4th edition, Arnold, London.
- Mackenzie, R.C. 1974. Highways and byways in thermal analysis, *Analyst* 99, 900-912.

- Malhotra, V. M. and Mehta, K. P. 1996. Pozzolanic and cementitious materials. Amsterdam, Gordon and Breach Science Publishers.
- Malinowski, R. and Garfinkel, Y. 1991. Prehistory of concrete. *Concrete International* 13, 62-68.
- Martinet, G., Deloye, F.X. and Le Roux, A. 1992. Natures et alterations des mortiers de restauration du Temple d'Amon a Karnak, *Bulletin de liaison des Laboratoires des ponts et chaussees* 182, pp. 21-26.
- Martinez-Ramirez, S., Blanco-Varela, M.T., Erena, I. and Gener, M. 2006. pozzolanic reactivity of zeolitic rocks from two different Cuban deposits: Characterization of reaction products. *Applied Clay Science* 32, 40-52.
- Massazza, F. 1998. Pozzolana and pozzolanic cements In: P.C. Hewlett, ed., *Lea's chemistry of cement and concrete*, 4th Edition, Butterworth Heinemann, pp. 471-635.
- Mehta, P. K. 1987. Natural pozzolans, in: V.M. Malhorta (Ed.), *Supplementary Cementing Materials for Concrete*, Canadian Government Publishing Center, Ottawa, pp. 3-20.
- Mehta, P.K. and Monteiro, P.J.M. 2006. *Concrete: Microstructure, properties, and materials*. 3rd edition, McGraw-Hill, 659 pp.
- Meier, W.M. 1968. *Molecular Sieves*. Society for Chemical Industry. London. p.10.
- Meier, W.M., Olson, D.H. and Baerlocher, C. 1996. *Atlas of zeolite structure types: 4th revised edn*. *Zeolites* 17, 1-230.
- Mertens, G., Snellings, R., Van Balen, K., Bicer-Simsir, B., Verlooy, P. and Elsen, J. 2009. Pozzolanic reactions of common natural zeolites with lime and parameters affecting their reactivity, *Cement and Concrete Research* 39, 233-240.
- Mielenz, R. C. 1950. *Materials for pozzolans, A report for the engineering geologist*. Petrographic Laboratory Report No Pet90B. USA, Department of Interior, Bureau of Reclamation, Branch of design and construction, Denver, Colorado, 25p.
- Ming, D.W., Allen, E.R., Galindo, C., Jr. and Henninger, D.L. 1993. Methods for determining cation exchange capacities and compositions of native cations for clinoptilolite. Pp. 31 - 35 in: *Memoirs of the 3rd International Conference on the Occurrence, Properties, and Utilization of Natural Zeolites* (G.R. Fuentes and J.A. Gonzales, editors). Vol. 2. International Conference Center, Havana, Cuba.

- Mostafa, N. Y., El-Hemaly, S. S. S., Al-Wakeel, E. I., El-Korashy, S. A. and Brown, P. W. 2001. Characterization and evaluation of the pozzolanic activity of Egyptian industrial by-products I: Silica fume and dealuminated kaolin. *Cement and Concrete Research* 31, 467-474.
- Mozgawa, W. 2000. The influence of some heavy metals cations on the FTIR spectra of zeolites. *Journal of Molecular Structure* 555, 299-304.
- Mozgawa, W. 2001. The relation between structure and vibrational spectra of natural zeolites. *Journal of Molecular Structure* 596, 129-137.
- Mozgawa, W., Sitarz, M. and Rokita, M. 1999. Spectroscopic studies of different aluminosilicate structures. *Journal of Molecular Structure* 511-512, 251-257.
- Mumpton, F. A. 1978. Natural zeolites: a new industrial mineral commodity. In L.B. Sand and F.A. Mumpton (eds) *Natural Zeolites: Occurrence, Properties, Use*. Pergamon Press, Elmsford, New York, 3-27.
- Mumpton, F. A. 1999. *Proc. Natl. Acad. Sci. U.S.A.* 96, 3463.
- Mumpton, F. A., and Ormsby, W. C., 1978. Morphology of zeolites in sedimentary rocks by scanning electron microscopy: in *Natural Zeolites: Occurrence, Properties, Use*, Sand, L. B., and Mumpton, F. A., eds., Pergamon Press, Elmsford, New York, 113-132.
- Mumpton, F.A. 1973b. Scanning electron microscopy and the origin of sedimentary zeolites. *Molecular Sieves. Proc. 3rd Int. Molecular Sieve Conf.*, pp. 159-161.
- O'Connor, B H. and Raven, M.D. 1988. Application of the Rietveld refinement procedure in assaying powdered mixtures. *Powder Diffraction* 3, 2-6.
- Oleson, J.P., Brandon, Ch., Cramer, S.M., Cucitore, R., Gotti E. and Hohlfelder, R.L. 2004. The ROMACONS project: a contribution to the historical and engineering analysis of hydraulic concrete in Roman maritime structures, *The International Journal of Nautical Archaeology* 33 (2), pp. 199-229.
- Ortega, E.A., Cheeseman, C., Knight, J. and Loizidou, M. 2000. Properties of alkali-activated clinoptilolite. *Cement and Concrete Research* 30, 1641-1646.
- Özaydin S., Koçer G. and Hepbaşlı A. 2006. Natural Zeolites in Energy Applications. *Energy Sources, Part A: Recovery, Utilization, and Environmental Effects* 28(15), 1425-1431.
- Özen, S. and Göncüoğlu, M.C. 2012. Origin of analcime in the Neogene Arikli Tuff, Biga Peninsula, NW Turkey, *Neues Jahrbuch für Mineralogie Abhandlungen* 189 (1), 21-34.

- Papadakis, M. and Venuat, M. 1966. Fabrication et utilization des liants hydrauliques, n.p.
- Passaglia E. and Galli G. 1991. Natural Zeolites: Mineralogy and Applications. *European Journal of Mineralogy* 3(4), 637-640.
- Paya, J., Monzo, J., Borrachero, M. V., Velazquez, S. and Bonilla, M. 2003. Determination of the pozzolanic activity of fluid catalytic cracking residue. Thermogravimetric analysis on FC3R-lime pastes. *Cement and Concrete Research* 33, 1085-1091.
- Pechar, F. and Rykl, D. 1985. Infrared spectra of natural zeolites. *Rozpr. Ceskosl. Akad. Ved, Praha*.
- Perraki, Th., Kakali, G. and Kontoleon, F. 2003. The effect of natural zeolites on the early hydration of Portland cement. *Microporous and Mesoporous Materials* 61, 205-212.
- Perraki, Th., Kakali, G. and Kontori, E. 2005. Characterization and pozzolanic activity of thermally treated zeolite. *Jornal of Thermal Analysis and Calorimetry* 82, 109-113.
- Poon, C. S., Lam, L., Kou, S. C. and Lin, Z. S. 1999. A study on the hydration rate of natural zeolite blended cement pastes. *Construction and Building Materials* 13, 427-432.
- Ramachandran, V.S. 2001. Thermal analysis: In: Ramachandran, V.S and Beaudoin, J.J (eds.) *Handbook of analytical techniques in concrete science and technology. Principles, techniques and applications*. Ottawa, Ontario, Canada: Noyes Publications/ William Andrew Publishing, LLC Norwich, New York, U.S.A.
- Rietveld, H. M. 1969. A profile refinement method for nuclear and magnetic structures. *Journal of Applied Crystallography* 2, 65-71.
- Rondelet, J. 1805. *L'art de batir*, Paris.
- Scrivener, K.L. 2004. Backscattered electron imaging of cementitious microstructures: understanding and quantification. *Cement and Concrete Composite* 26 (8), 935-945.
- Sersale, R. 1980. *Chemistry of Cement*, Proc. 7th Symp., sous theme IV-1, Paris.
- Sersale, R. 1992. *Advances in Portland and blended cements: Proc. 9th Int. Conf. Chemistry of Cement*, I, Natl. Counc. Cement and Building Materials, New Dehli, India, pp. 261-302.
- Sersale, R. and Frigione, G. 1983. Utilization of the quarry dust of the Neapolitan yellow tuff for the manufacture of blended cements, *La Chimica E L'Industria* 65 (7-8), 479-481.

- Sersale, R. and Frigione, G. 1985. Natural zeolites as constituents of blended cements. *Studies in Surface Science and Catalysis* 24, 523-530.
- Shi, C. and Day, R.L. 2000. Pozzolanic reaction in the presence of chemical activators Part I. *Peaction Kinetics, Cement and Concrete Research* 30, 51-58.
- Snyder, R.L. and Bish, D.L. 1989. Quantitative analysis. In *Mineralogical Society of America Reviews in Mineralogy* 20, 101-144.
- Stark, J. and Wicht, B. 1999. Zur historie des gipses. *ZKG International*, 10, 527-533.
- Taylor, H.F.W. 1990. *Cement Chemistry*. London; Akademik Press Limited, 475pp.
- Taylor, H.F.W. 1997. *Cement Chemistry*, Academic Press Ltd., London.
- Thornton, G. 1996. *Cast in concrete: Concrete Construction in New Zealand 1850-1939*, Auckland: Red Books.
- Treacy, M.J. and Higgins J.B. 2001. *Collection of Simulated XRD Powder Patterns for Zeolites*, 4th edition. Elsevier, Amsterdam.
- Tröger, W. E. 1982. *Optische Bestimmung der gesteinsbildenden Minerale*. E. Schweizerbart'sche Verlagsbuchhandlung, Stuttgart, Germany.
- Tsitsishvili G. V., Andronikashvili T. G., Kirov G. M. and Filizova L. D. 1992. *NaturalZeolites*. Ellis Horwood Limited, Chichester, UK.
- Tunca, O. 2004. La Revolution Neolithique, *Bulletin de la Societe Royale des Sciences de Liege* 73 (4), 211-223.
- Turkmenoglu, A.G. and Tankut, A. 2002. Use of tuffs from central Turkey as admixture in pozzolanic cements assessment of their ptrographical properties. *Cement and Concrete Research* 32, 629-637.
- Ulusoy, G. and Albayrak, M. 2009. Mineralogical and technological properties of the zeolites from Foça (İzmir), Bigadiç (Balıkesir) and Gördes (Manisa). *Mineral Res. Exp. Bull.*, 139, 61-74.
- Urhan, S. 1987. Alkali silica and pozzolanic reactions in concrete. Part 1: interpretation of published results and an hypothesis concerning the mechanism. *Cement and Concrete Research* 17, 141-152.

- USGS (United States Geological Survey. 2008 Minerals Yearbook. <http://minerals.usgs.gov/minerals/pubs/commodity/zeolites/myb1-2008-zeoli.pdf>.
- Uzal, B. and Turanlı, L. 2007. Properties and hydration of cementitious systems containing low, moderate and high amounts of natural zeolites. PhD thesis.
- Uzal, B. and Turanlı, L. 2012. Blended cements containing high volume of natural zeolites: Properties, hydration and paste microstructure. *Cement and Concrete Composites* 34, 101-109.
- Uzal, B., Turanlı, L., Yücel, H., Göncüoğlu, M.C. and Çulfaz, A. 2010. Pozzolanic activity of clinoptilolite: A comparative study with silica fume, fly ash and a non-zeolitic natural pozzolan, *Cement and Concrete Research* 40, 398-404.
- Vicat L.J. 1818. *Recherches experimentales sur les chaux de construction, les betons et les mortiers ordinaires*, Goujon, Paris, 49p.
- Vicat, L.J. 1837. *Mortars and cements*, Ed. Michael Wingate, Donhead publishing, 302p.
- Villar-Cocina, E., Frias, M., Valencia-Morales, R. and Sanchez de Rojas, M.I. 2006. An evaluation of different kinetic models for determining the kinetic coefficients in sugar cane straw-clay ash/lime system. *Advances in Cement Research* 18 (1), 17-28.
- Virta, R.L. 2002. *Annual Report on Zeolites*, U.S. Geological Survey, Zeolites.
- Vitruvius, P.M. 1826. *Archetecture*, book ii, chapter vi. English translation by Joseph Gwilt, London.
- Welton, E. J. 1984. *SEM Petrology Atlas*. The American Association of Petroleum Geologist, USA, 237 pp.
- Wilson, M.J. 1994. *Clay Mineralogy: Spectroscopic and Chemical Determinative Methods*. Chapman & Hall, New York, 367 pp.
- Wittry, D. B. 1958. *Electron Probe Microanalyzer*. US Patent No: 2916621, Washington DC, US Patent and Trademark Office.
- Yağmurlu, F. 1983. Akhisar doğusu Neojen topluluğunun jeolojisi ve kömür potansiyeli. Doktora Tezi, DEÜ Fen Bil. Enst., İzmir, 217s.
- Yılmaz, H. 1977. Beğenler-Geçtin köyleri KB yöresinin (Gördes) stratigrafik, tektonik ve petrografik incelenmesi. *EÜ Fen Fak. Dergisi*, A 1-2, 143-169.

Yılmaz, B., Uçar, A., Öteyaka, B. and Uz, V. 2007. Properties of zeolitic tuff (Clinoptilolite) blended portland cement. *Building and Environment* 42, 3808-3815.

Zhang, Z., Guo, J. and Liang, C. 1995. Contribution of zeolite to the hydration of cement. In: Mumpton FA, editor, Program and abstracts, Zeolite'93, 4th international conference on occurrence, properties, utilization of natural zeolites, Int. Comm. Natural Zeolites, Brockport, New York, p. 221-3.

CURRICULUM VITAE

PERSONAL INFORMATION

Surname, Name: Özen, Sevgi
Nationality: Turkish (TC)
Date and Place of Birth: 21 September 1978, Ankara
Marital Status: Single
Phone: +90 312 210 57 09
Fax: +90 312 210 57050
email: ozsevgi@metu.edu.tr

EDUCATION

Degree	Institution	Year of Graduation
MS	METU Geological Engineering	2008
BS	AÜ Geological Engineering	2000
High School	Aydınlıkevler High School, Ankara	1996

WORK EXPERIENCE

Year	Place	Enrollment
2005-2013	METU Department of Geological Engineering	Research Assistant

FOREIGN LANGUAGES

Advanced English

PUBLICATIONS

Özen, S. and Göncüoğlu, M.C. 2012. Origin of analcime in the Neogene Arikli Tuff, Biga Peninsula, NW Turkey, Neues Jahrbuch für Mineralogie Abhandlungen 189 (1), 21-34.

HOBBIES

Swimming, Running